

# Ernest Henry Cu-Au deposit



## LOCATION

### Geological Domain

Canobie Domain

### Co-ordinates

Latitude: 20° 26' 42" S, Longitude: 140° 42' 30" E

MGA Zone 54: 469250 E, 7739267 N

## NATURE OF MINE

### Mined Commodities

Cu, Au, Ag (1997-present), Fe (2011-2013)

### Mining Method

Open Pit (1997-2011) and underground (2011-present) mining;

### Depth of Mining

1000 m (underground); 650 m (open cut)

## PRODUCTION AND DIMENSIONS

### Mineralised bodies

The main body Cu-Au mineralisation occurs in a single south-plunging shoot which in some areas has a lower grade "interlens" zone (O'Brien, 2016). A new body of mineralisation (Ernie Junior) with a similar plunge has recently been recognised below the main Ernest Henry mineralised body (Sullivan, 2016)

### Dimensions

The Ernest Henry orebody defines a strongly cylindrical body with a down-plunge extent of at least 1.8km. At the northern (up-plunge) end of the orebody the shoot is approximately 400m wide and 200m high. Halfway down dip it is approximately 375m wide by 175m high, and it tapers to an equal width and height of approximately 150m at the southern down-plunge end of the orebody. The Ernie Junior mineralised body appears to have a length of approximately 1200m and a maximum width and height of approximately 200m (Sullivan, 2016)

### Orientation of Mineralised bodies

The main Ernest Henry orebody is semi-cylindrical and plunges approximately 40° directly to the south. The Ernie Junior body appears to have a similar orientation and lies below the main orebody (Sullivan, 2016)

### Historic Production

1.56mT Cu metal at 1.05% Cu (Ozmin database as of 2011)

2.0 mOz Ag at 0.43g/t Au (Ozmin database as of 2011)

### Recent Production

Production from 1/9/2016 to 30/9/2017 was 6.04m tonnes of ore at a grade of 1,13% Cu and 0.57g/t Au, for total production of 64,619t Cu, 83,941oz Au and 61,115oz Ag (Evolution quarterly reports)

### Resource

	Ernest Henry Resource (06/17)		
	Tonnage (mT)	Cu (%)	Au (g/t)
Measured	12.1	1.33	0.7
Indicated	68.7	1.15	0.59
Inferred	9	1.1	0.5
<b>Total</b>	<b>89.8</b>	<b>1.17</b>	<b>0.6</b>

(Evolution annual report 2017, resource as of 30/06/17)

### Reserves

Current reserves are 59.45mT of ore at 1.02% Cu and 0.5g/t Au for 607kT of Cu and 964kOz Au (Evolution annual report 2017)

### Total In-Situ Metal

Current global resource is 89.8mT of ore at 1.17% Cu and 0.6g/t Au for 1,050kT of Cu and 1,720kOz Au (Evolution annual report 2017)

## HOST ROCKS

### Mine Stratigraphy

The Ernest Henry orebody is hosted within altered intermediate metavolcanics of the Mount Fort Constantine Volcanics, along with associated carbonate and calc-silicate rocks which may be the equivalent of the Corella Formation. Ubiquitous shear zones and lack of exposure make interpretation of stratigraph-

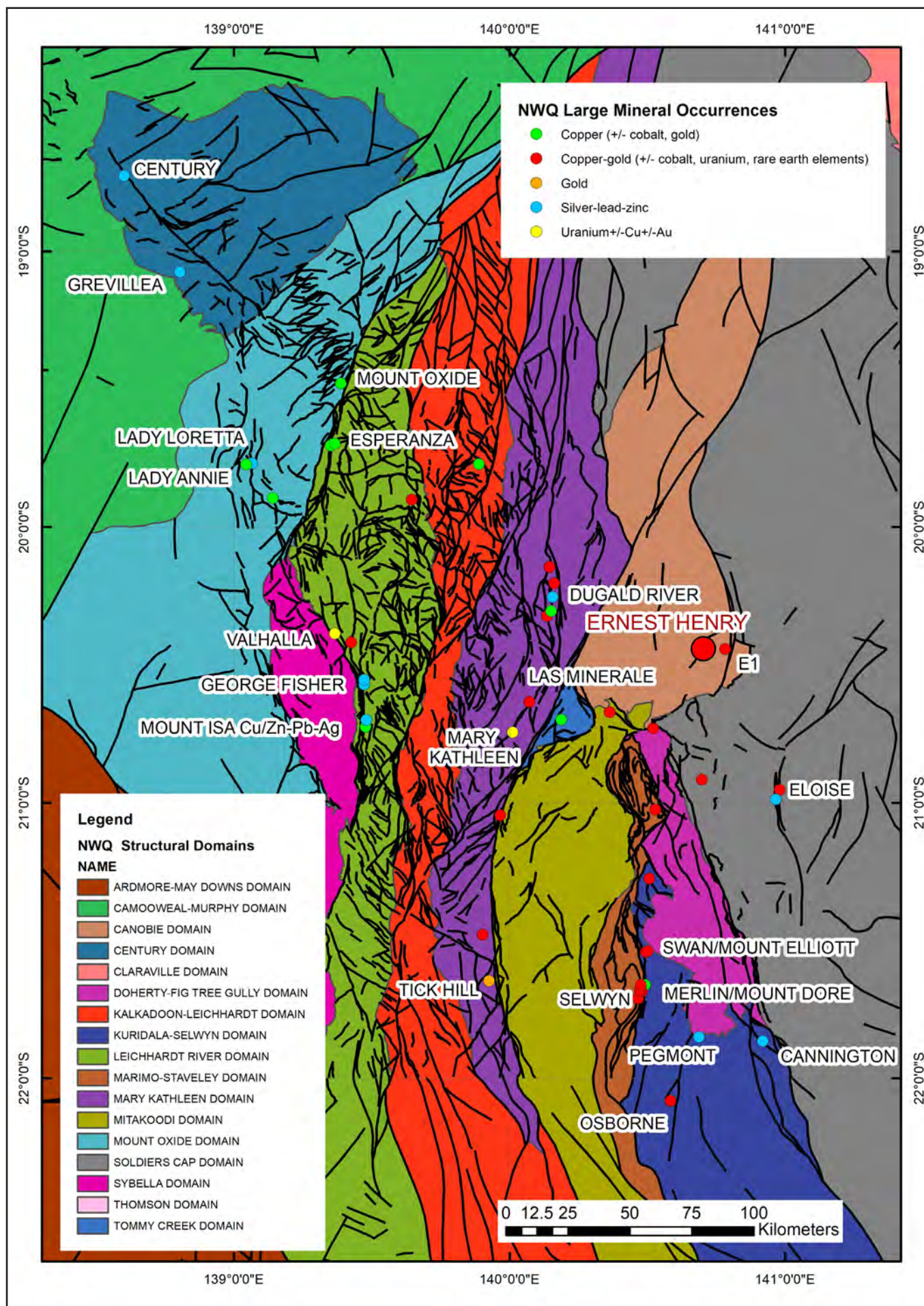


Figure 3.1. Regional location of Ernest Henry shown with respect to the Mount Isa Structural Domain Map from the 2010 NWQMEP GIS

## METAMORPHISM

### Metamorphic Grade

Regional metamorphism in the Ernest Henry area is interpreted to have reached amphibolite facies during D2 of the Isan Orogeny (Mark et al 2006)

## STRUCTURAL CHARACTERISTICS

### Structural Setting

The Ernest Henry orebody occurs within a SE-dipping sequence of altered meta-andesites bounded above and below by SE-dipping shear zones. The footwall shear zone dips to the southeast and is approximately parallel to the Cu-Au orebody. The hangingwall shear also dips to the southeast, but shows a pronounced inflection to a southwest dip in magnetic data which coincides with the position of the Ernest Henry shoot.

### Structural History

The structural history of the rocks exposed in the Ernest Henry mine and environs can be summarised as follows:

- Deposition of the Mount Fort Constantine Volcanics and associated metasediments (possible Corella formation equivalents) at approximately 1740Ma
- Emplacement of the Ernest Henry diorite bodies at approximately 1660Ma.
- NNW-SSE shortening resulting in thrusts and ENE-trending folds in rocks exposed to the south of the Mount Fort Constantine region. Some of the ENE-trending folds visible in the magnetics within the metasedimentary package to the south of Ernest Henry may be related to this event, and Mark et al (2006) recognised a layer-parallel S1 foliation at Ernest Henry.
- E-W shortening associated with the Isa D2 deformation event, which appears to have produced the NNW-trending folds recognised at E1 to the southeast of Ernest Henry (Case et al, 2017), and may be associated with the N-S trending synform recognised by Murphy et al (2017) in the hangingwall of Ernest Henry. Mark et al (2006) described the nature of S2 as a syn-peak metamorphic crenulation and penetrative fabric but did not provide details of orientation.
- Mark et al (2006) correlated the dominant fabric within the mine with regional S3, which was reported to take the form of a heterogeneous foliation and local crenulations. Foliations within the mine area are broadly parallel to the strike and dip of lithological units, showing a moderate southeast dip. The SE-dipping orientation of the shear zones temporally associated with this

ic relationships difficult

### Major Host Rock

The main host rock is a variably altered plagioclase-phyric meta-andesitic rock interpreted to be the equivalent of the Mount Fort Constantine Volcanics (approx 1740Ma; Page and Sun 1998) which are exposed 10km to the southwest of the deposit (Mark et al 2006)

### Minor Host Rock

Intercalated metasedimentary units include (Mark et al 2006):

- biotite-and muscovite-rich schist;
- biotite psammite;
- graphitic (andalusite) schist;
- banded scapolitic calc-silicate rock; and
- cordierite-muscovite schist

A distinctive "marble matrix breccia" zone underlies the main mineralised body and may either be entirely hydrothermal or include a component of primary marble (Mark et al

2006)

## INTRUSIVE ROCKS IN REGION

### Granitoids

A large body of metadiorite occurs immediately to the southwest of Ernest Henry and structurally overlies the shoot in cross section. The diorite is dated at approximately 1660Ma (Mark et al, 2006; Pollard and McNaughton, 1997)

Magnetic interpretation and drilling also show the existence younger granites likely to be the time equivalent of the Narku and Mount Margaret batholiths which cover an age range from 1530Ma to 1500Ma (Mark et al, 2006)

### Mafic Intrusives

n/a

### Other

n/a

Figure 3.2. Regional location of Ernest Henry overlain on an image of total magnetic intensity from the GADDS data for the region

foliation suggests a temporal association with the Isan D4 deformation and its associated NW-SE shortening.

- Late NW and NE-trending faults which overprint these features are visible in aeromagnetic images.

### Major Structural Styles

The host sequence to Ernest Henry is strongly deformed, with most rocks showing moderate to intense foliation development. Alteration and mineralisation is associated with hydrothermal veining and brecciation.

### Nature and Orientation of Controlling Structure

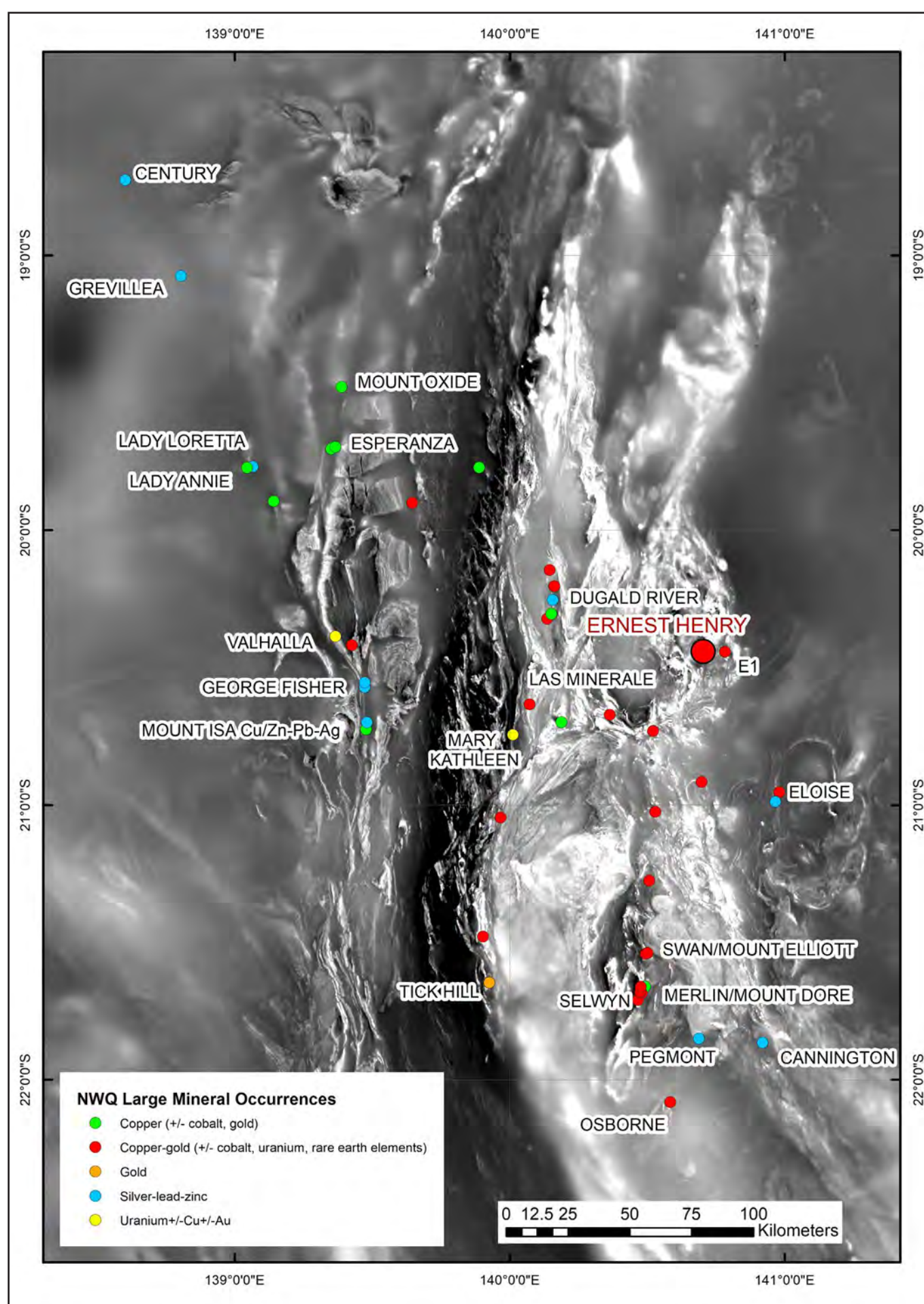
The Ernest Henry plunges directly south within a southeast-dipping series of shear zones which form the upper and lower bounds to the orebody, as well as cutting through a less-mineralised "interlens zone" (O'Brien, 2016). The Ernest Henry shoot is generally portrayed in a section parallel to the plunge of the orebody, and in this section the body is clearly bounded by a footwall shear zone which contains a mixture altered metavolcanics and carbonate-bearing marble matrix breccia and by a hangingwall shear zone which broadly marks the boundary between the metavolcanic package below and a package of intensely albitised rocks and metasediments above. What is less clear is the nature of the structure which forms the control that imposes the extreme pipe-like geometry of the orebody. This has variably been attributed to:

- Flexures in the shear fabrics of the hangingwall, footwall and intervening structures (Coward, 2001) leading to localised dilation.
- The intersection between the dipping package of shear zones and rock packages with a group of steep north-trending faults (Austin et al, 2017)
- The presence of a minor south-plunging synclinal axis in rocks above the orebody which is spatially coincident with the plunge of the orebody, with mineralisation localised on the west limb of the synform and interpreted to have formed subsequent to folding (Murphy et al, 2017).

### WALLROCK ALTERATION

#### General Characteristics

Ernest Henry occurs in a district with pervasive hydrothermal alteration, in which there are very few examples of unaltered rock encountered in drillholes. The orebody is hosted in mafic to intermediate volcanics of the Mount Fort Constantine Volcanics, and there is a protracted history of regional pre-mineralisation and syn-metamorphic Na-Ca alteration which is overprinted by post-peak metamorphic mineralisation and inner alteration (Mark et al 2006)



#### Inner (Ore) Zone

Syn-ore K-feldspar alteration proximal to mineralisation takes the form of K-(Ba) feldspar with variably abundant quartz and calcite veins, with mineralisation itself taking the form of clast- to matrix-supported breccias with magnetite, pyrite, calcite, biotite, K-(Ba) feldspar, chalcopyrite, barite, molybdenite, arsenopyrite, quartz, electrum, garnet, amphibole, rutile, sphalerite, galena, coffinite, and monazite (Mark et al, 2006).

#### Outer Zone

Alteration at Ernest Henry occurs within a regional envelope of Na-Ca alteration which affects the Mount Fort Constantine Volcanics and surrounding lithologies, as described by Mark et al (2006). This alteration takes the albitisation, minor scapolite and diopside alteration, with minerals including actinolite, tremolite, titanite, diopside, albite, scapolite, calcite, apatite, magnetite, pyrite and quartz. This alteration is evident in the occurrence of regionally extensive zones of elevated magnetic response in the Mount Fort Constantine

Volcanics to the northeast and southwest of Ernest Henry. K-feldspar alteration is also extensive, with biotite-magnetite +/- garnet alteration occurring in volcanic rocks (Mark et al, 2006). Geochemical data suggest that the Potassic alteration occurs in an envelope of up to 2km away from the orebody.

#### Mass/Volume Change

Rusk et al (2010) noted a higher proportion of dilation and mineralisation related to breccia infill in the upper parts of the shoot, grading downward into greater proportions of replacement in the deeper parts of the shoot.

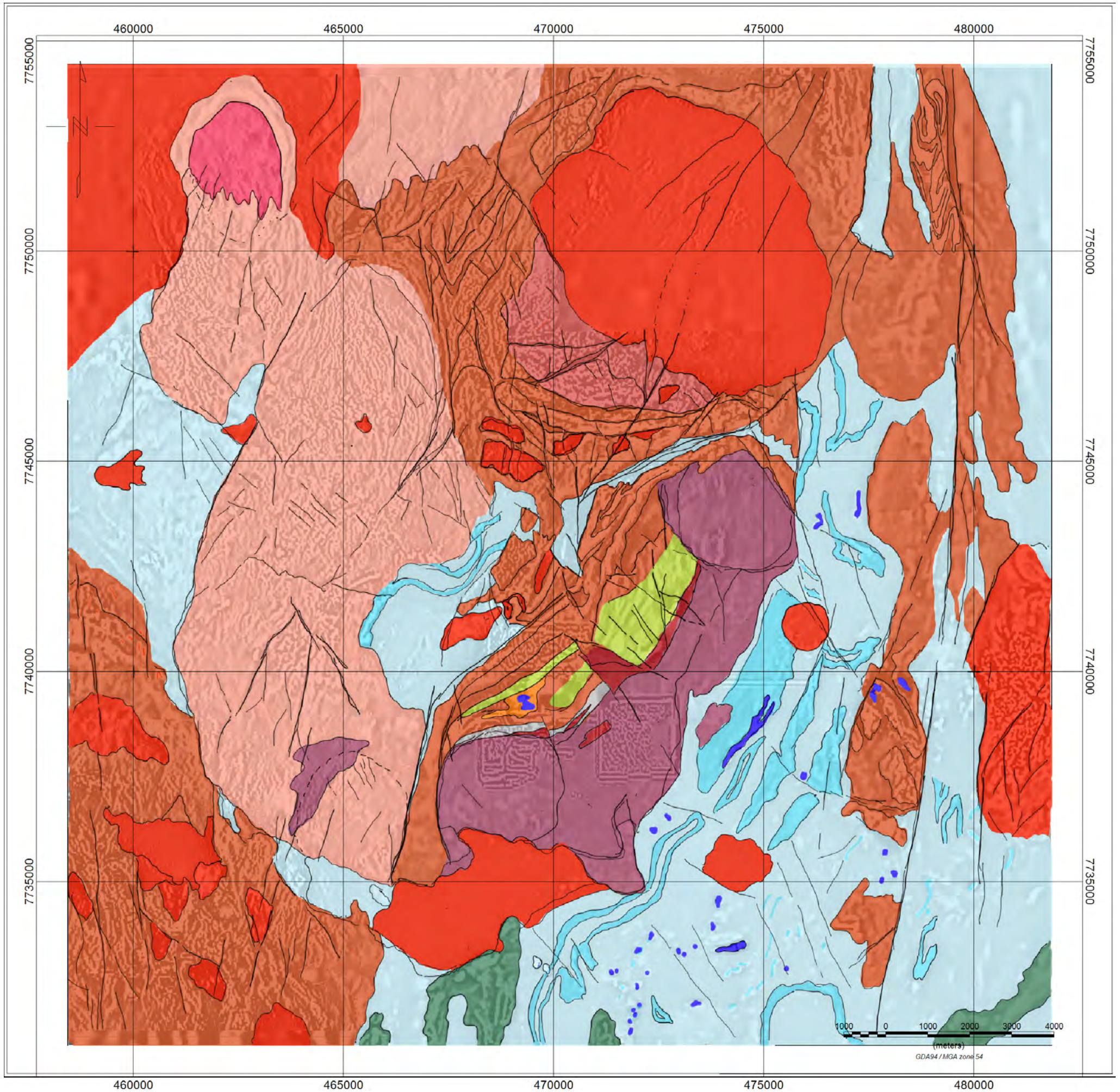
### INNER HALO

#### Extent

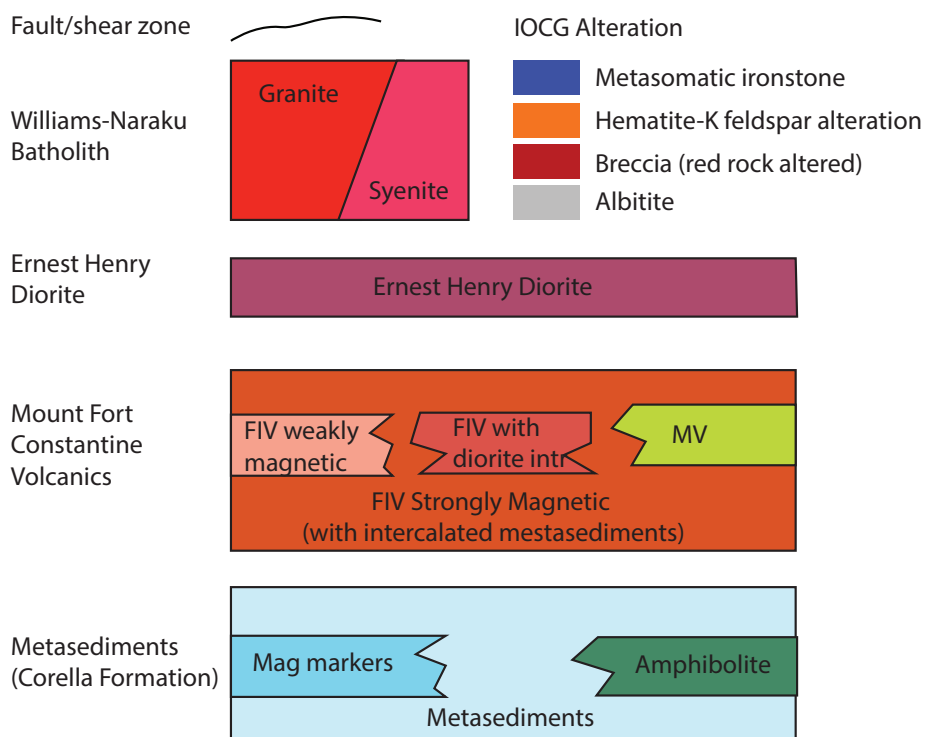
The footprint of the main Ernest Henry shoot at the unconformity at a 0.1% Cu cutoff is approximately 500m in a NW-SE direction and 350m in a NE-SW direction.

#### Geophysical Expression

- The area of the Ernest Henry orebody



LEGEND



DATA SOURCES

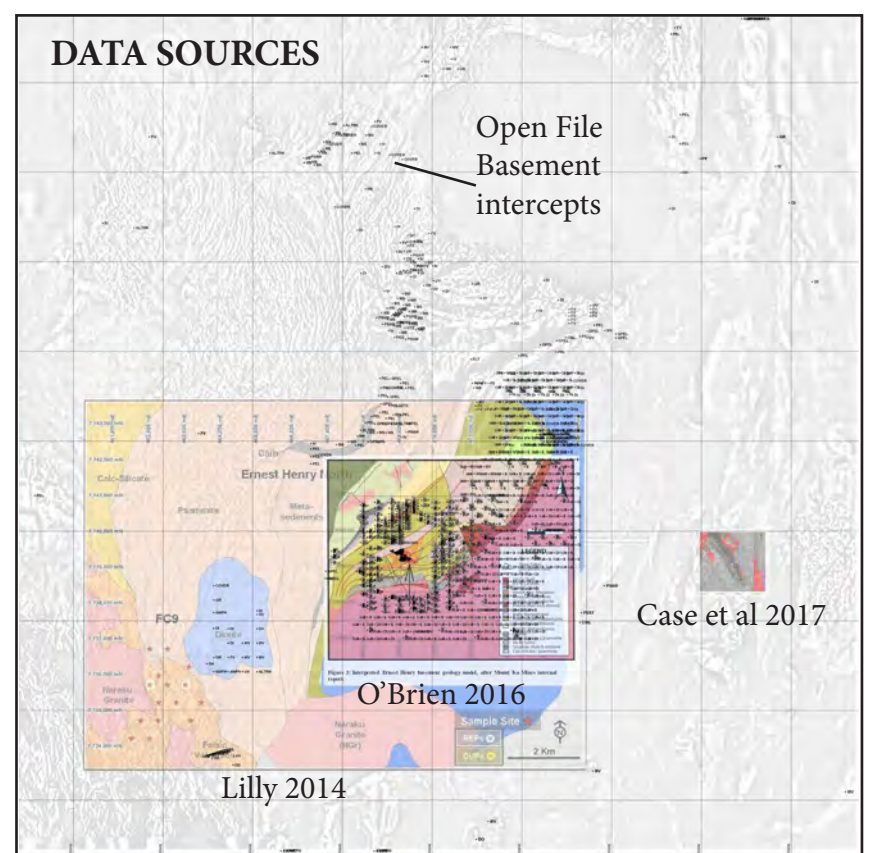


Figure 3.3. (Facing page) Geological interpretation map based on merged open file 50m-spaced aeromagnetic surveys, lithologies from open file drill data, and published maps from the Ernest Henry (Lilly, 2014; O'Brien, 2016) and E1 areas (Case et al, 2017). Map Projection GDA94, MGA54.

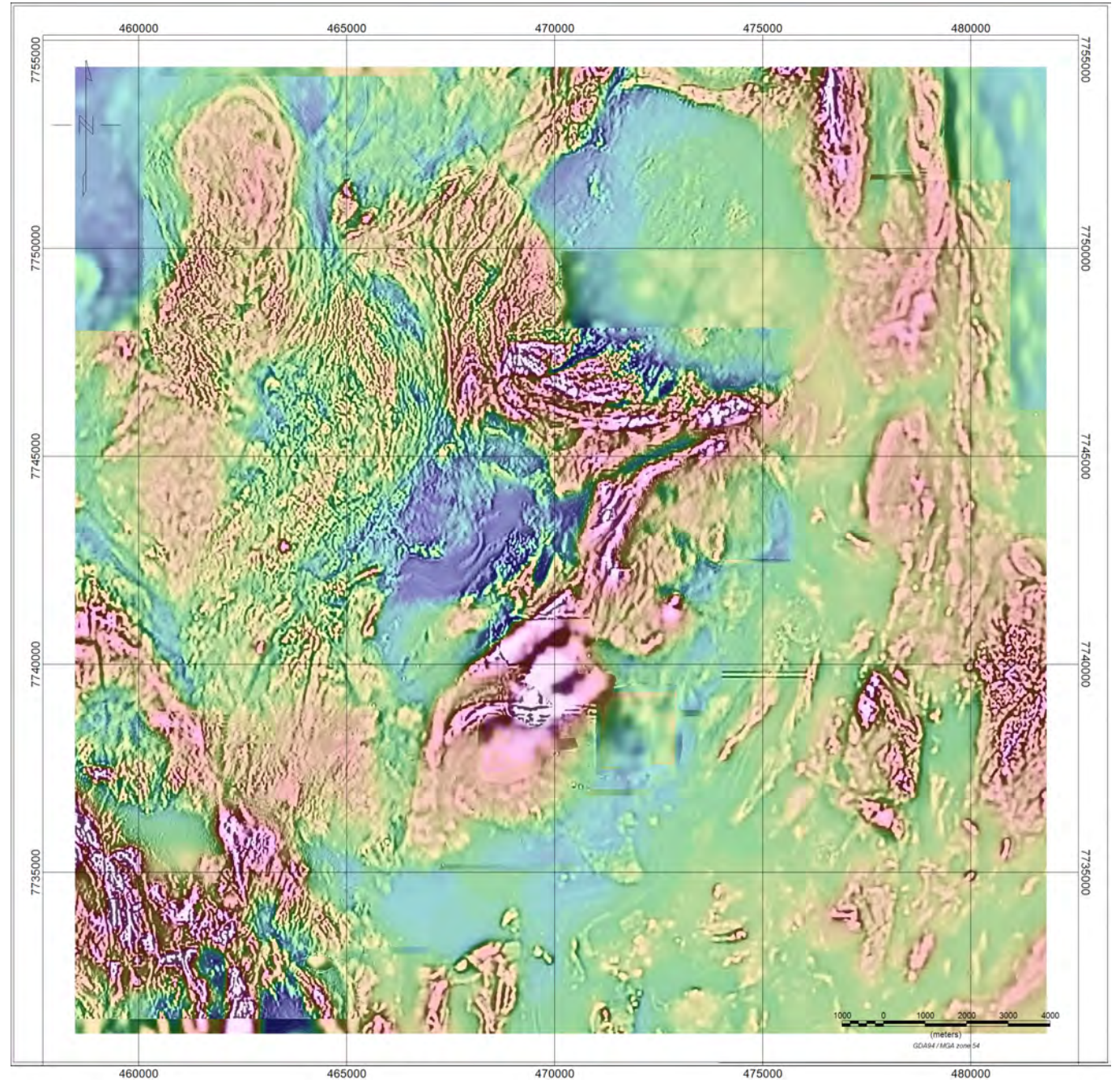


Figure 3.4. Composite aeromagnetic image merging 200m-spaced and 50m-spaced surveys over the area surrounding Ernest Henry - colour Reduced to the Pole magnetics with gaussian stretch overlain on first vertical derivative of RTP. Map Projection GDA94, MGA54.

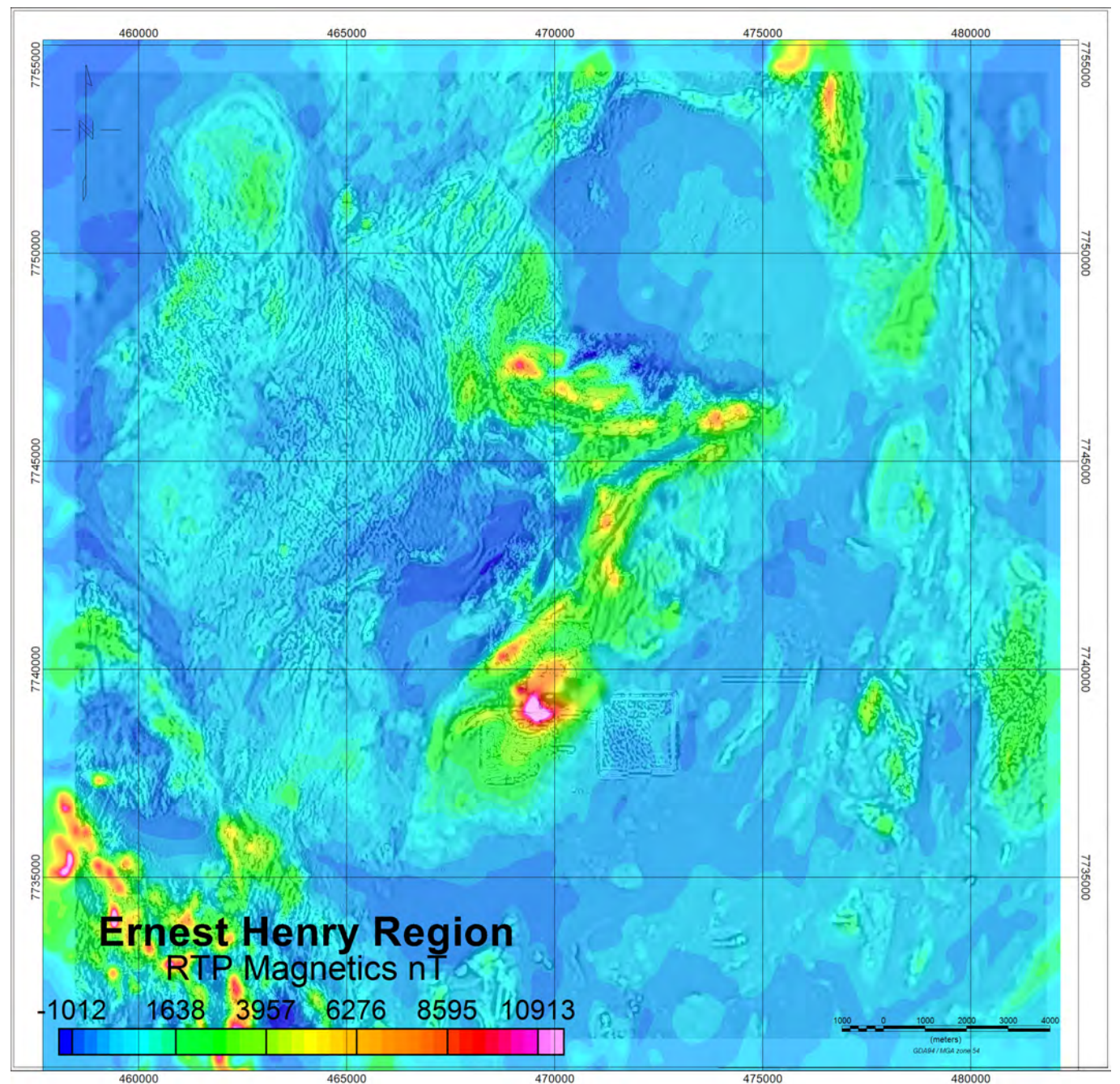


Figure 3.5. Composite aeromagnetic image merging 200m-spaced and 50m-spaced surveys over the area surrounding Ernest Henry - colour Reduced to the Pole magnetics with minimal stretch overlain on first vertical derivative of RTP. Map Projection GDA94, MGA54.

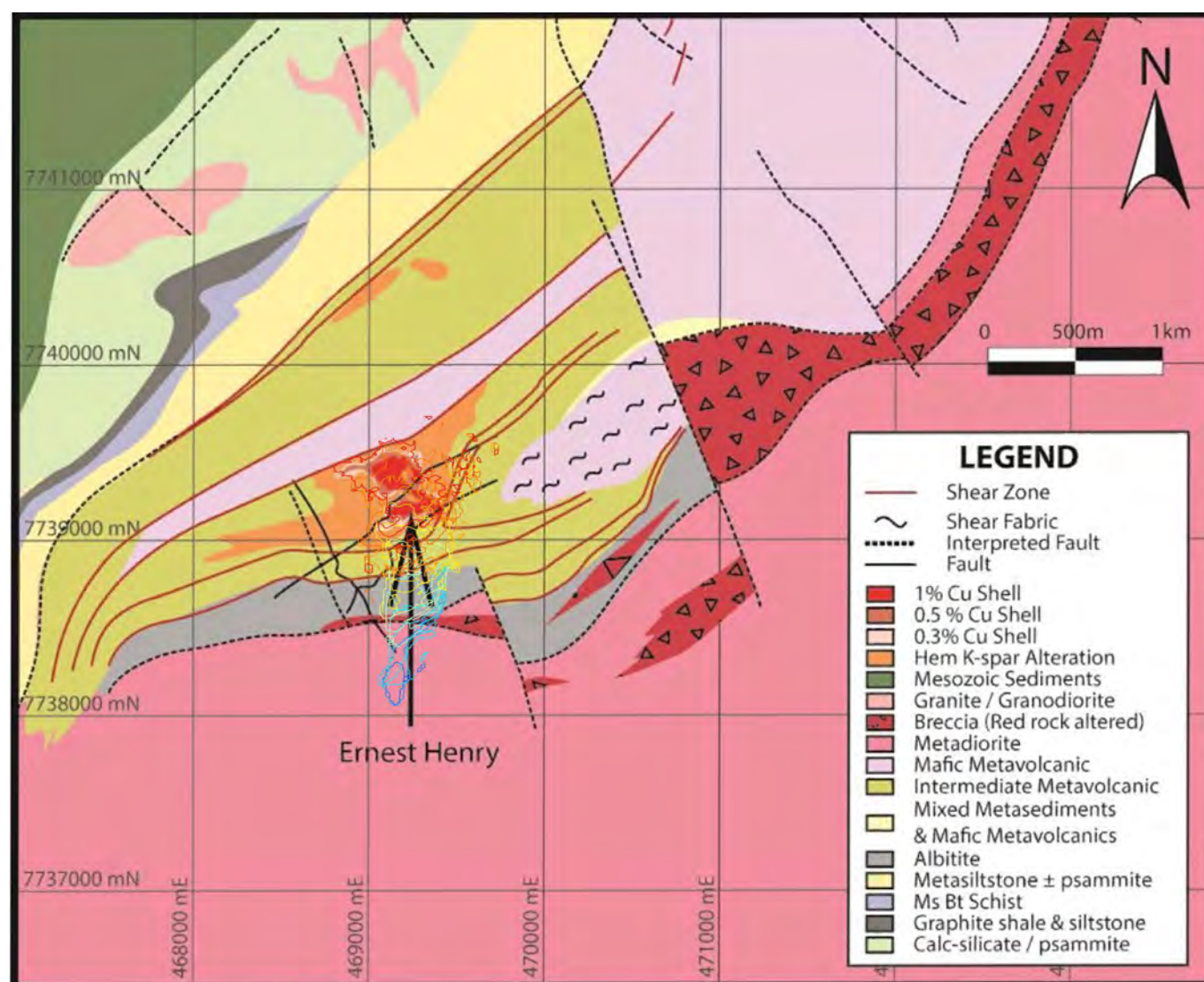


Figure 3.6. Geological interpretation map of the Ernest Henry area from O'Brien (2016) derived from company mapping and interpretation. Colour outlines extending to the south of Ernest Henry depict a series of horizontal out lines through the 0.5% Cu equivalent grade shell, and show the southward plunge of the orebody. Map Projection AGD84, AMG54.

### Exploration Geochemistry

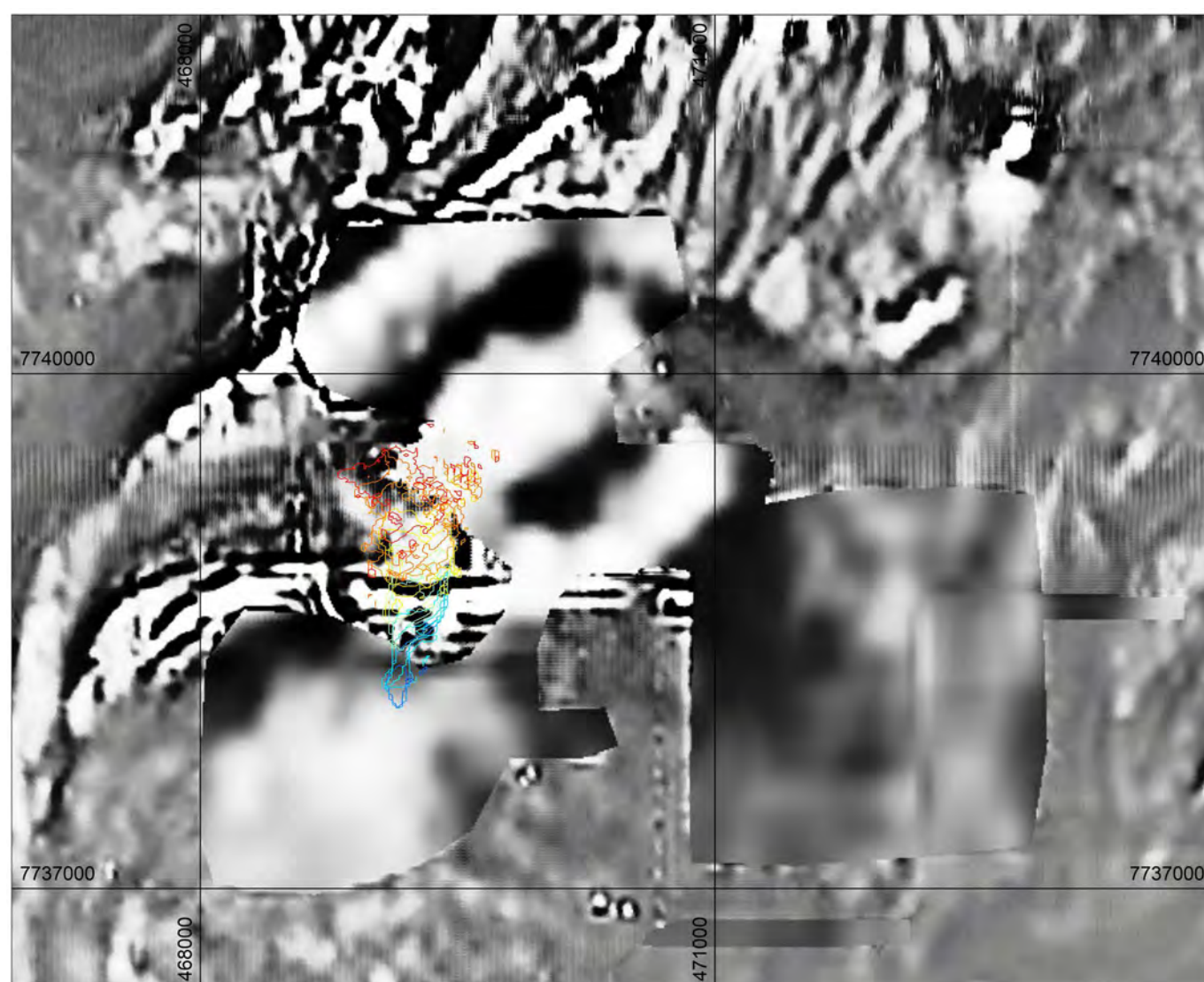
- The Ernest Henry orebody occurs under 40-50m of younger cover, comprising (Lilly and Hannan, 2016):
  - Several metres of black soil
  - Up to 20 metres of Tertiary clastic rocks
  - Up to 30 metres of Mesozoic sediments including shales and sands of the Walumbilla Formation and clastics of the Gilbert River Formation
- Geochemical expressions of the mineralisation include the following (Lilly and Hannan, 2016):
  - Cu anomalies of up to 500ppm in samples at the Proterozoic-Mesozoic unconformity
  - Anomalies of Mo, As and W of >5ppm developed in Mesozoic shales overlying the deposit
  - Ag anomalies detectable at surface in partial extraction methods such as Mobile Metal Ions (MMI)
  - Peripheral Br and Cl anomalies in Enzyme Leach surveys
- Soil gas orientation surveys showed a moderate Cu response to the south of the Ernest Henry pit, as well as anomalous responses in Ce, Co, Ga, La, and U (Lilly et al, 2014)

has an associated 7000-10000nT magnetic anomaly in ground magnetics (Webb and Rowston, 1995). However, Austin et al (2017) showed that the main contributors to this anomaly were more strongly magnetised rocks in the hangingwall and footwall to the actual deposit.

- The area of the orebody also has a 1.7mGal gravity anomaly due to the high concentration of magnetite in the orebody and associated alteration (Webb and Rowston, 1995)
- The supergene enriched part of the orebody contained chalcocite and

native copper and produced a strong ground Transient Electromagnetic (TEM) anomaly. Subsequent study showed that primary mineralisation did not produce a TEM response (Webb and Rowston 1995).

- The mineralisation also showed a discernible chargeability anomaly in dipole-dipole induced polarisation surveys, interpreted to be related to a mixture of responses relating to primary and supergene mineralisation (Webb and Rowston, 1995)



### Lithogeochemistry

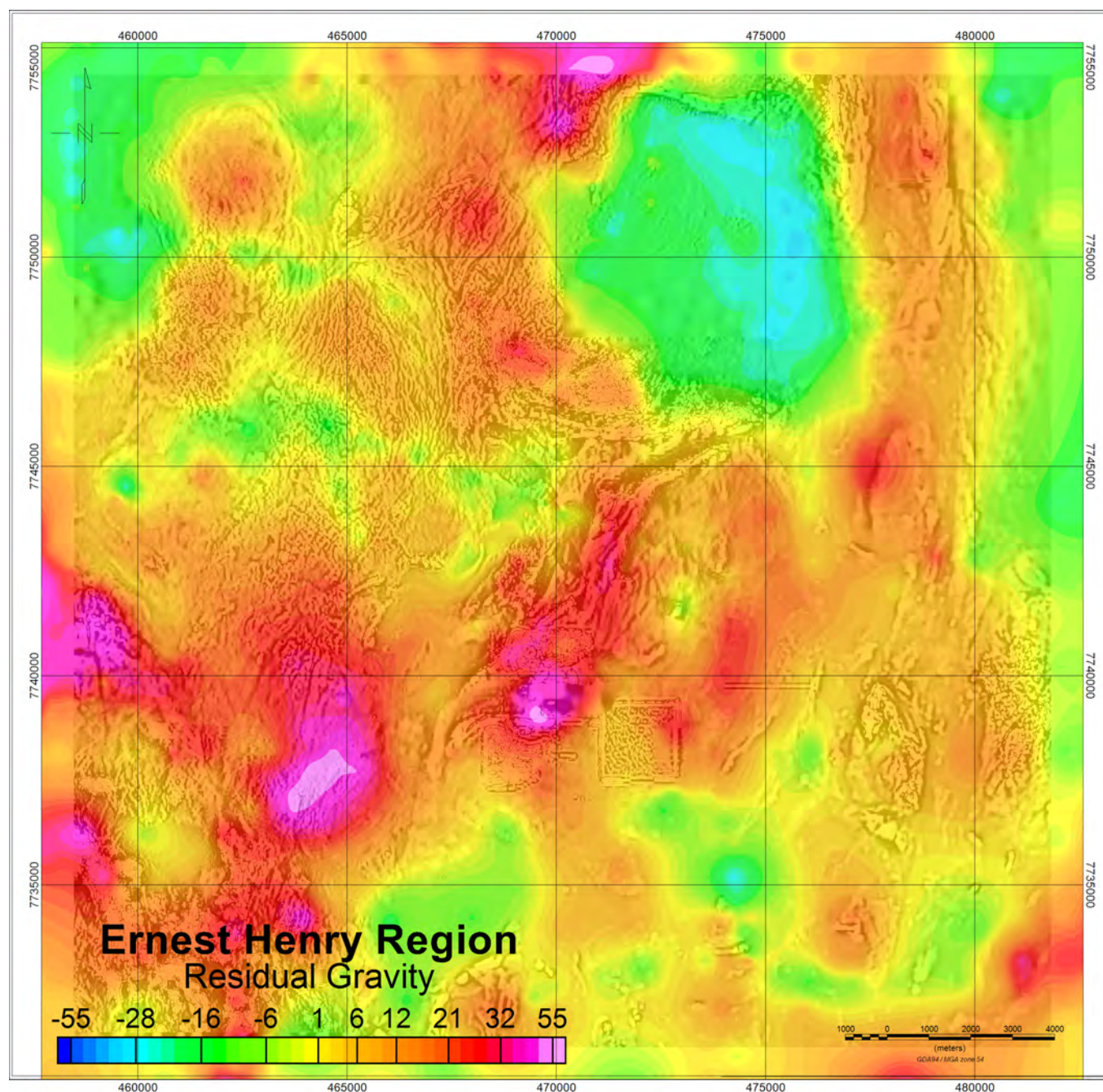
- The Ernest Henry orebody is lithologically heterogeneous, and the nature of the halo is different depending on the search direction as compared to the distribution of rock units and structures:
  - In a northeast direction (in what is most likely to be the equivalent stratigraphy to that hosting Ernest Henry) the resource and sterilisation drilling shows a zone of elevated K which extends approximately 1km to the northeast of the orebody. This signature also continues to the southwest, though the signature

Figure 3.7. Merged 50m-spaced and 200m-spaced aeromagnetic survey data near Ernest Henry, Greyscale first vertical derivative. Colour outlines extending to the south of Ernest Henry depict a series of horizontal out lines through the 0.5% Cu equivalent grade shell, and show the southward plunge of the orebody. Map Projection GDA94, MGA54.

Figure 3.8. Residual open file gravity over the Ernest Henry area, based on subtraction of a 1000m upward continuation from the infinite slab bouguer data. Map Projection GDA94, MGA54.

is less simple in this direction. Mark et al (2006) interpreted this assemblage to overprint Na-Ca alteration.

- To the southeast, in the structural hangingwall of the system, Na predominates over K, and the Na-rich signature is very extensive along strike. Fe, Mn and Co are also elevated in the sterilisation drilling to the south of the orebody in the hangingwall.
- To the northwest, in the footwall of the deposit, there is a distinctive Ca-rich zone which may correspond to the area of marble matrix breccia. Other halo elements that extend to the northwest into the footwall include Ag, U, Ba and Bi
- Analysis of zoning within the Potassic zone which extends to the northeast of Ernest Henry shows a number of elements which are elevated within 100-200m of the orebody including Cu, Mo, Co As P and Ni



### Mineralogy

- Mark et al (2006) analysed the distribution of a number of mineral assemblages associated with Ernest Henry. Notable patterns included:
  - Overlapping northeast trends of Albite (albite, titanite, quartz) and Na-Ca alteration (actinolite, tremolite, titanite, diopside, albite, scapolite, calcite, apatite magnetite, pyrite, quartz) occurring in the hangingwall of the deposit
  - A broadly N-S trending zone of K-feldspar alteration mapped as passing from the footwall into the hangingwall, with a zone of garnet-K-feldspar also defining a broadly N-S trend in the footwall
  - Mark et al (2006) also mapped a broadly N-S zone of pyrite enrichment which is broadly coincident with the zone of K-feldspar

Figure 3.9. Residual open file gravity over the Ernest Henry area, based on subtraction of a 1000m upward continuation from the infinite slab bouguer data. Shaded from the northwest with contour overlay. Yellow outline shows the position of the final Ernest Henry pit, and the black solid shows the near-unconformity expression of Ernest Henry. Map Projection GDA94, MGA54.

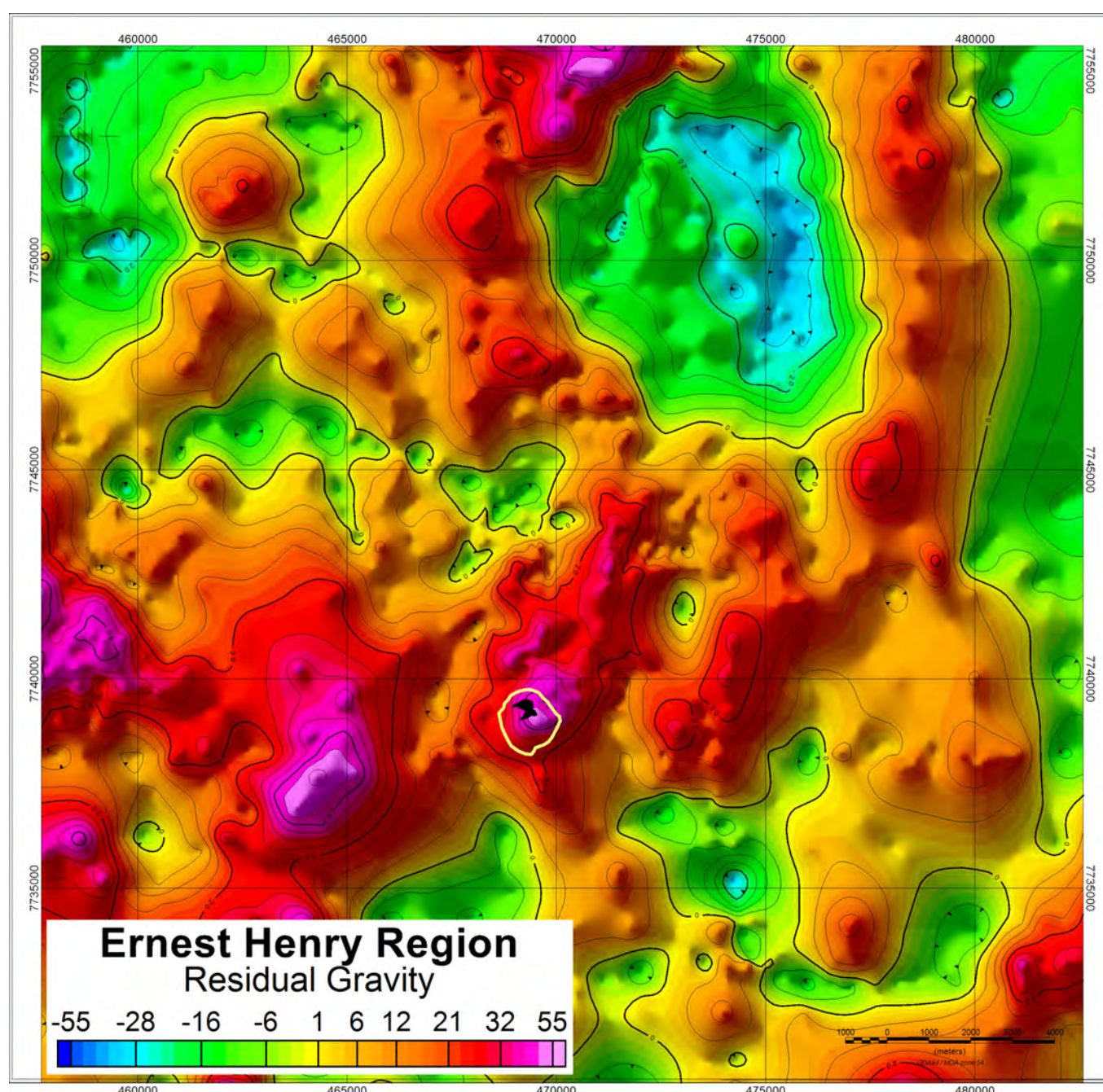


Figure 3.10. Summary of Ernest Henry rock-types (from EHM company poster.)

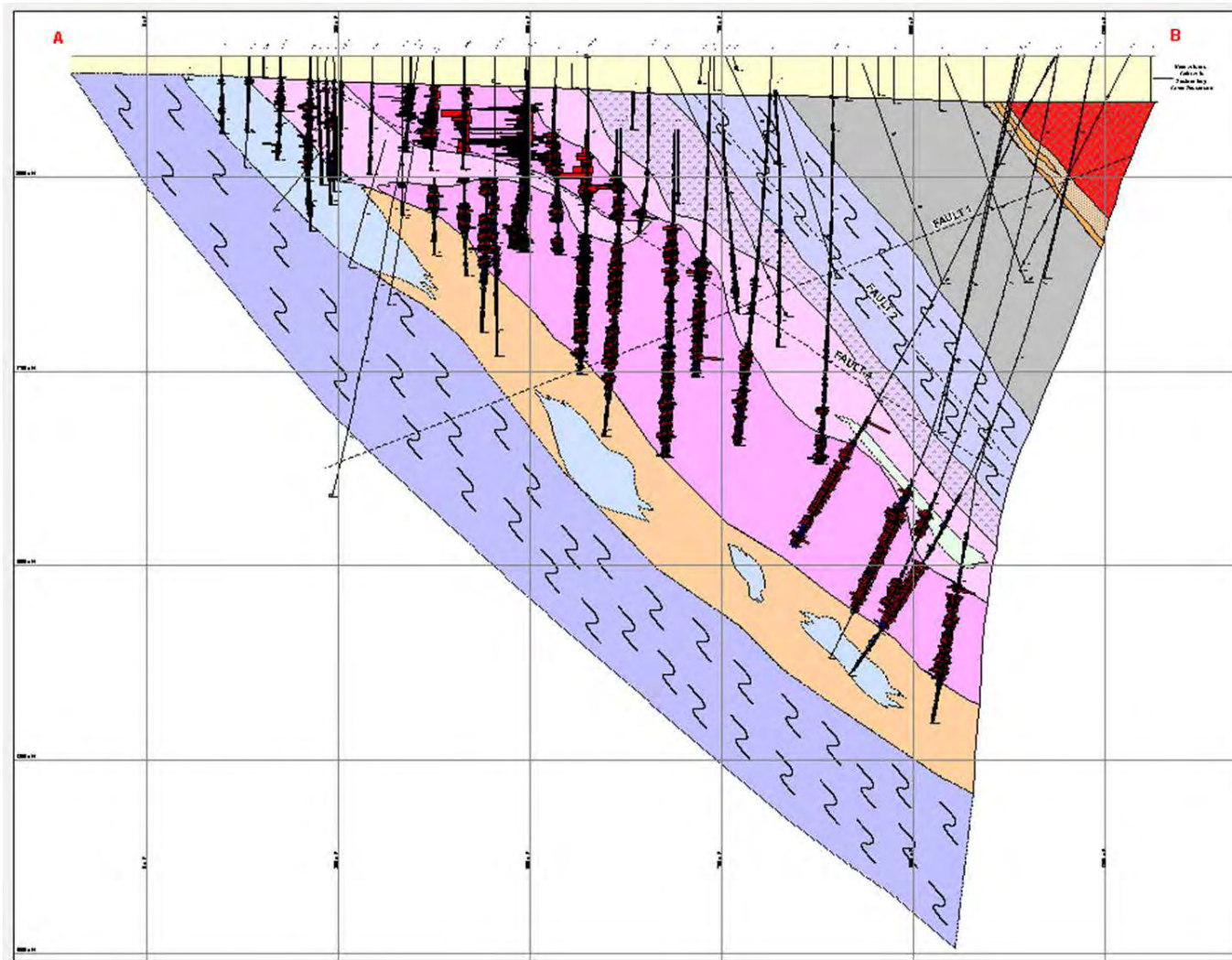
 Footwall Shear Zone (SCH3/SCH4)  
Moderately to strongly foliated mafic-intermediate meta volcanic rocks, mostly occurring as biotite-calcite schist. Rocks typically exhibit variable biotite-calcite-magnetite-actinolite +/- garnet alteration and carbonate veining



 Marble Matrix Breccia (MMB)  
Irregularly developed breccia bodies occurring between the footwall shear and the base of the ore body. The breccia comprises strongly k-feldspar altered clasts with matrix fill comprising calcite-biotite-magnetite-amphibole-pyrite. Clasts commonly exhibit biotite altered 'reaction rims'



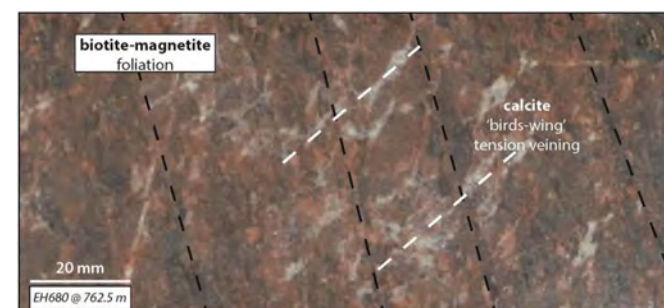
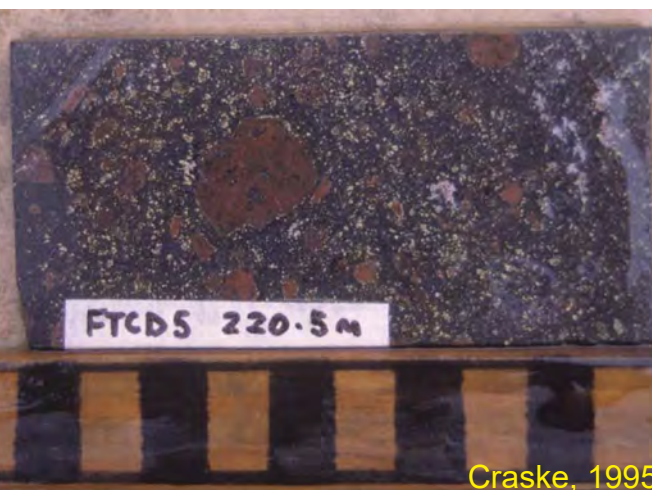
 Footwall Breccia Unit (FV-FV1)  
Variably brecciated metavolcanic rocks between the orebody and the footwall shear. Breccia textures vary from matrix and clast supported to weak crackle styles. Characteristic alt'n minerals: k-feldspar-magnetite-actinolite -garnet-chlorite +/- muscovite



 Ore Breccia (FV2)  
Matrix to clast supported hydrothermal breccia, 5-50%, 5-50mm dia subrounded breccia clasts with intense k-feldspar alteration set in matrix comprising magnetite-biotite-calcite-barite-pyrite-chalcocopyrite



 Crackle Breccia (FV-FV1)  
Variably k-feldspar magnetite-biotite altered intermediate metavolcanic rocks with variably weak to strongly developed crackle breccia textures, Breccia fill mostly comprises ragged 'birds-wing' textured calcite veins



O'Brien, 2016



**Hanging Intermediate Metavolcanic (HIV)**  
Plagioclase phyric metaandesite with variable porphyritic and amygdaloidal textures. Phenocrysts typically weakly-intensely altered to hematitic k-feldspar, ground mass moderately to strongly biotite-magnetite altered



**Hangingwall Shear Zone (SCH3/SCH4)** Moderately to strongly foliated biotite-magnetite schist, protolith comprised HIV and FGAB (shear developed at boundary). Remnant phenocrysts commonly rotated and stretched parallel to foliation. Alteration mostly biotite-magnetite-k-feldspar



**Metadiorite (DI)**  
Medium grained, equigranular, massive textured leucocratic metadiorite. Plagioclase typically strongly albitised with patchy Fe-ox staining, mafics mostly hornblende +/- biotite with selective titanite replacement



**Bt-Mt Schist/Mafic Metavolcanic (SCH3/MMV)** Moderately foliated biotite-magnetite schist as discrete unit between Hangingwall Shear and HIV. Rock is possible deformed mafic metavolcanic. Alteration comprises strong biotite-magnetite overprinted by characteristic calcite-actinolite-apatite +/- garnet



**Fine-grained Albitite (FGAB)** Typically massive fine-grained rock affected by variable Na-Ca alteration. Rock mostly grey-brown and comprises intense pervasive albitite alteration. Towards the top of the unit, grey albitite commonly overprinted by pink albitite-actinolite-titanite



**Polymict Breccia (PBX)**  
Poorly sorted clast-supported polymictic breccia which occurs at the contact with the metadiorite. Breccia typically comprises <50mm dia. subangular-subrounded Breccia dasts of albitised metaseds HIV/diorite and calc-silicate, matrix chlorite altered



**Metasiltstone (SSL) - Psammite (SAN) - Calc-Silicate (CAS)** Mixed package of metasedimentary rocks comprising meta siltstone -f-grained psammite (variably albitised) and calc-silicate. Calc-silicate rocks typically comprise albitite-scapolite-actinolite-epidote-calcite-quartz



Hydrothermal Alteration	Mineralogy (vein and alteration)	General Alteration Characteristics	Rock Types	Hydrothermal Styles	Spatial relations to Cu–Au mineralisation	Main Chemical Associations
<i>Pre-ore Sodic alteration</i>						
Albitization	albite, titanite, quartz	fine-grained albitization minor titanite, mainly present in altered diorite	diorite, siliciclastic metasedimentary rocks, plagioclase phyrlic volcanic rocks, calc-silicate rocks	pervasive fine-grained alteration, fracture-controlled breccias, veining	Present over whole area, although lack of preserved alteration in the vicinity of the orebody rare in hanging wall rocks and ore breccia clasts	Na
Na–Ca alteration	actinolite, tremolite, titanite, diopside albite, scapolite, calcite, apatite magnetite, pyrite, quartz	fine-grained albitization minor scapolite and diopside alteration minor titanite, mainly present in altered diorite	diorite, plagioclase phyrlic volcanic rocks, siliciclastic metasedimentary rocks, calc-silicate rocks	Fracture-related hydrothermal breccia, crackle veining, pervasive alteration	Pervasive throughout term lease, but overprinted by K-feldspar alteration in the vicinity of the ore breccia. Most intense hydrothermal breccias along NE trending fractures	Na, Ca
Magnetite-apatite	magnetite, apatite, actinolite, quartz calcite, quartz	massive fine- to coarse-grained magnetite alteration	plagioclase phyrlic volcanic rocks	hydrothermal veining, localized pervasive alteration	Present within NE trending fracture systems in the footwall to the deposit	Fe, P, Mg
<i>Potassic alteration</i>						
Biotite–magnetite	biotite, magnetite, K-(Ba) feldspar titanite, quartz	pervasive biotite alteration minor fine-grained K-feldspar with biotite	plagioclase phyrlic volcanic rocks, siliciclastic metasedimentary rocks	pervasive alteration, rare veining	Pervasive throughout the term lease, and affects all major rock types	K, Rb, Fe, Ba, Mn, Cl
Garnet–K-feldspar–biotite	garnet, biotite, K-feldspar, amphibole quartz, magnetite, pyrite, chalcopyrite	fine- to medium-grained biotite and garnet alteration	plagioclase phyrlic volcanic rocks, siliciclastic metasedimentary rocks	hydrothermal breccias, localized crackle veining, local pervasive alteration	Present largely in the footwall to the deposit, and occurs up to 1.5 kilometres from the orebody.	Fe, Mn, K, Ba, Cl, Cu, Co
<i>Syn-ore</i>						
K-feldspar	K-(Ba) feldspar, quartz, rutile, calcite	equigranular fine- to medium-grained K-feldspar alteration	plagioclase phyrlic volcanic rocks, siliciclastic metasedimentary rocks diorite, calc-silicate rocks	pervasive alteration of volcanic rocks, veining	Most intense in the vicinity of the orebody, although occurs as crackle veins up to 2 kilometres from the orebody	K, Rb, Ba, Cl, Cu, Co Ni, As
Sericite	sericite, quartz	pervasive fine- to medium-grained white mica alteration of K-feldspar altered volcanic rocks	plagioclase phyrlic volcanic rocks	pervasive alteration, localized crackle veining	Overprints K-feldspar altered volcanic rocks, within 400 m of the orebody	K, H
<i>Cu–Au mineralisation</i>						
Breccia	magnetite, pyrite, calcite, biotite, K-(Ba) feldspar, chalcopyrite, barite, molybdenite, arsenopyrite, quartz, electrum, garnet, amphibole, rutile sphalerite, galena, coffinite, monazite	equigranular K-feldspar alteration minor biotite alteration minor garnet and amphibole alteration in calc-silicate rocks minor arsenopyrite and pyrite alteration in siliciclastic metasedimentary rocks	plagioclase phyrlic volcanic rocks, calc-silicate rocks, siliciclastic metasedimentary rocks	infill-supported hydrothermal breccia, distal crackle veining, distal alteration	Exhibits localization from inner ore breccia to outer crackle veining Elevated Co, As and S up 150 m from ore breccia	Fe, K, Ba, S, Cu, Au, Mn, Ca, C, Sr, Co, As, Mo, Sb, U, Ag, F, Cl
Late veining	K-(Ba) feldspar, magnetite, pyrite, chalcopyrite, fluorite, molybdenite, calcite, garnet, quartz, barite, rutile	no demonstrable alteration	Stage 1 ore breccia	fracture-related veining and breccia	No demonstrable core-margin zonation within ore breccia	Fe, K, Ba, S, Cu, Au, Mn, Ca, C, Sr, Co, As, Mo, Sb, U, Ag, F, Cl

Table 3.1. Summary of Ernest Henry alteration characteristics, from Mark et al (2006)

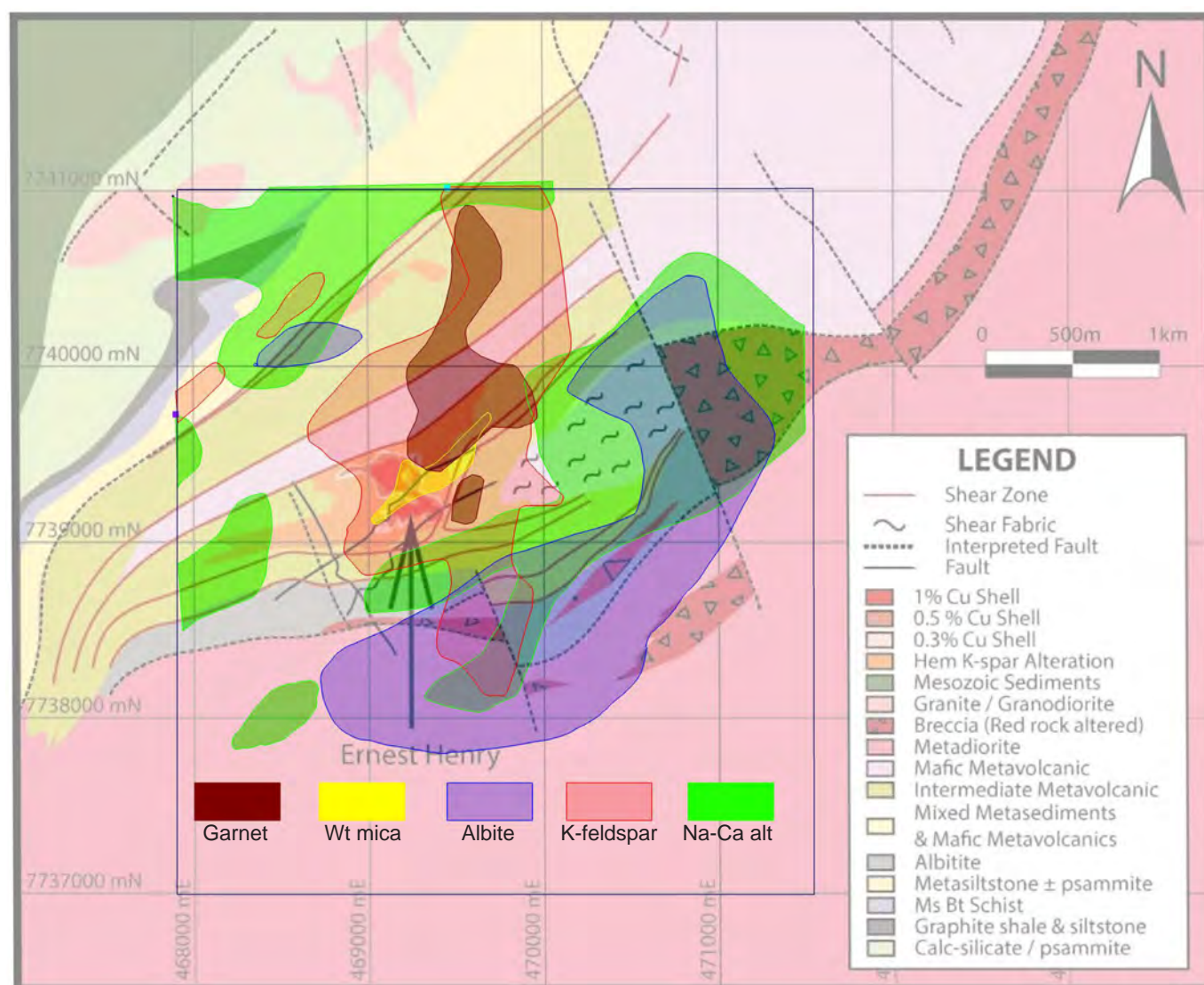


Figure 3.11. Spatial distribution of alteration suites from Mark et al (2006) overlain on the Ernest Henry geological map (O'Brien, 2016). Map Projection AGD84, AMG54.

Figure 3.12. Mineral paragenesis from Mark et al (2006). Line thickness denotes abundance.

OUTER HALO

Extent

- The widespread cover and regional extent of Na-Ca alteration make it difficult to precisely define the outer halo of the Ernest Henry system. However, the maximum extent of geochemical signatures potentially attributable to Ernest Henry (as opposed to regional Na-Ca alteration) is about 2km to the northeast and approximately 1.5km in all other directions

Geophysical Expression

- Whilst the strongest magnetic anomalies occur in association with the hangingwall shoot and footwall to Ernest Henry and are not laterally continuous, the zone of elevated magnetic signature continues for approximately 1km to the northeast.
- Mapping of a zone of elevated pyrite extending approximately 1.5km to the north of Ernest Henry and approximately 1km to the south suggests that the halo should be detectable through IP surveying
- While the strongest local gravity anomaly occurs associated with the Ernest Henry ore system, the belt of Mount Fort Constantine Volcanics extending to the northeast also defined a gravity high.
- The 100-150m, 150-200m and 200-300m depth slices of the recently released Isa East airborne EM survey highlight Ernest Henry and the surrounding region as containing conductive sources, though it is unclear whether this response is related in any way to surface infrastructure associated with the mine. The survey aircraft increased altitude to more than 400m over the pit and infrastructure.

Exploration Geochemistry

- Lilly et al (2014) also reported multi-element MMI anomalies in Cu and Mo associated with a zone 4km to the northeast of Ernest Henry, and MMI surveying over the similarly-covered E1 deposit to the southeast of Ernest Henry showed distinct MMI anomalies in Ag, Au, Cu, Co, Mo, Mn and U.

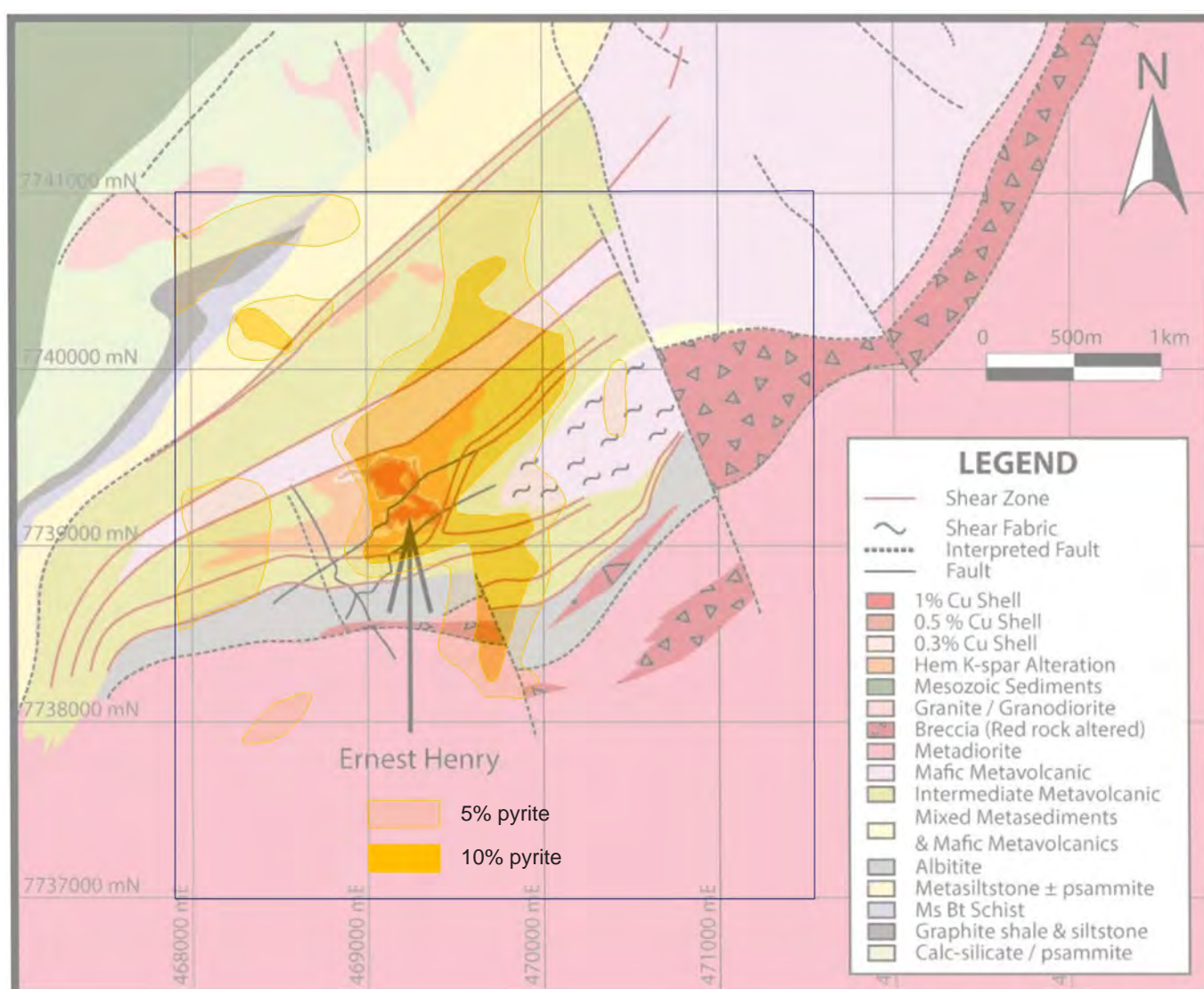
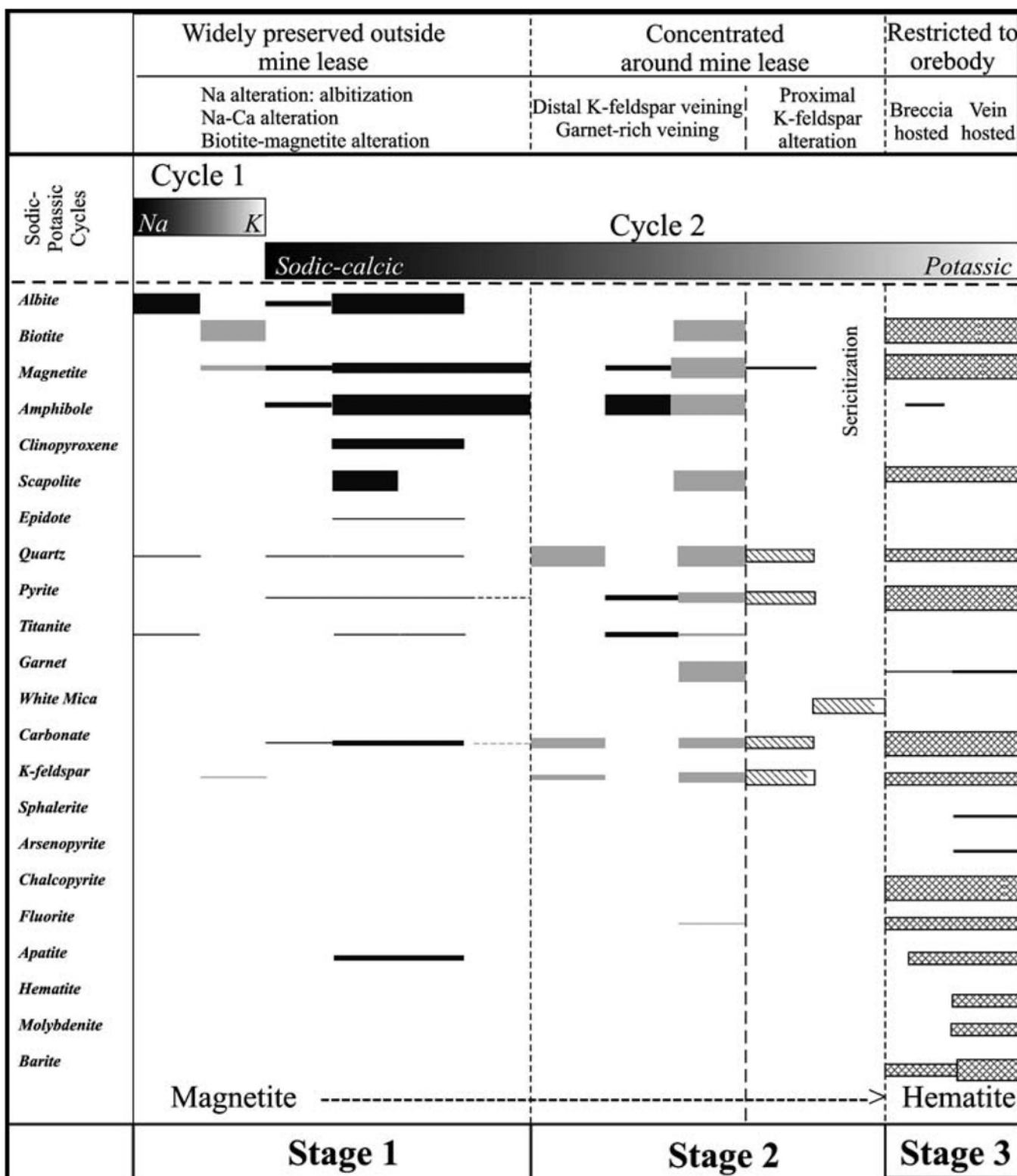


Figure 3.13. Spatial distribution of pyrite percentage from Mark et al (2006) overlain on the Ernest Henry geological map (O'Brien, 2016). Map Projection AGD84, AMG54.

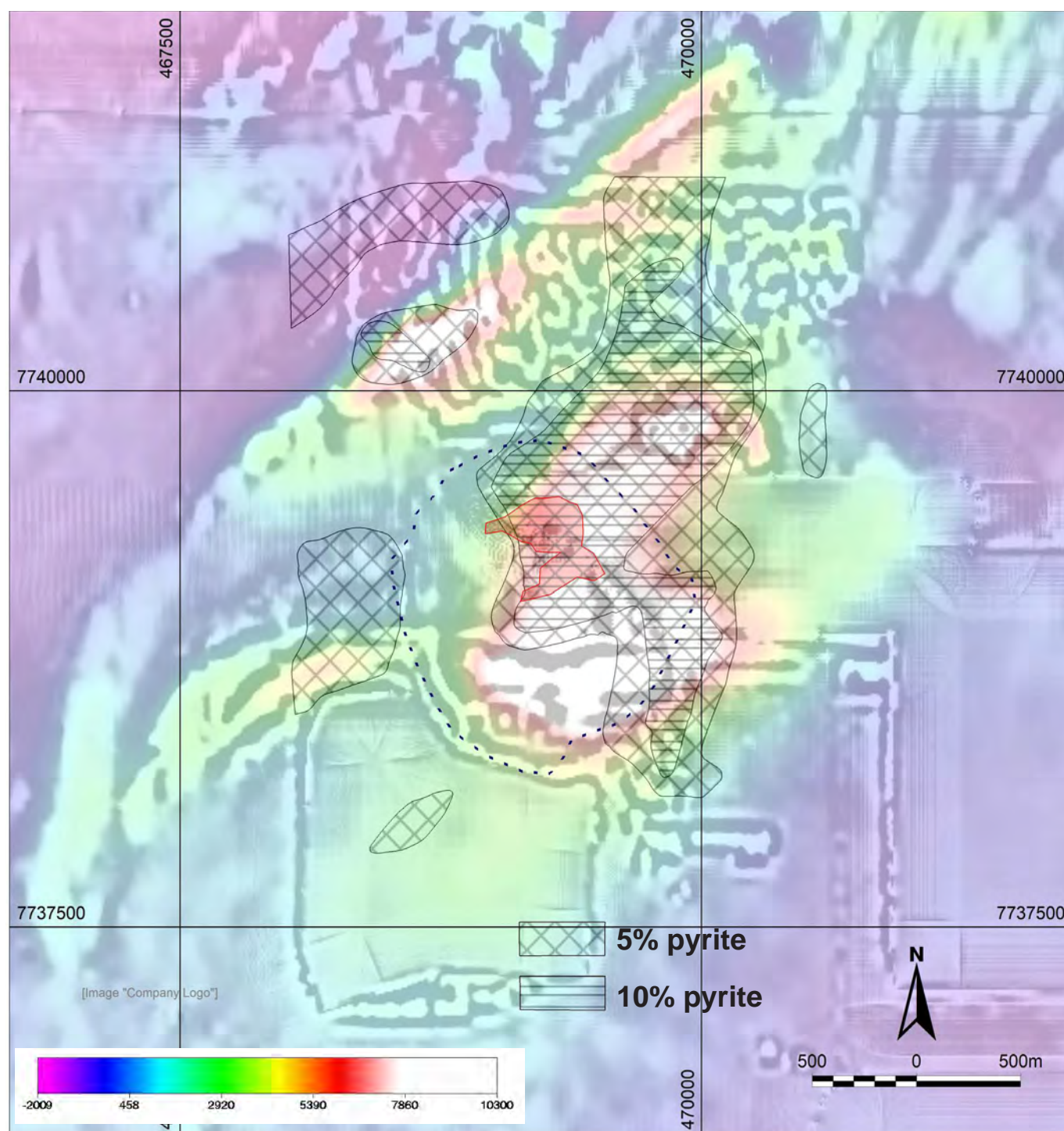


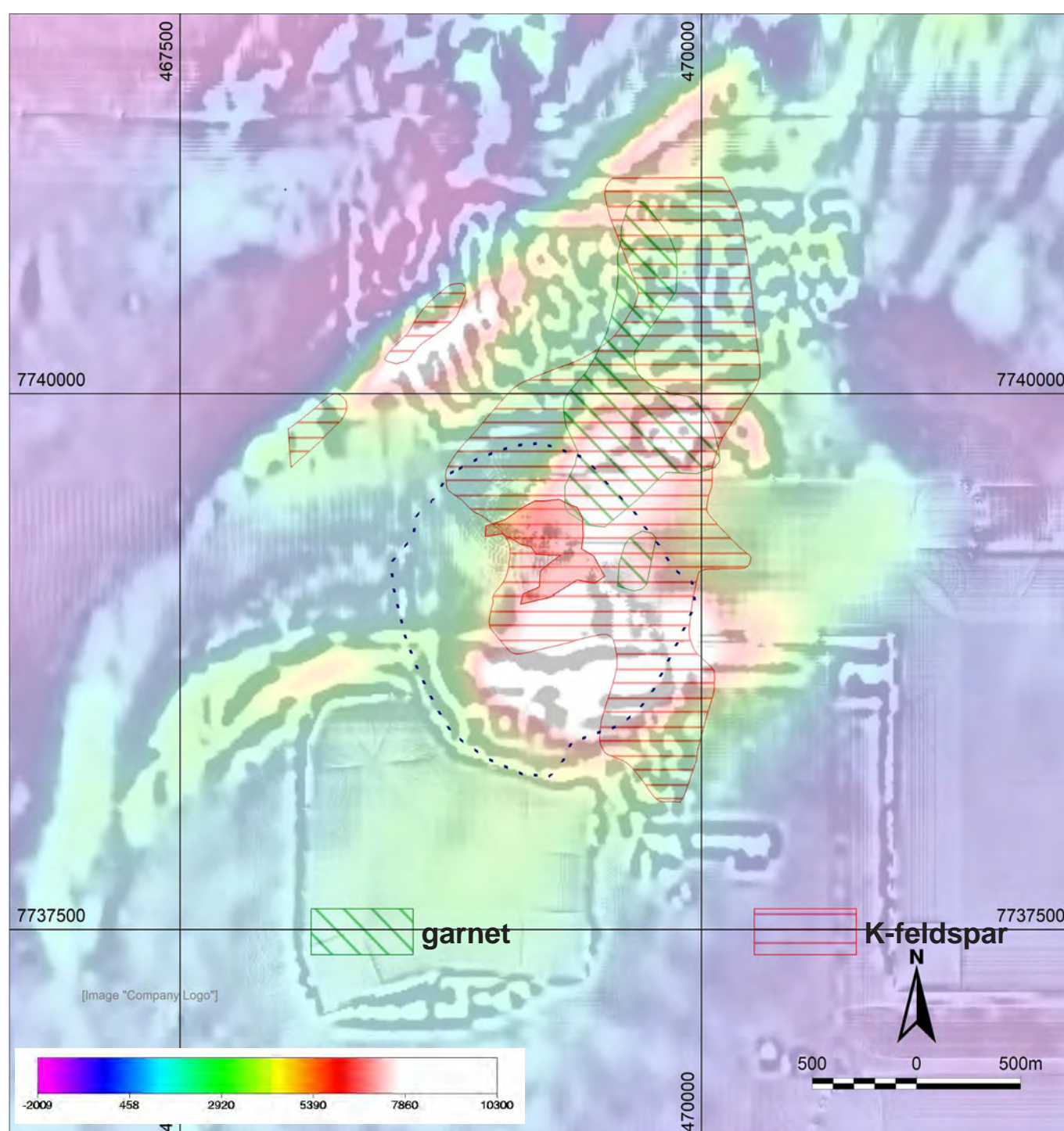
Figure 3.14. Spatial distribution of pyrite percentage from Mark et al (2006) overlain colour RTP magnetics with greyscale VD-automatic gain control image. The zone of abundant pyrite coincides with the orebody itself as well as the magnetite-enriched zone of K-feldspar alteration to the northeast of Ernest Henry, and crosses into the hangingwall on a N-S trend. Map Projection AGD84, AMG54.

### Lithogeochemistry

- Analysis of multielement drill data in the Ernest Henry region highlights the following elements as defining a broader outer halo associated with the Ernest Henry system – Bi, Ba, Fe, K and As

### Mineralogy

- Consideration of the paragenetic diagram of Mark et al (2006) suggests a number of minerals whose occurrence is diagnostic of the Ernest Henry orebody and halo as opposed to the regional Na-Ca suite. These include fluorite, barite, higher abundances of pyrite, quartz, higher abundances of carbonate, F-rich biotite and Ba-rich K-feldspar.
- Mark et al (2006) compared the composition of biotite and K-feldspar in proximal and distal settings to the orebody, and found that proximal biotites tended to be fluorine-bearing while distal biotites were low in F. In addition, K-feldspars proximal to mineralisation had up to 3% Ba, while more distal K-feldspar showed Ba less than 1%.
- Rusk et al (2010) showed that magnetites associated with Ernest Henry had relatively high Mn/Ti ratios, and that magnetites at Ernest Henry were more Mn-enriched than other hydrothermal magnetite in the region.
- Rusk et al (2010) also reported that apatite at Ernest Henry is unusually high in fluorine and arsenic compared to other apatites sampled in the region



### TIMING OF MINERALIZATION

#### Relative Timing

Mineralisation is interpreted by Mark et al (2006) to be associated with veining and brecciation which has overprinted the main foliation-forming and metamorphic event. Mineralisation is interpreted to be broadly synchronous with the intrusion of the Naraku batholith.

#### Absolute age

- Ar-Ar dating of amphibole associated with pre-mineralisation Na-Ca alter-

Figure 3.15. Spatial distribution of K-feldspar and garnet from Mark et al (2006) overlain colour RTP magnetics with greyscale VD-automatic gain control image. The zone of K-feldspar coincides with the orebody itself as well as the magnetite-enriched zone to the northeast of Ernest Henry, and crosses into the hangingwall on a N-S trend. Map Projection AGD84, AMG54.

Figure 3.16. Spatial distribution of albite and Na-Ca alteration from Mark et al (2006) overlain colour RTP magnetics with greyscale VD-automatic gain control image. Both zones define a northeast trend coinciding broadly with the strongly magnetic marker in the hangingwall of the Ernst Henry system, broadly defined as the Marshall Shear.. Map Projection AGD84, AMG54.

ation produced ages of approximately 1610Ma (Twyerould, 1997)

- U-Pb dating of titanite associated with pre-mineralisation Na-Ca vein infill produced an age of approximately 1530Ma (Mark et al, 2006), and U-Pb dating of titanite associated with pre-ore bi-mt alteration produced an age of approximately 1514Ma (Mark et al, 2006)
- Ar-Ar dating of biotite and muscovite temporally associated with mineralisation produced ages around 1500Ma (Twyerould, 1997)

### GENETIC MODEL

Ernest Henry is interpreted to be formed as the result of circulation of oxidised, saline, high-temperature Cu-bearing fluids driven by the synchronous intrusion of the Williams-Naraku batholith suite into dilatant zones of competency and redox contrast such as that represented by the footwall, hangingwall and ore sequences at Ernest Henry (eg Oliver et al, 2008; Austin et al, 2017; Murphy et al 2017)

### POST-FORMATION MODIFICATION

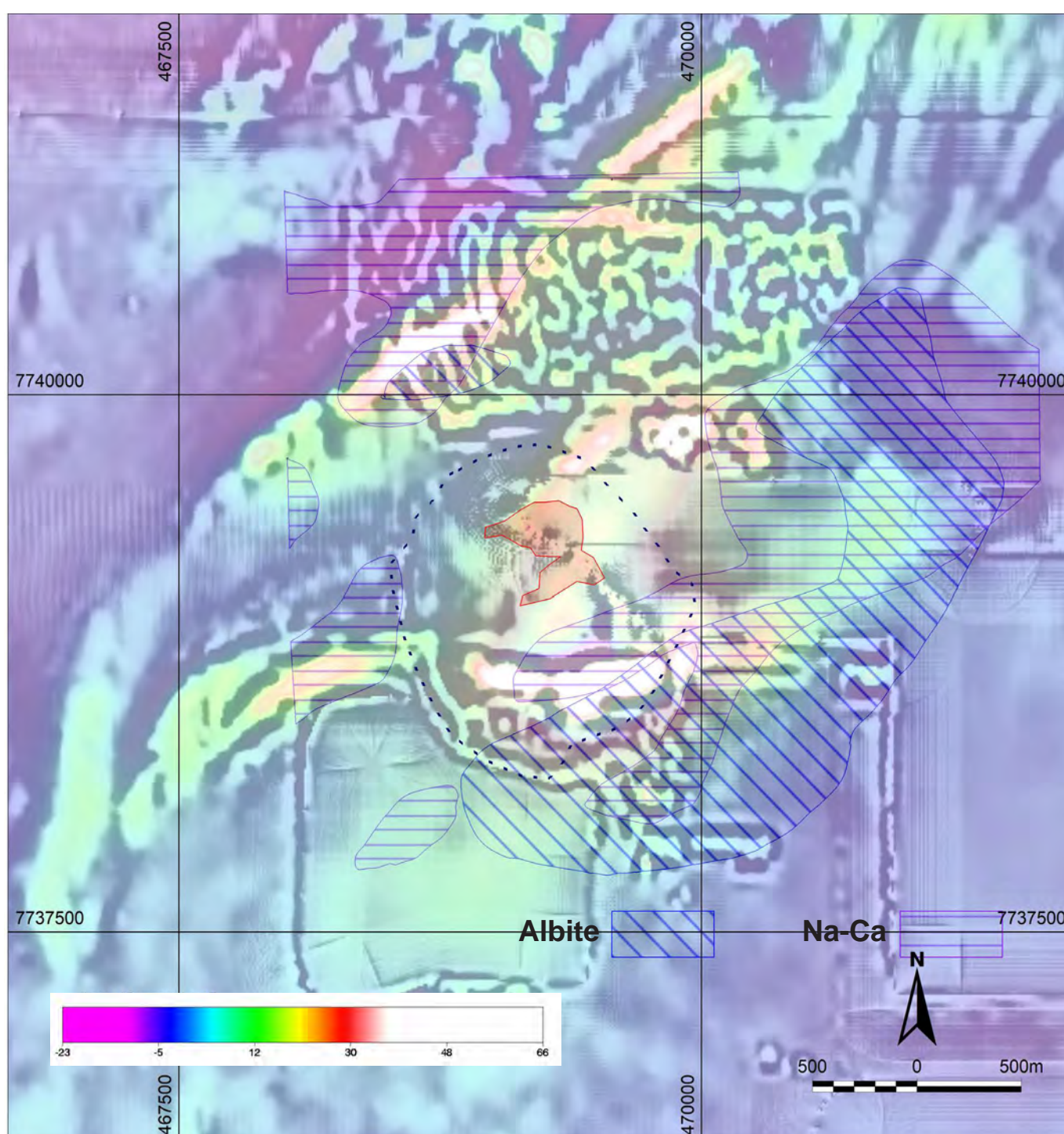
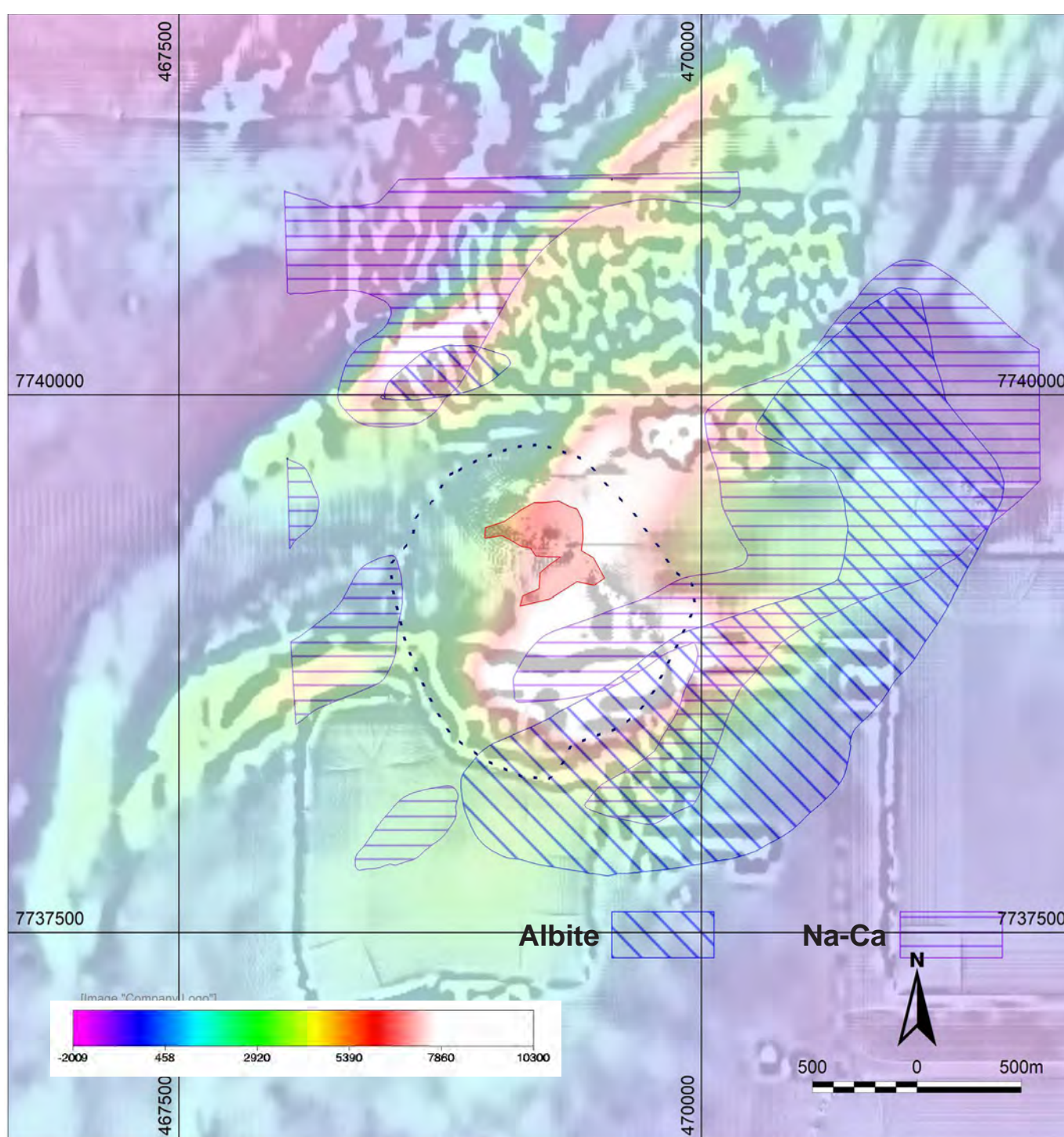
- Faulting
- Burial by Mesozoic and tertiary sediments
- Surface weathering

### EXPLORATION

#### Discovery Method

The Ernest Henry deposit was discovered on the basis of drilling of a ground TEM anomaly associated the Ernest Henry magnetic anomaly. It was discovered in October 1991 (Lilly et al 2017).

Figure 3.17. Spatial distribution of albite and Na-Ca alteration from Mark et al (2006) overlain colour first vertical derivative magnetics with greyscale VD-automatic gain control image. Both zones define a northeast trend coinciding broadly with the strongly magnetic marker in the hangingwall of the Ernst Henry system, broadly defined as the Marshall Shear.. Map Projection AGD84, AMG54.



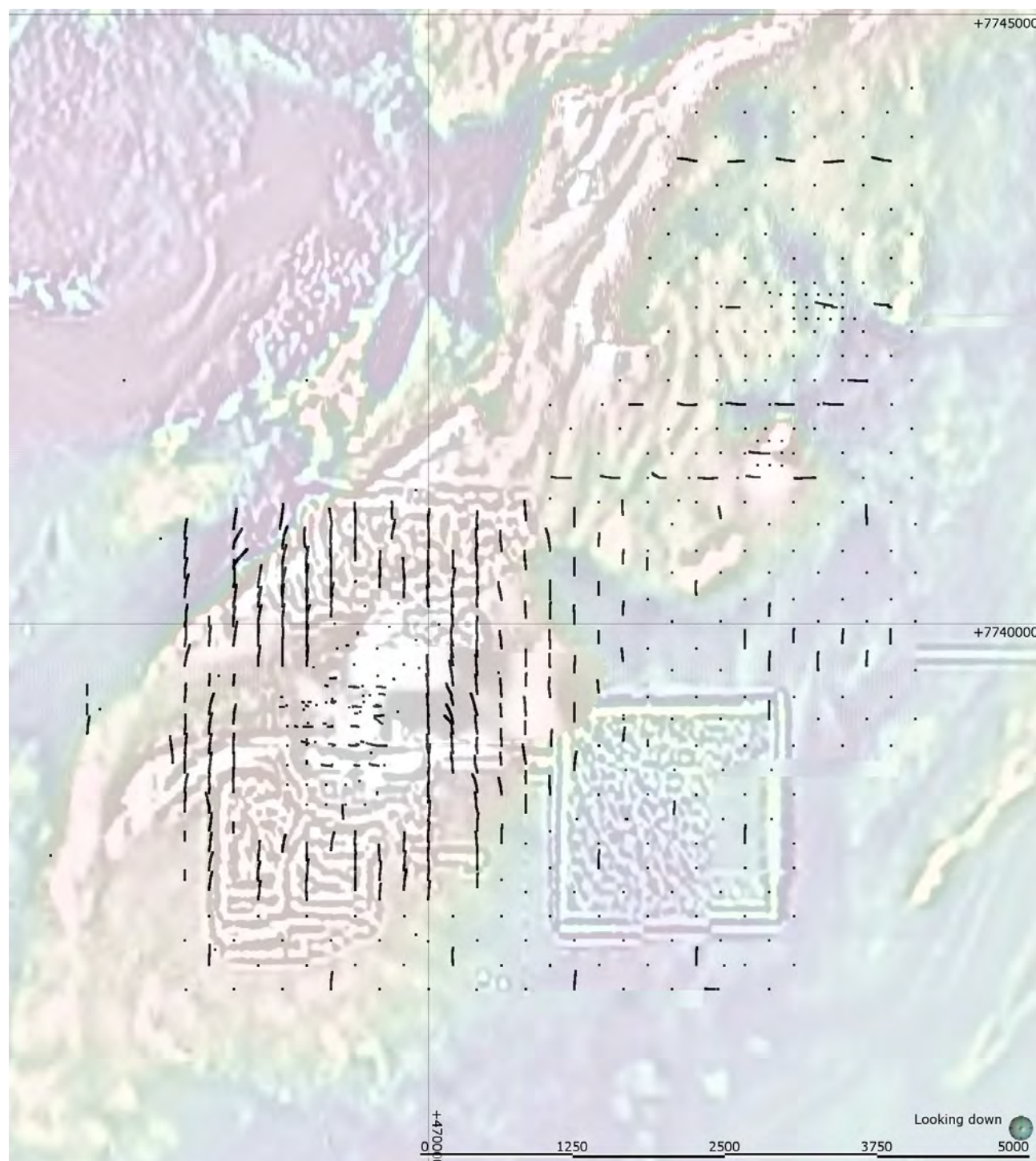


Figure 3.18. Index map showing the distribution of drillholes used in the analysis of lithogeochemical zoning associated with the Ernest Henry area. Map Projection AGD84, AMG54.

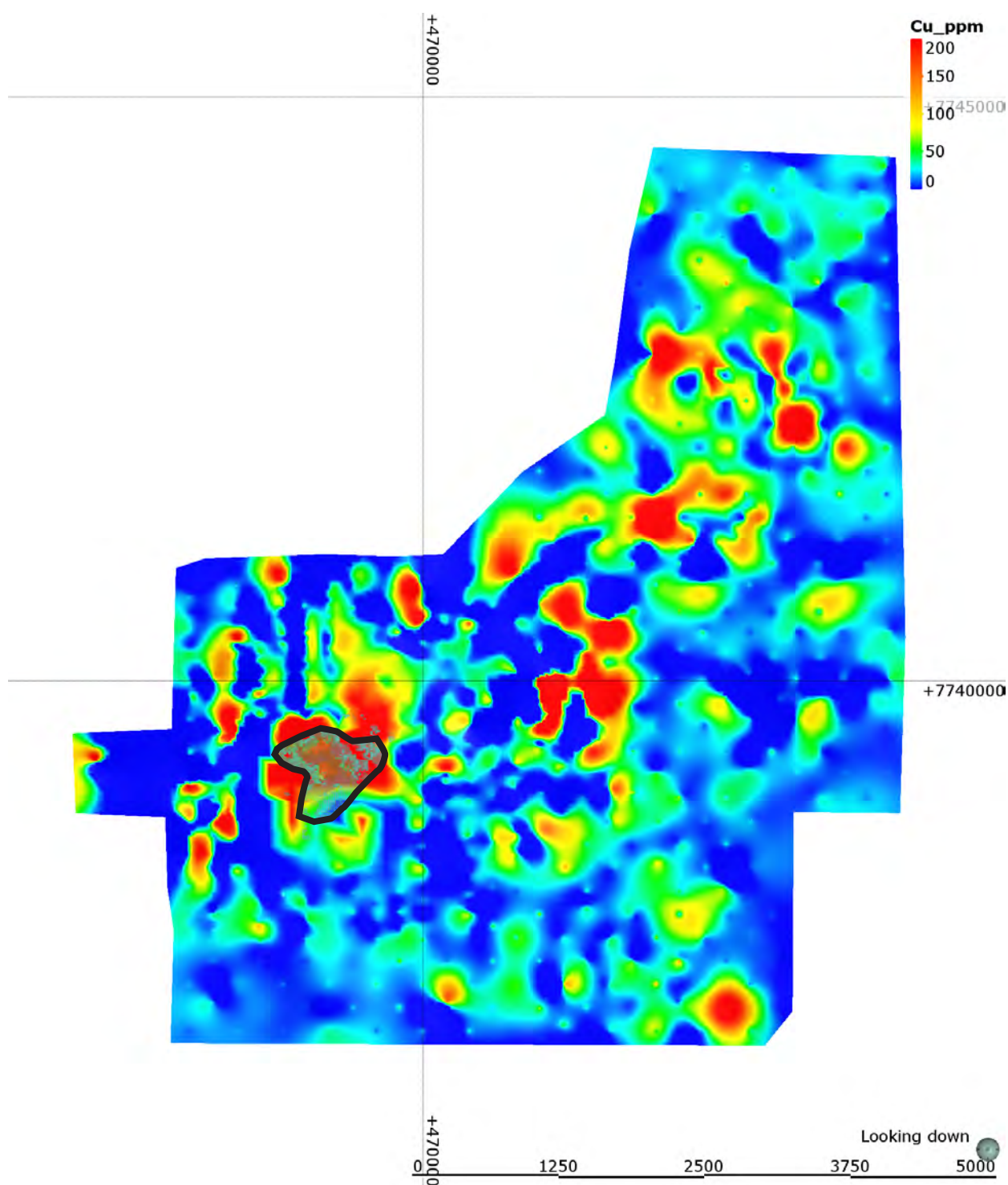


Figure 3.19. Image showing an evaluation of Cu values on the Proterozoic unconformity surface from the multi-element drill dataset, based on a non-directional Leapfrog™ linear interpolant. Solid line denotes the approximate position of the near-surface trace of the Ernest Henry ore outline. Map Projection AGD84, AMG54. Image below shows a 3D perspective view of Cu shells from Austin et al (2017), showing the southerly plunge of the orebody as well as an apparent northerly-dipping intersecting structure down plunge.

Figure 3.20. Image showing an evaluation of Co values on the Proterozoic unconformity surface from the multi-element drill dataset, based on a non-directional Leapfrog™ linear interpolant. Solid line denotes the approximate position of the near-surface trace of the Ernest Henry ore outline. Map Projection AGD84, AMG54. Image below shows a 3D perspective view of Co shells from Austin et al (2017), showing the southerly plunge of the orebody as well as an apparent northerly-dipping intersecting structure down plunge.

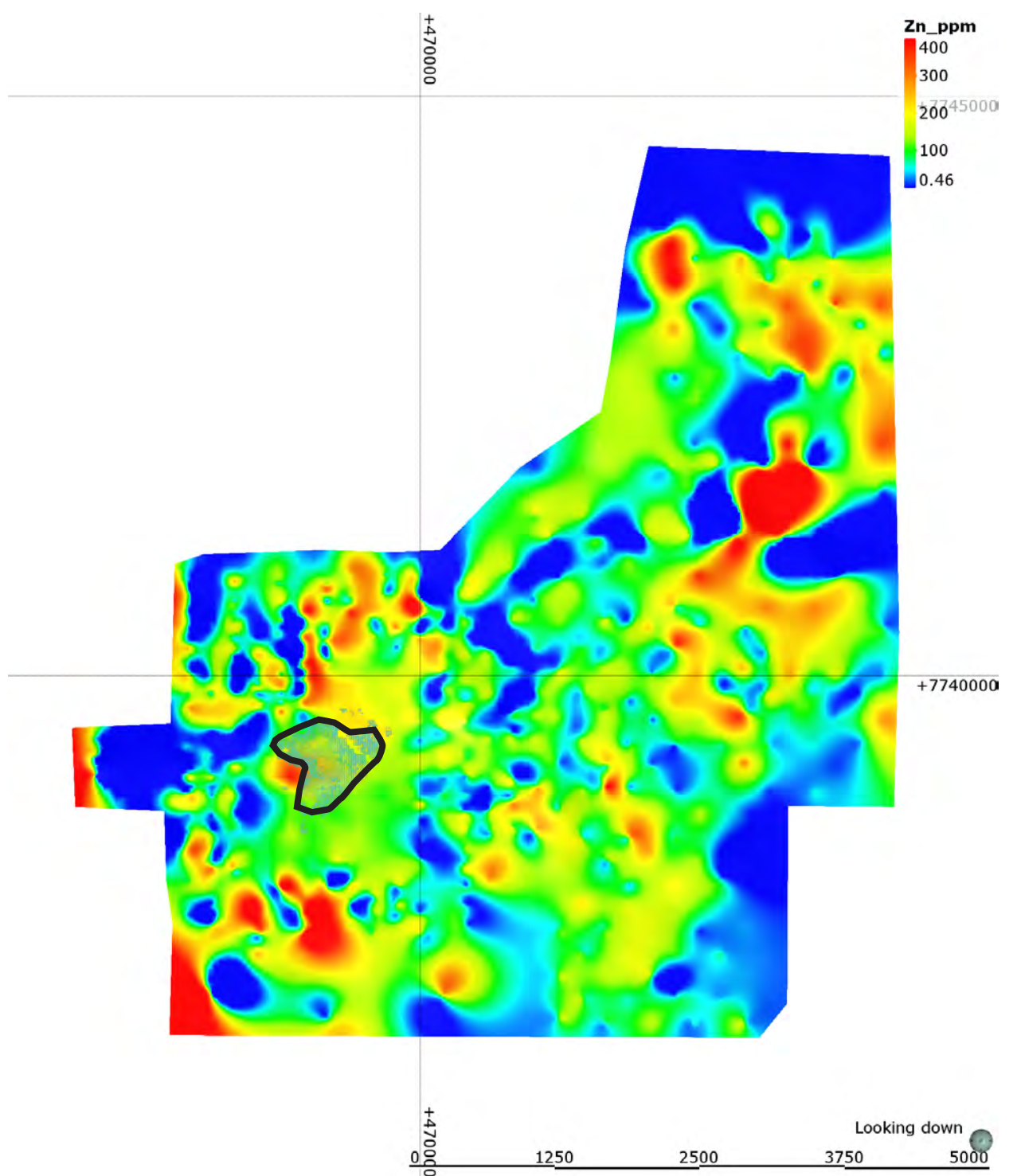
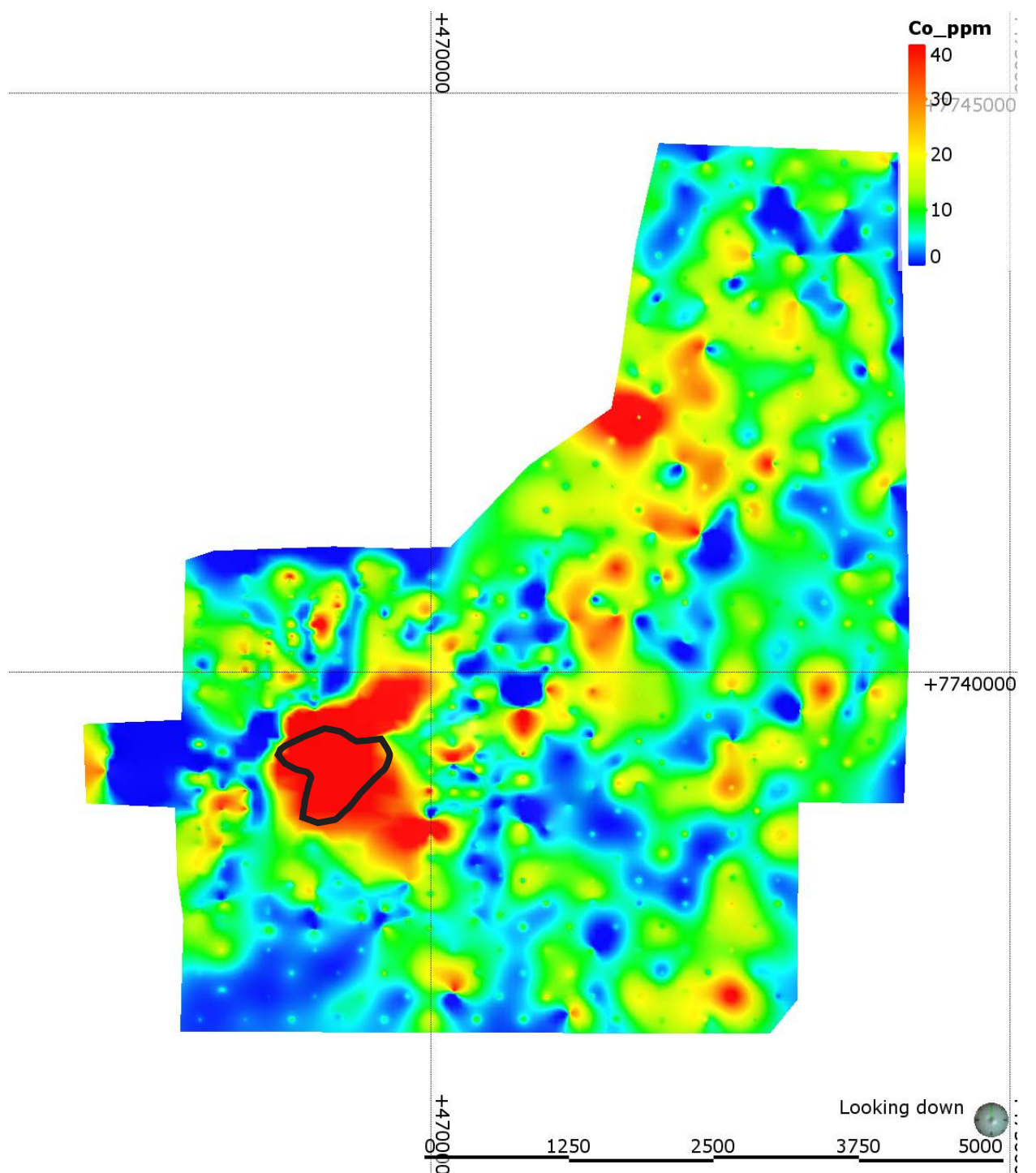


Figure 3.21. Image showing an evaluation of Zn values on the Proterozoic unconformity surface from the multi-element drill dataset, based on a non-directional Leapfrog™ linear interpolant. Solid line denotes the approximate position of the near-surface trace of the Ernest Henry ore outline. Map Projection AGD84, AMG54.

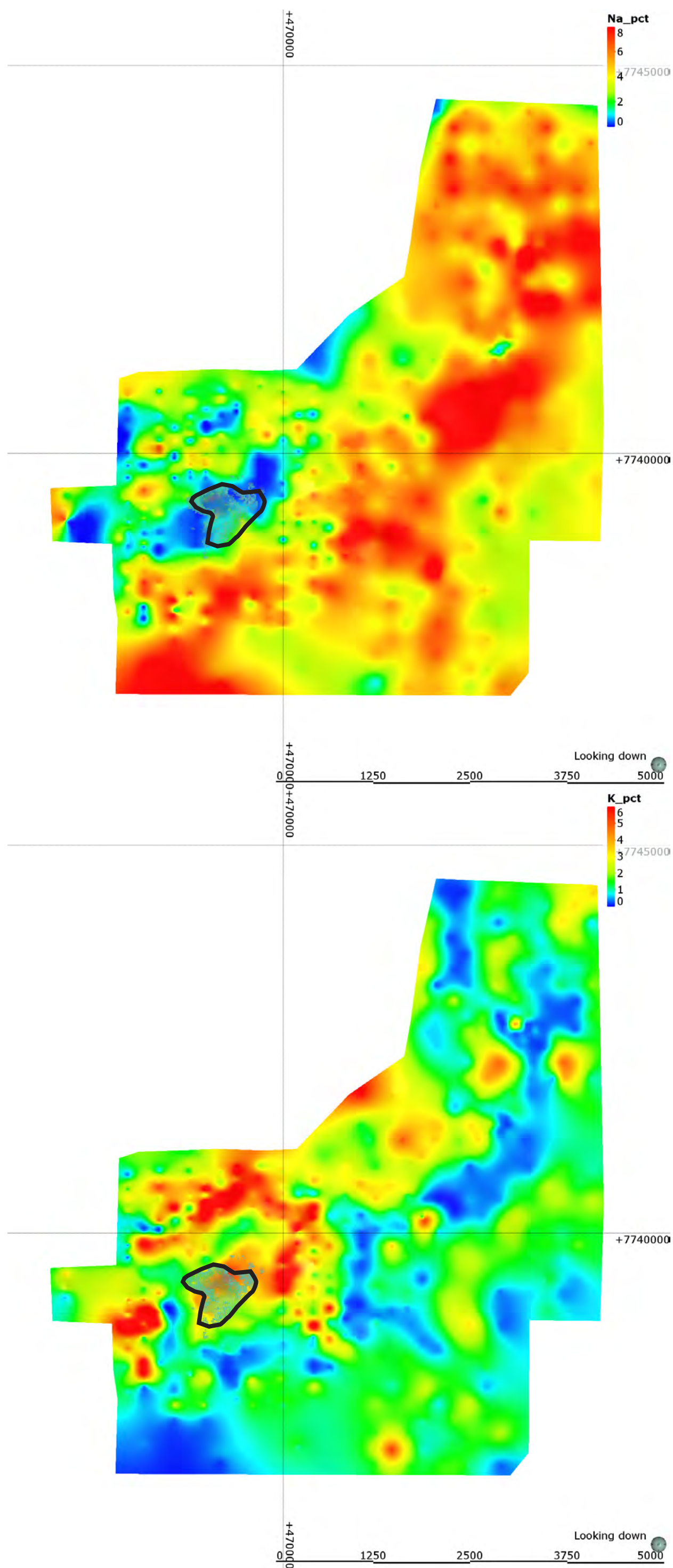


Figure 3.22. Image showing an evaluation of Na values on the Proterozoic unconformity surface from the multi-element drill dataset. Based on a non-directional Leapfrog™ linear interpolant. Solid line denotes the approximate position of the near-surface trace of the Ernest Henry ore outline. Higher values of Na occur in the hangingwall to the deposit and in the diorite, as well as some areas of the foot-wall. Map Projection AGD84, AMG54.

Figure 3.23. Image showing an evaluation of K values on the Proterozoic unconformity surface from the multi-element drill dataset. Based on a non-directional Leapfrog™ linear interpolant. Solid line denotes the approximate position of the near-surface trace of the Ernest Henry ore outline. The K-rich zone extends to the north, northeast and southwest of the Ernest Henry orebody. The distribution of K is likely to be a composite effect of the K-feldspar and biotite alteration suites. Map Projection AGD84, AMG54.

Figure 3.24. Image showing an evaluation of Ca values on the Proterozoic unconformity surface from the multi-element drill dataset. based on a non-directional Leapfrog™ linear interpolant. Solid line denotes the approximate position of the near-surface trace of the Ernest Henry ore outline. Ca is elevated in the immediate footwall of the deposit, possibly related to the occurrence of the marble matrix breccia. Map Projection AGD84, AMG54.

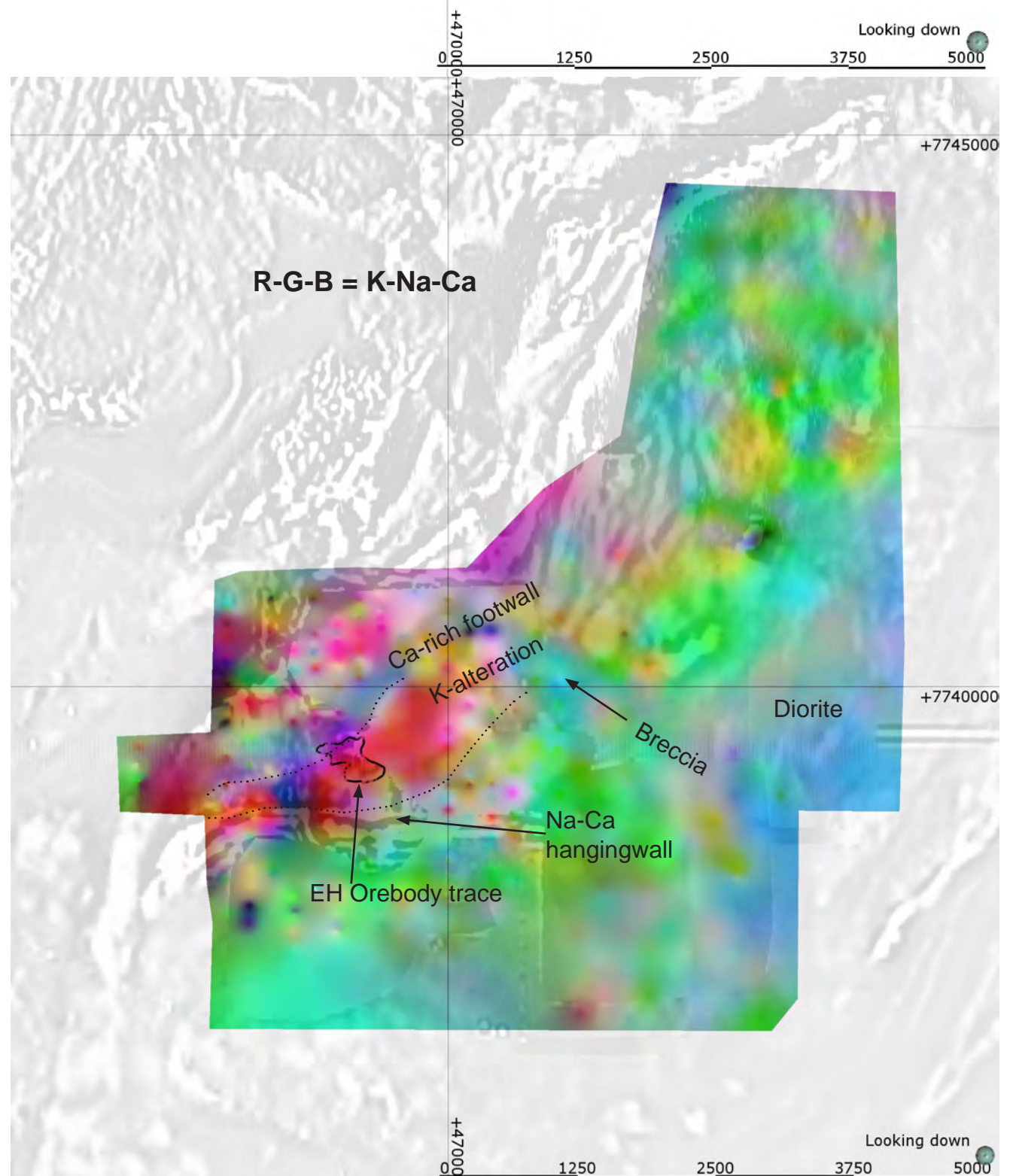
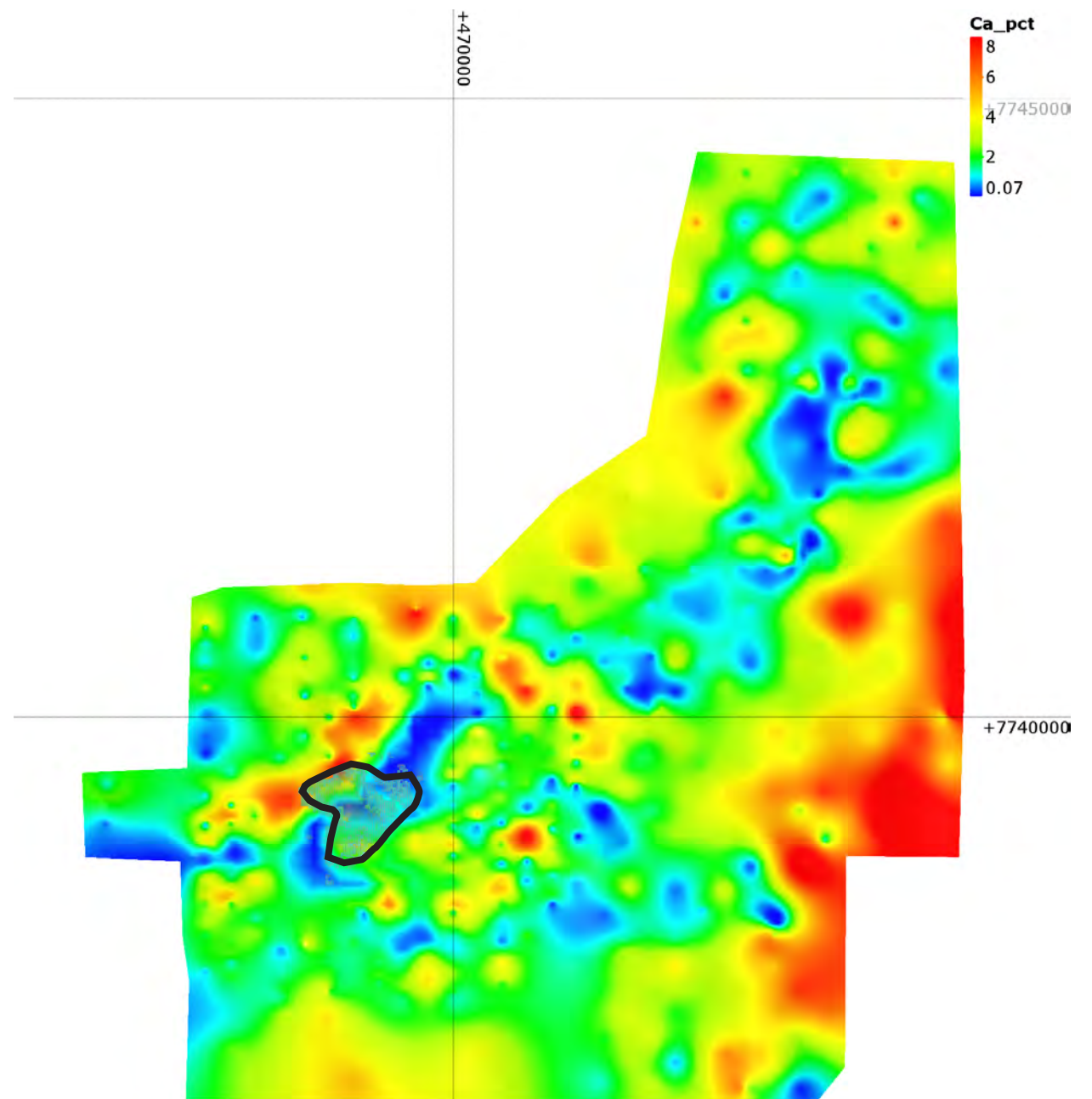


Figure 3.25. Image showing a 3-colour composite evaluation of K, Na and Ca values on the Proterozoic unconformity surface from the multi-element drill dataset. Based on a non-directional Leapfrog™ linear interpolant. Solid line denotes the approximate position of the near-surface trace of the Ernest Henry ore outline. Map Projection AGD84, AMG54.

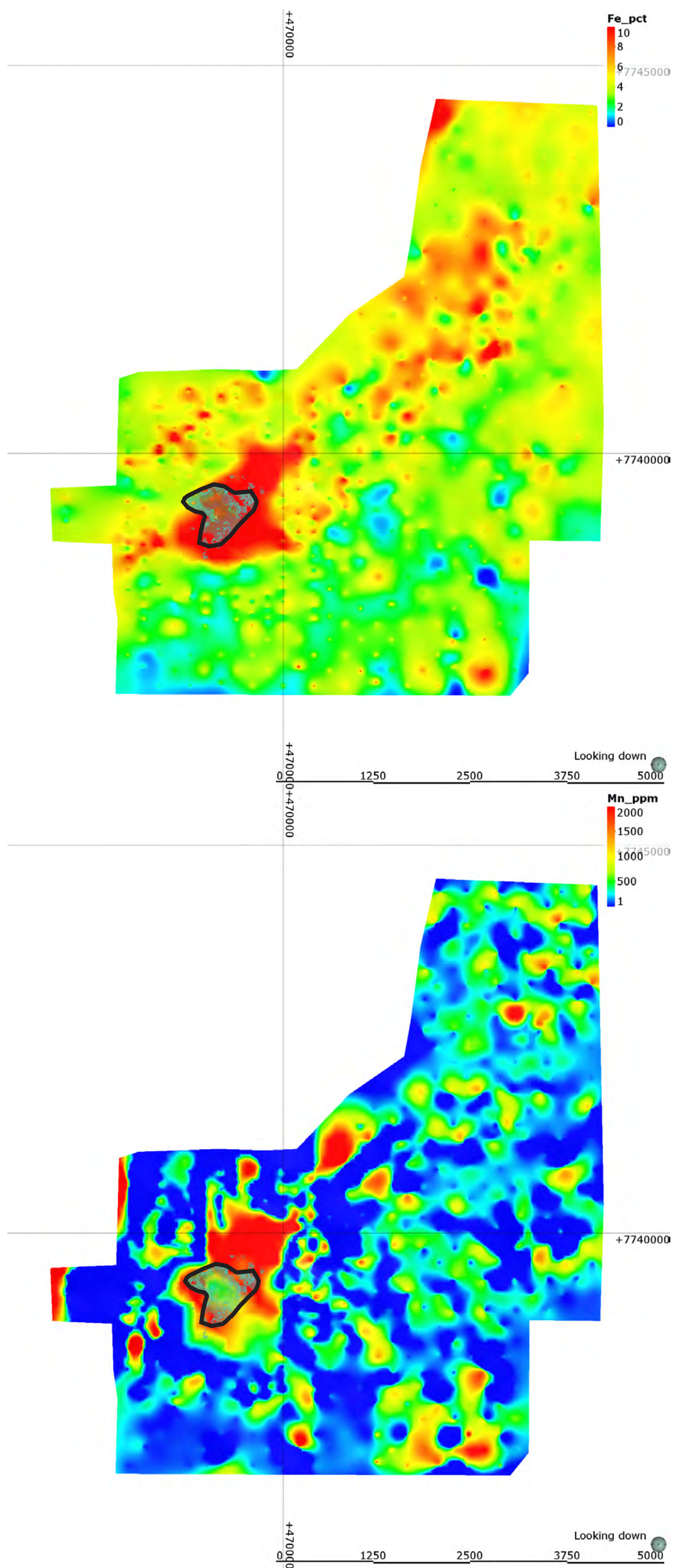


Figure 3.26. Image showing an evaluation of Fe values on the Proterozoic unconformity surface from the multi-element drill dataset. Based on a non-directional Leapfrog™ linear interpolant. Solid line denotes the approximate position of the near-surface trace of the Ernest Henry ore outline. Higher values of Fe extend northeast from Ernest Henry and extend into the hangingwall. Map Projection AGD84, AMG54.

Figure 3.27. Image showing an evaluation of Mn values on the Proterozoic unconformity surface from the multi-element drill dataset. Based on a non-directional Leapfrog™ linear interpolant. Solid line denotes the approximate position of the near-surface trace of the Ernest Henry ore outline. Mn shows a broadly similar distribution to Fe. The distribution of K is likely to be a composite effect of the K-feldspar and biotite alteration suites. Map Projection AGD84, AMG54.

Figure 3.28. Image showing an evaluation of P values on the Proterozoic unconformity surface from the multi-element drill dataset. Based on a non-directional Leapfrog™ linear interpolant. Solid line denotes the approximate position of the near-surface trace of the Ernest Henry ore outline. Map Projection AGD84, AMG54.

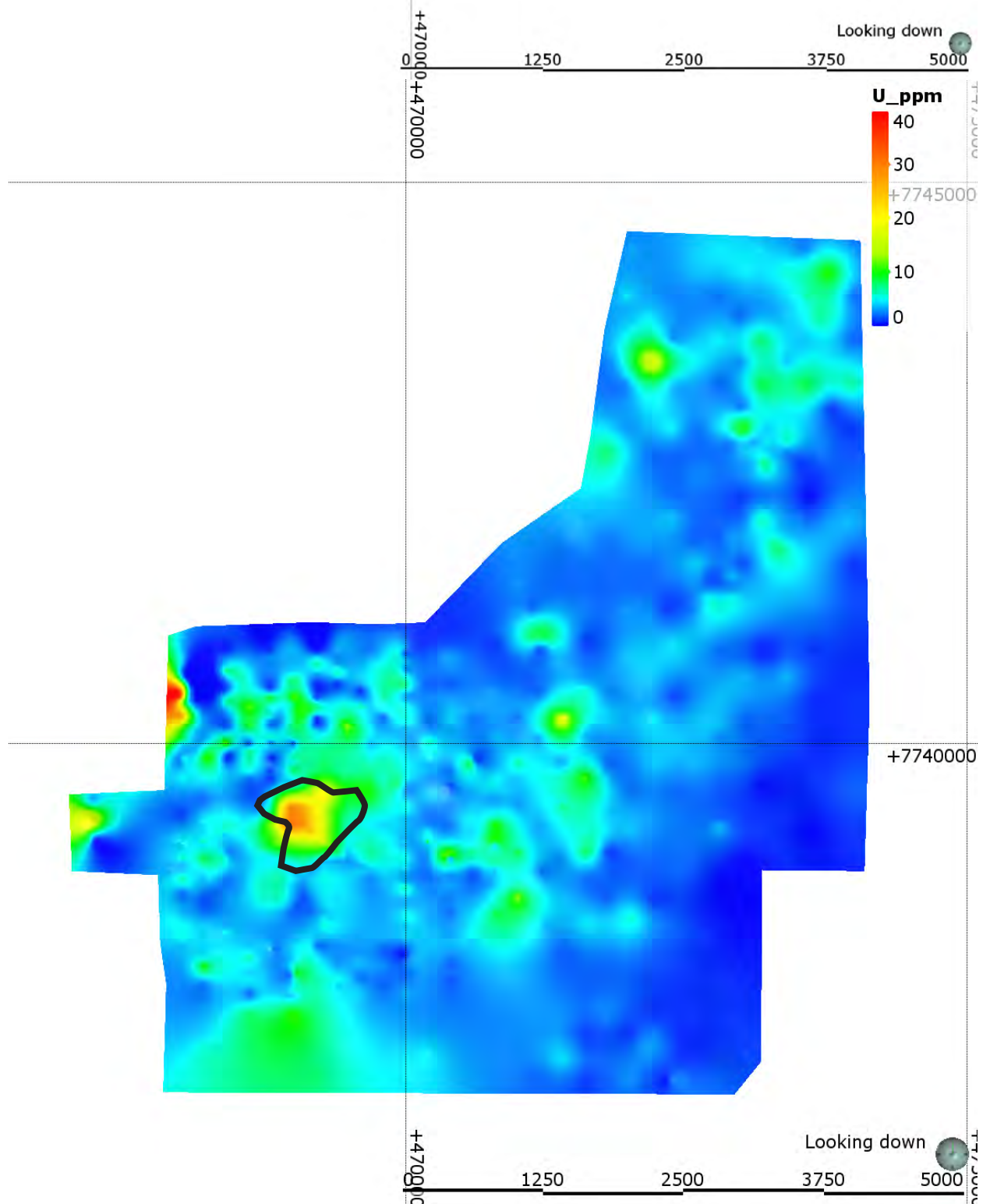
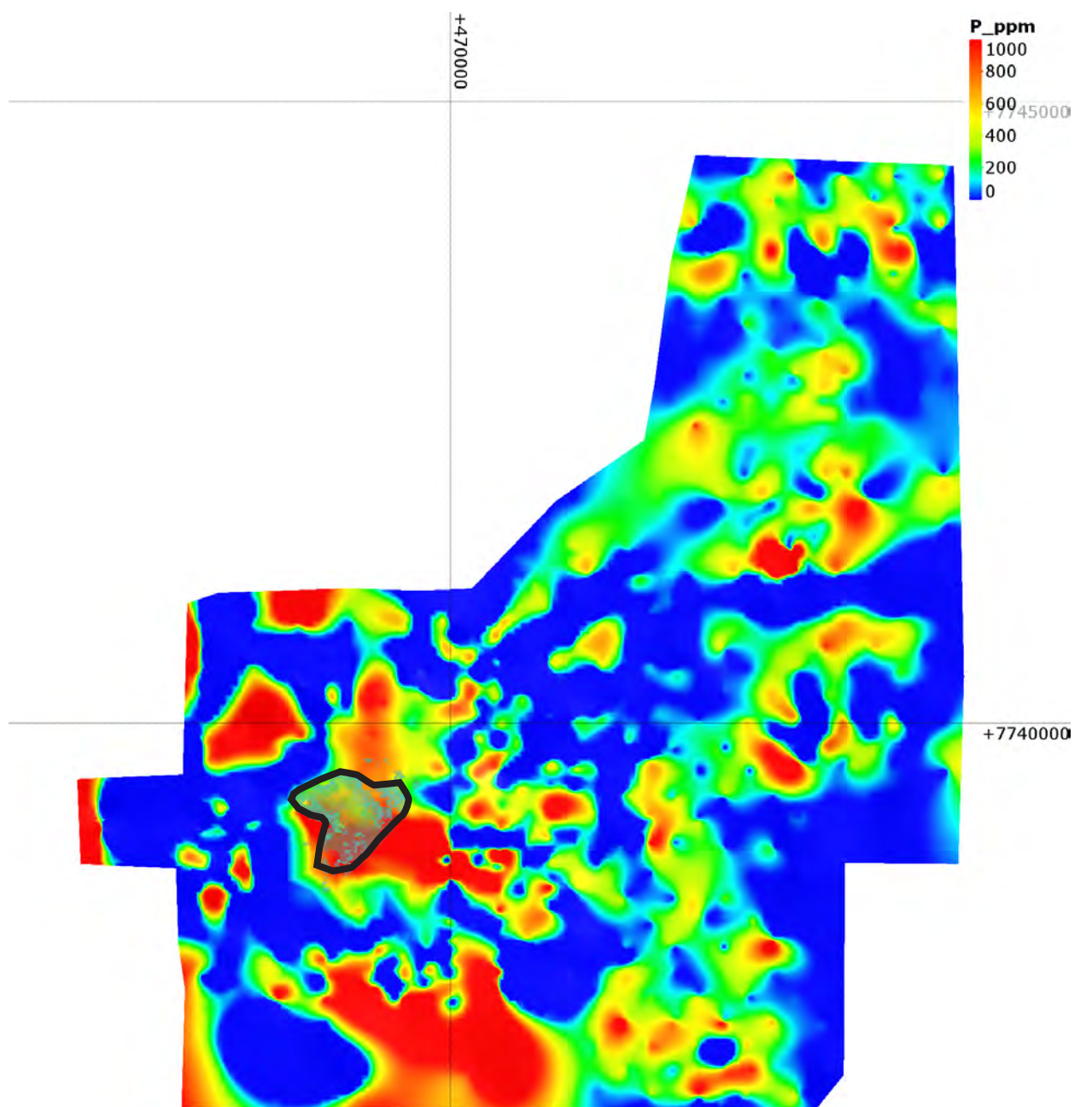


Figure 3.29. Image showing an evaluation of U values on the Proterozoic unconformity surface from the multi-element drill dataset. Based on a non-directional Leapfrog™ linear interpolant. Solid line denotes the approximate position of the near-surface trace of the Ernest Henry ore outline. Map Projection AGD84, AMG54.

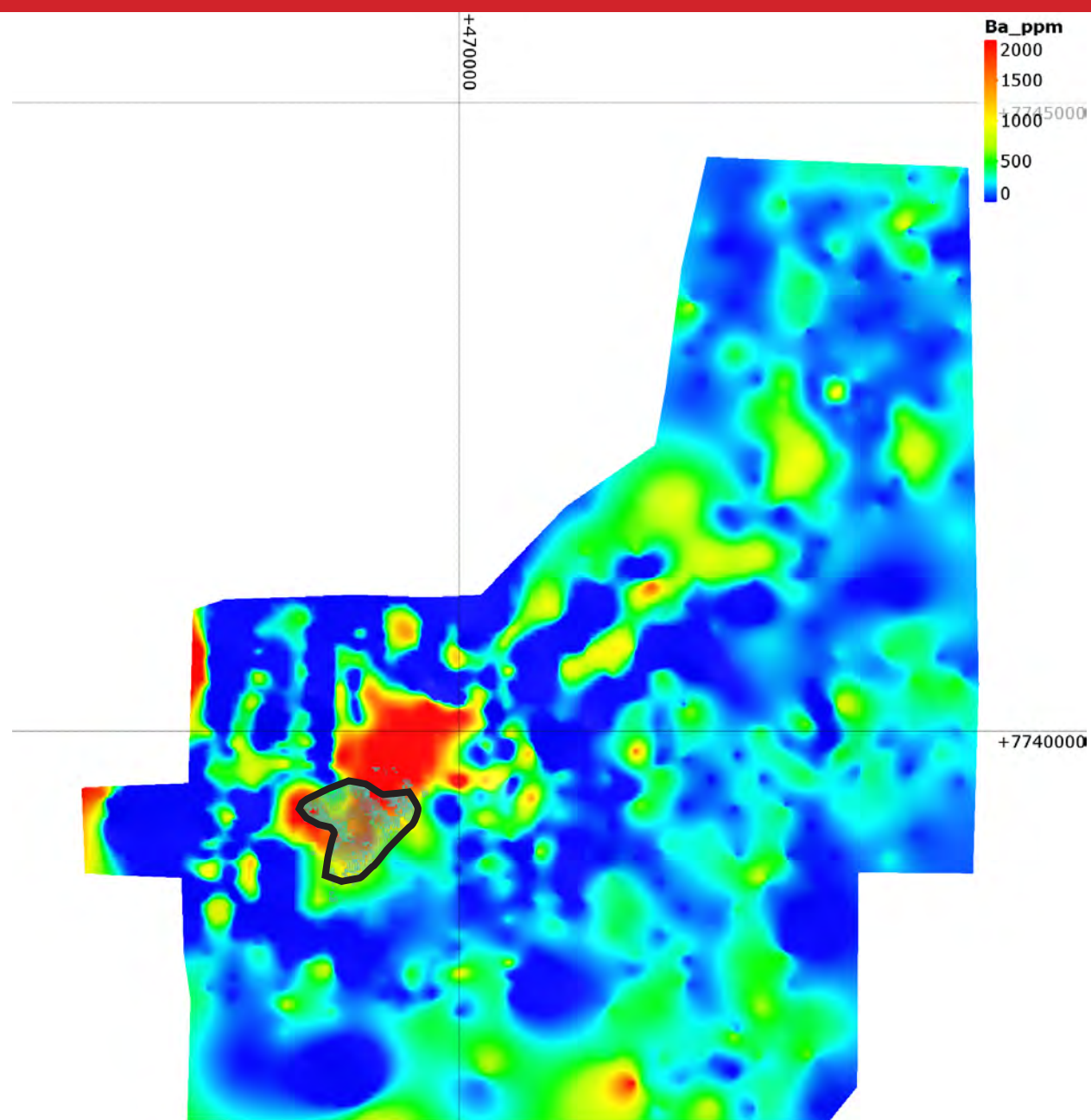


Figure 3.30. Image showing an evaluation of Ba values on the Proterozoic unconformity surface from the multi-element drill dataset. Based on a non-directional Leapfrog™ linear interpolant. Solid line denotes the approximate position of the near-surface trace of the Ernest Henry ore outline. Higher values of Ba are broadly coincident with the K-feldspar alteration zone. Map Projection AGD84, AMG54.

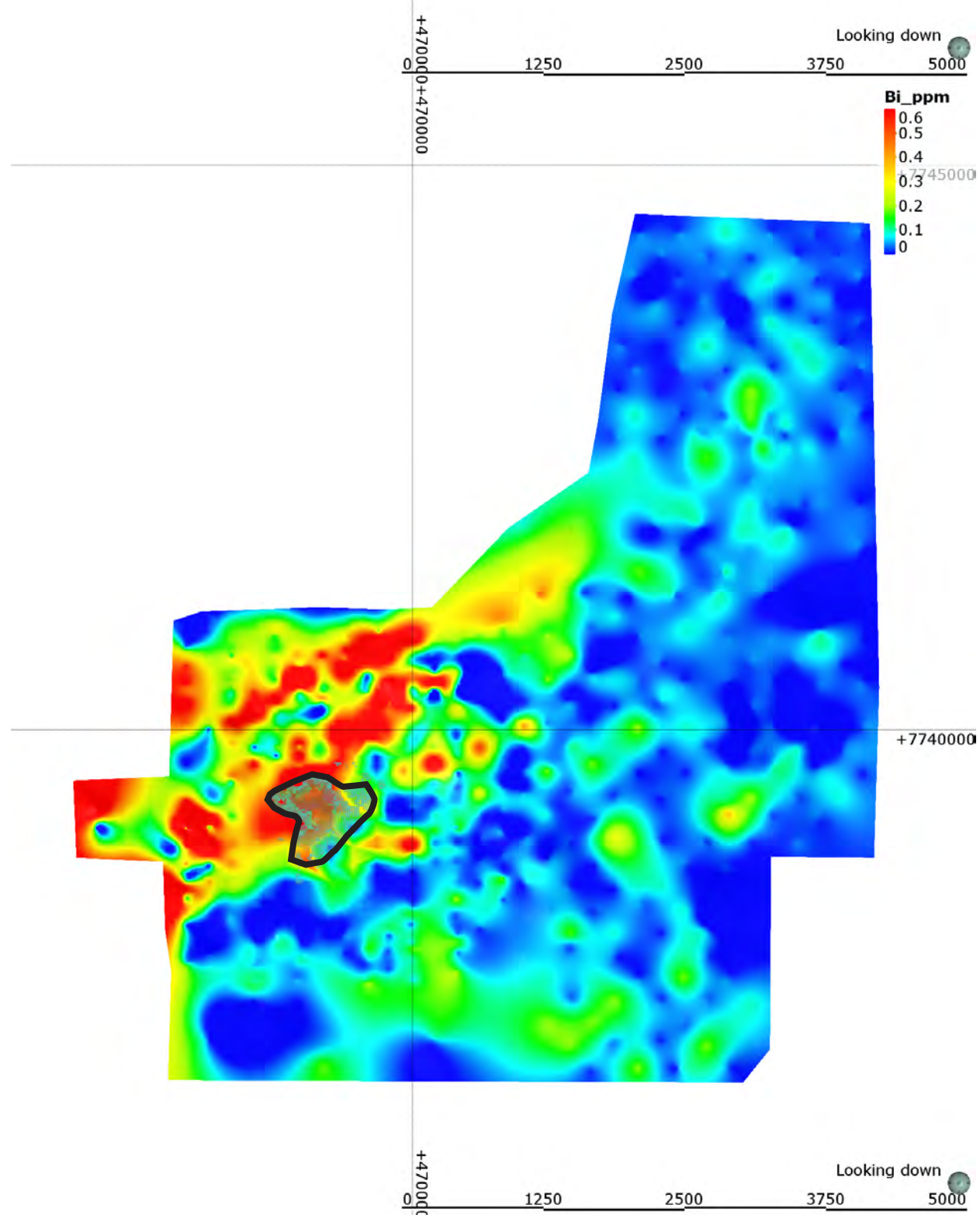


Figure 3.31. Image showing an evaluation of Bi values on the Proterozoic unconformity surface from the multi-element drill dataset. Based on a non-directional Leapfrog™ linear interpolant. Solid line denotes the approximate position of the near-surface trace of the Ernest Henry ore outline. Zones of elevated bi appear to coincide with both the K-feldspar alteration zone and the biotite-magnetite zone in the footwall of Ernest Henry. Map Projection AGD84, AMG54.

Figure 3.32. Image showing an evaluation of Sb values on the Proterozoic unconformity surface from the multi-element drill dataset. Based on a non-directional Leapfrog™ linear interpolant. Solid line denotes the approximate position of the near-surface trace of the Ernest Henry ore outline. Higher values of Sb are broadly coincident with the K-feldspar alteration zone. Map Projection AGD84, AMG54.

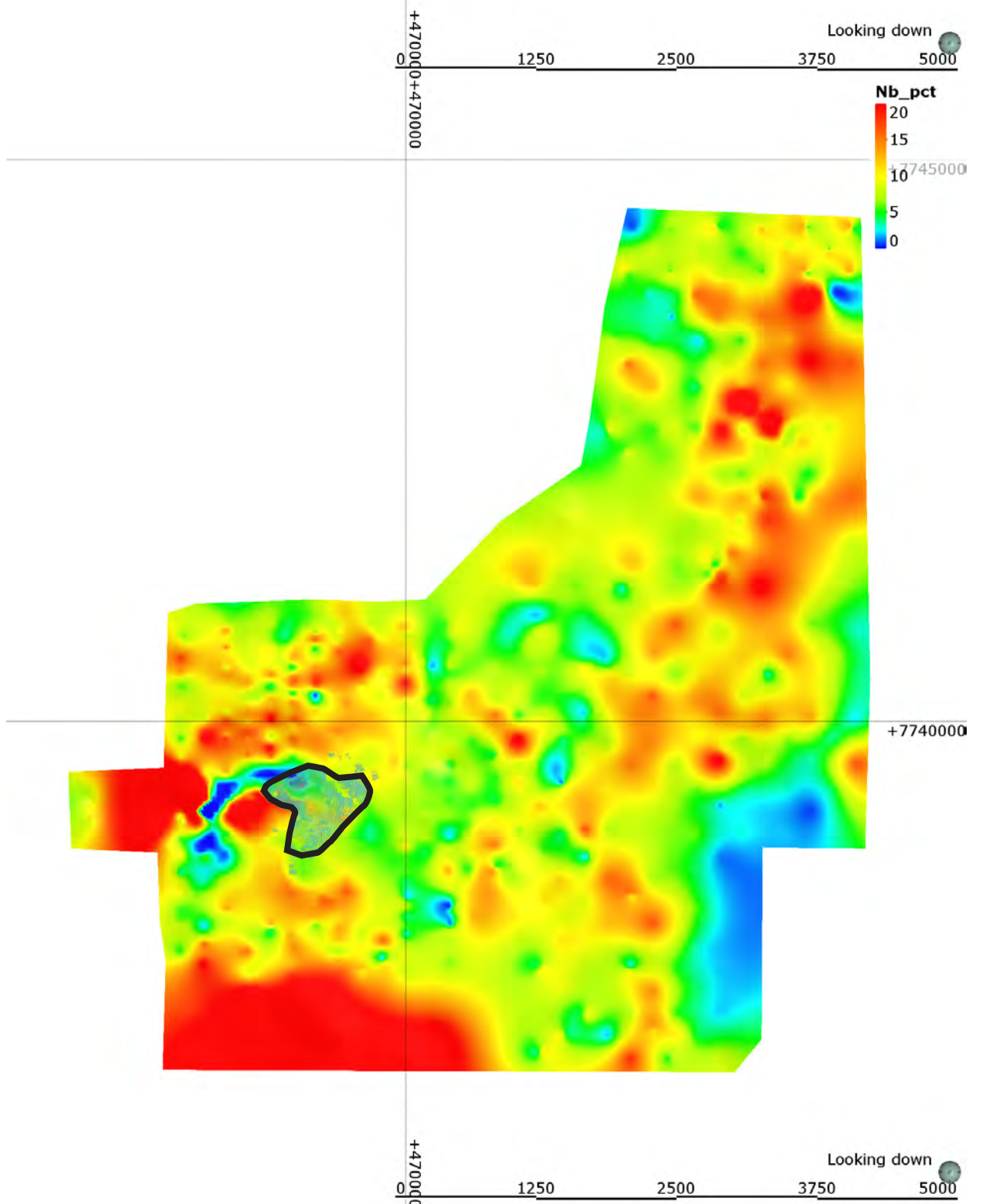
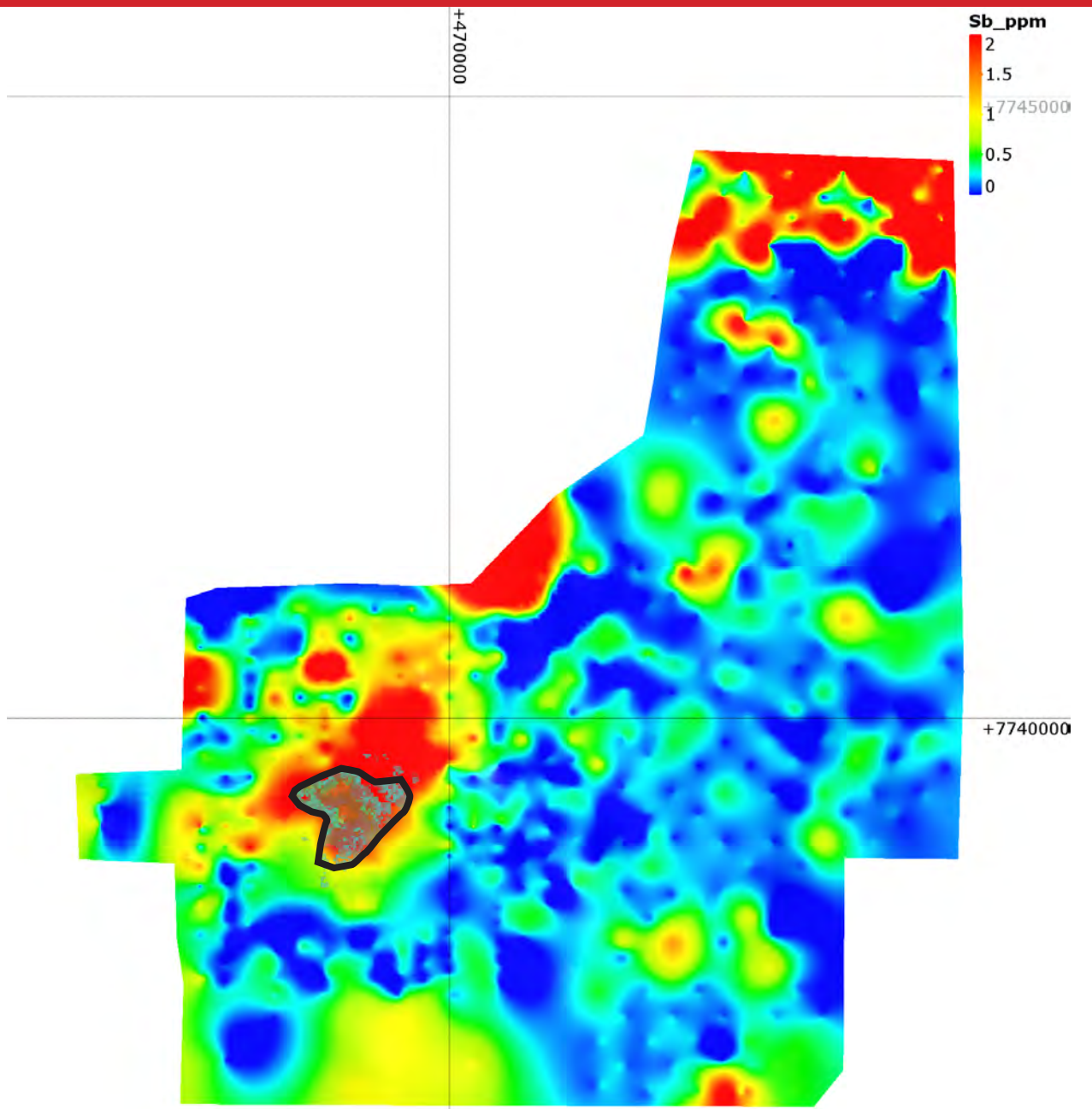


Figure 3.33. Image showing an evaluation of Nb values on the Proterozoic unconformity surface from the multi-element drill dataset. Based on a non-directional Leapfrog™ linear interpolant. Solid line denotes the approximate position of the near-surface trace of the Ernest Henry ore outline. Map Projection AGD84, AMG54.

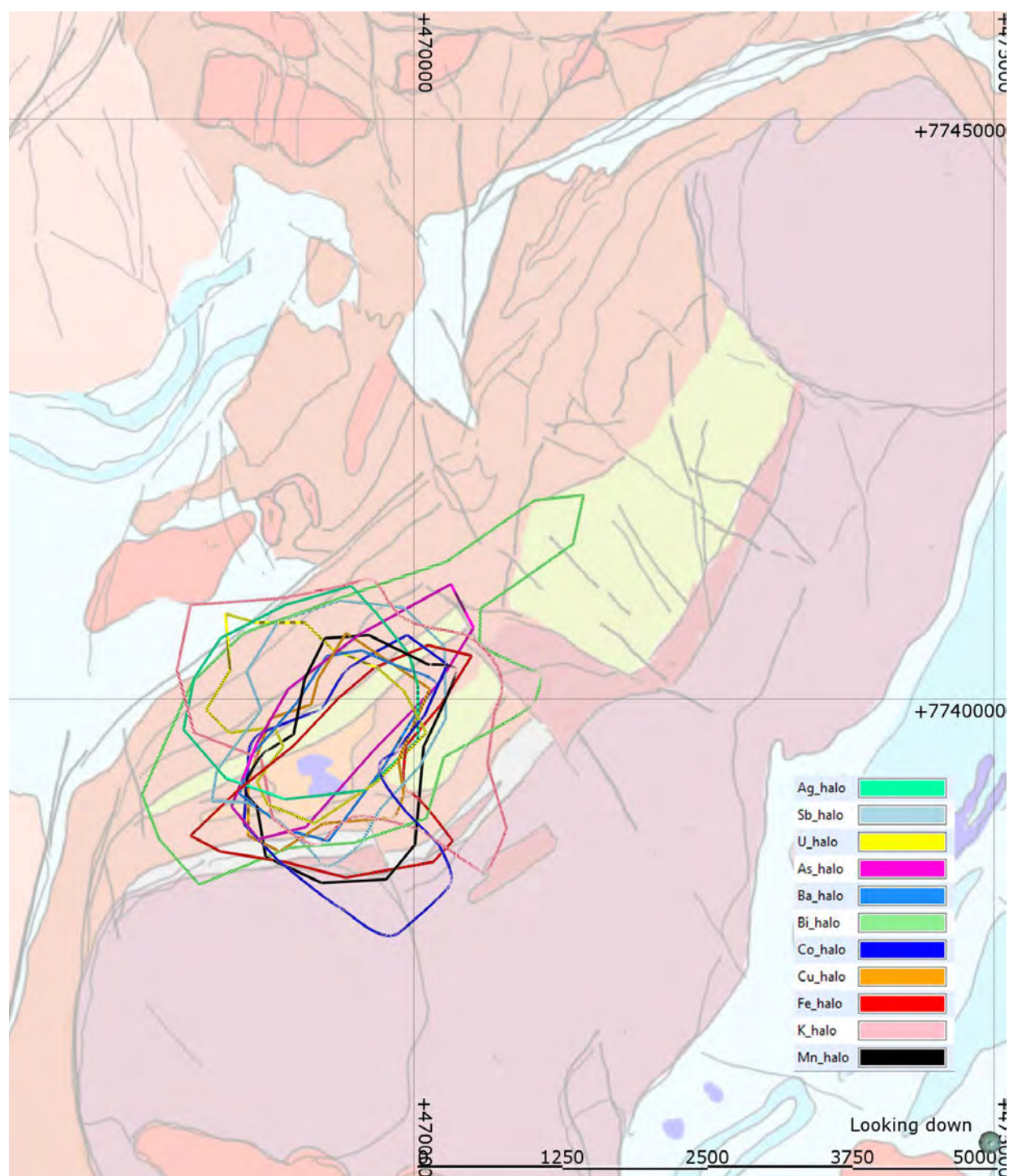


Figure 3.34. Composite outlines showing approximate distribution of elevated values for a range of elements in the Ernest Henry region drill dataset, superimposed on the schematic interpretation map. Map Projection AGD84, AMG54.

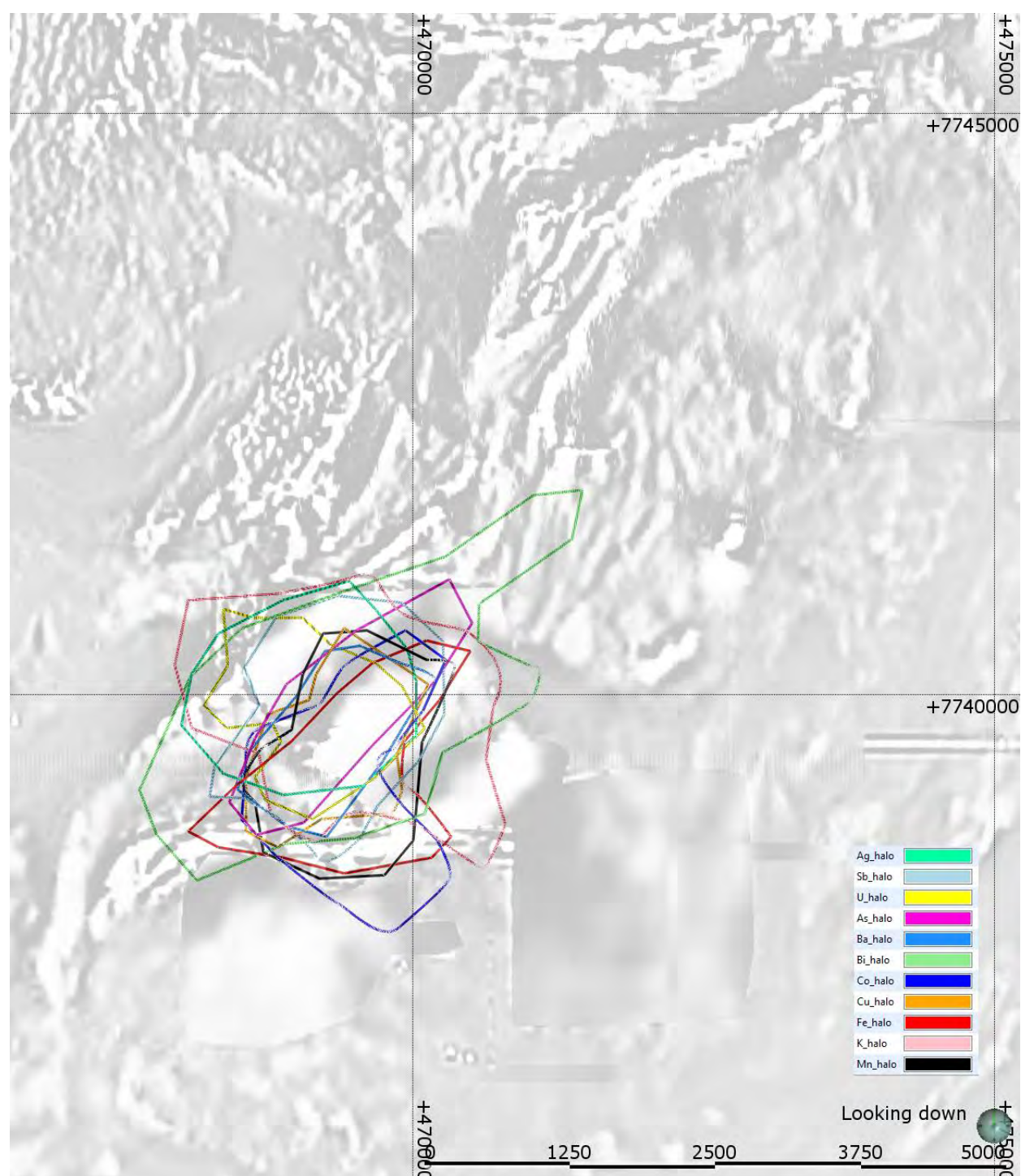


Figure 3.35. Composite outlines showing approximate distribution of elevated values for a range of elements in the Ernest Henry region drill dataset, superimposed on greyscale first vertical derivative. Map Projection AGD84, AMG54.

Figure 3.36. Series of graphs plotting assay values as a function of distance from the 0.5% Cu (eq) shell for the area of strong potassic alteration to the Northeast of Ernest Henry. This area has been singled out as it appears to contain a package of rocks which are most likely to be the lateral equivalent of the Ernest Henry orebody. The box plotted in the diagram below shows the area from which the assay results were obtained in order to make these plots. See text for further discussion.

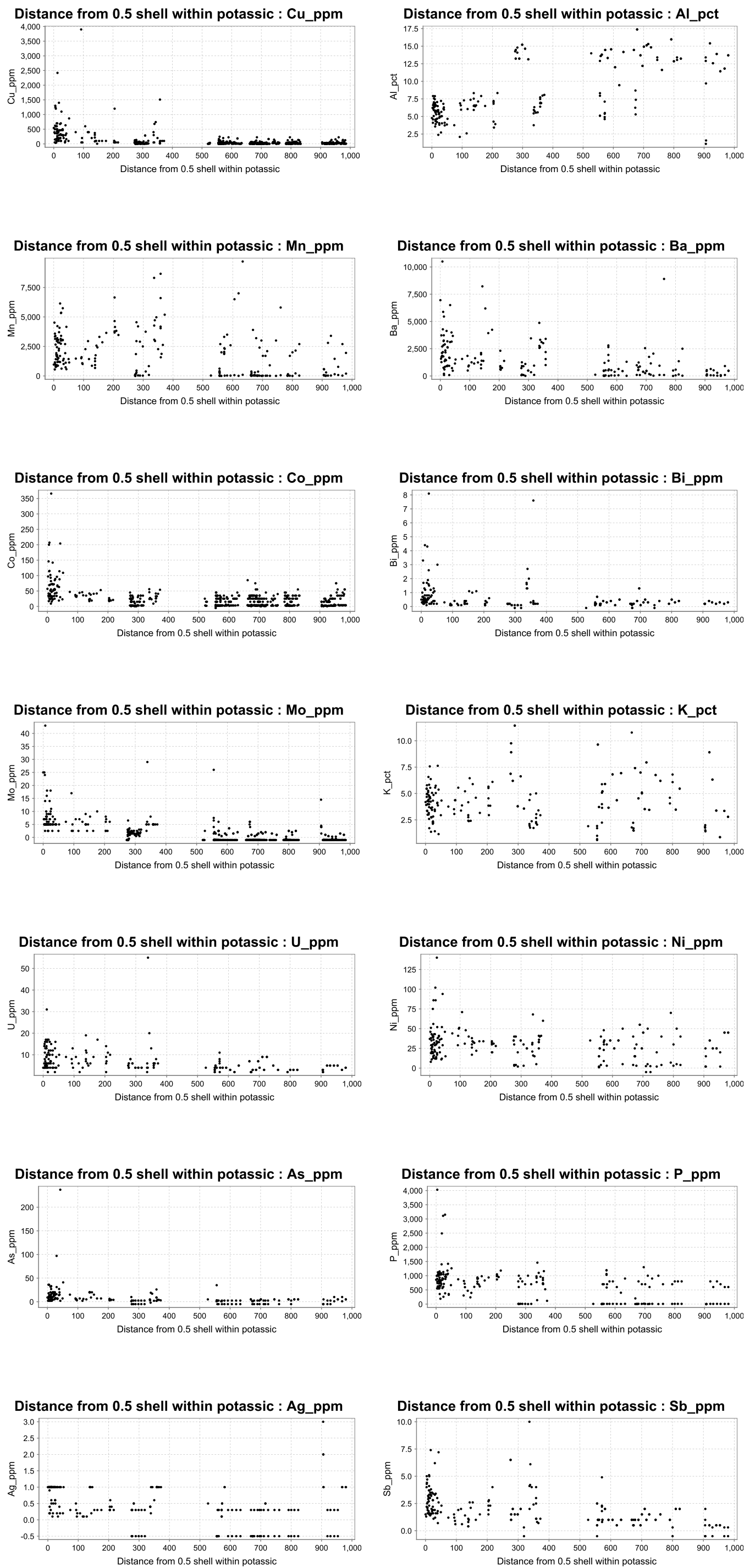
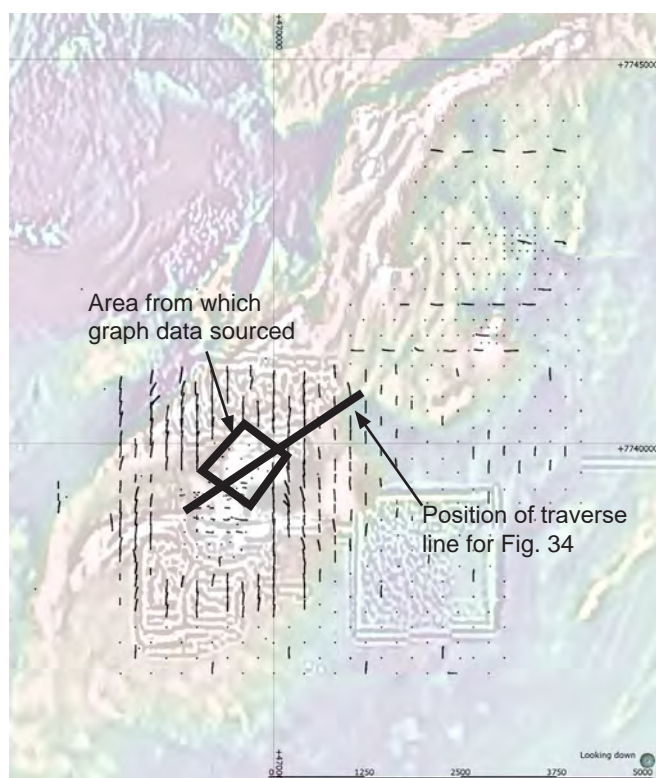
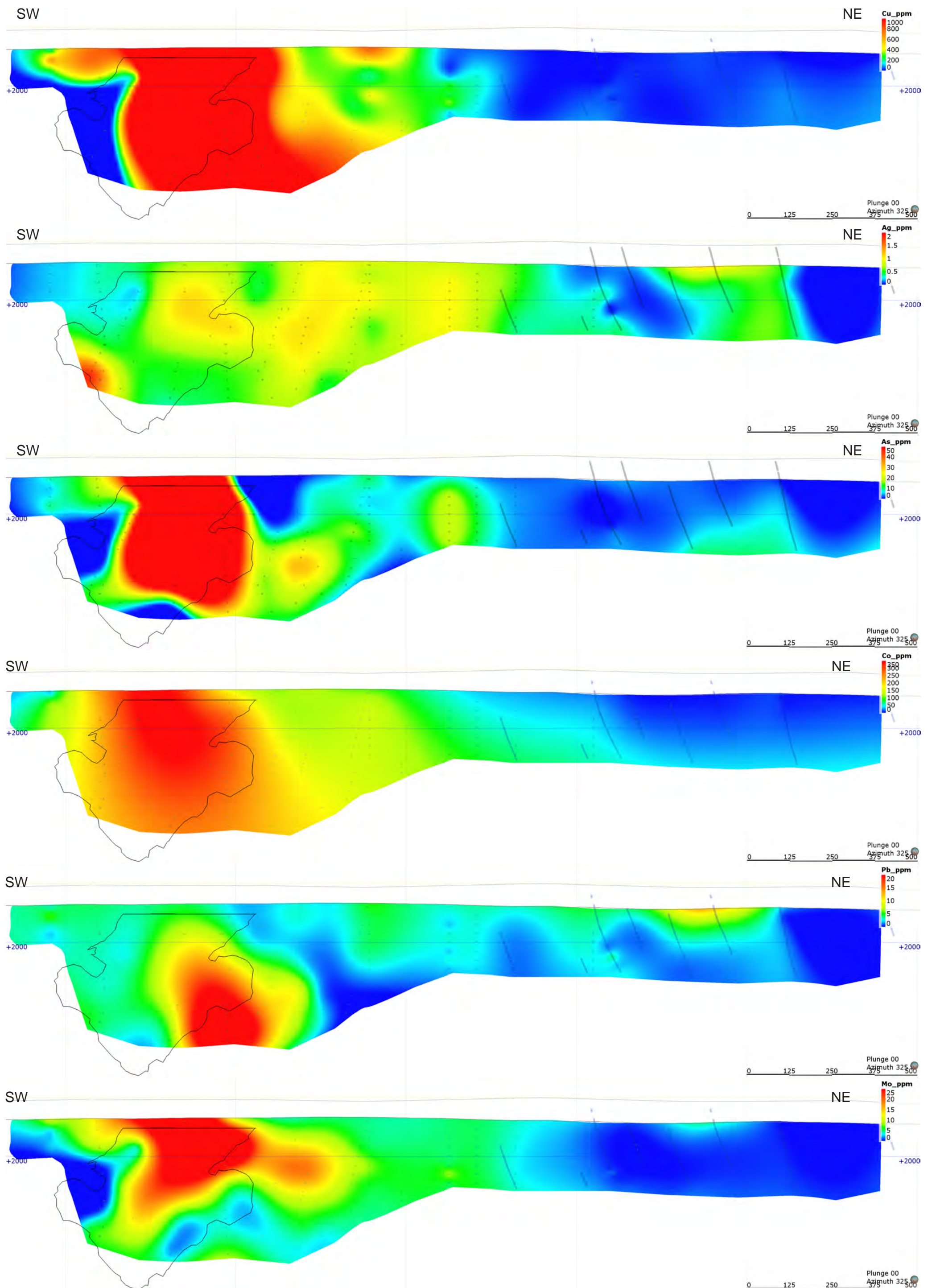
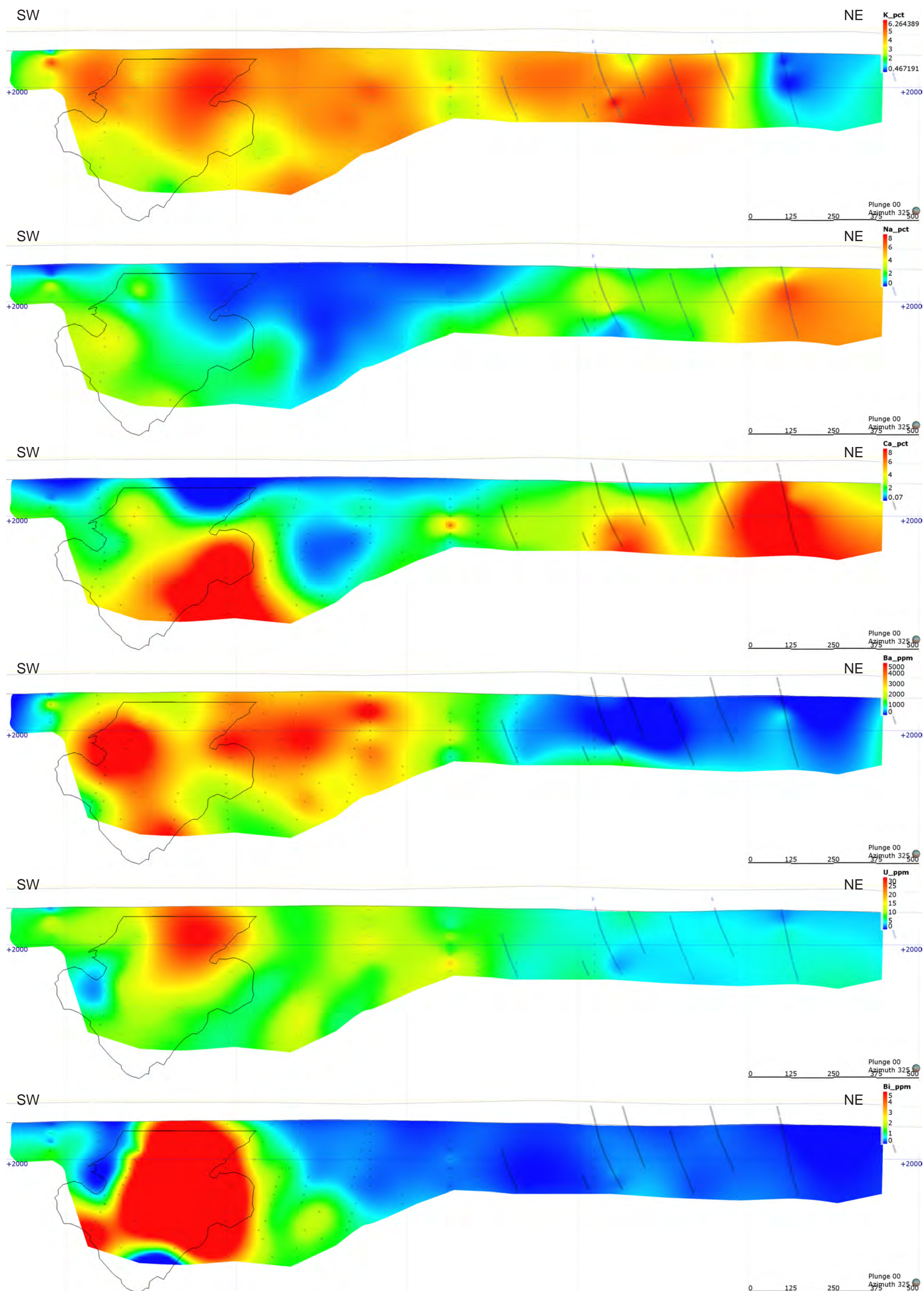


Figure 3.37 (on next pages). Series of element plots on a NE-trending surface clipped to the extent of drilling. Element plots are derived from a non-directional Leapfrog™ linear interpolant of drillhole assay values. Outline shows the outline of the Ernest Henry orebody at a 0.3% Cu equivalent cutoff. The traverse line is interpreted to pass through a zone of K-feldspar-altered metavolcanics which appear likely to be the less-mineralised equivalent of the Ernest Henry host rocks.





(see previous page for Figure 3.caption)



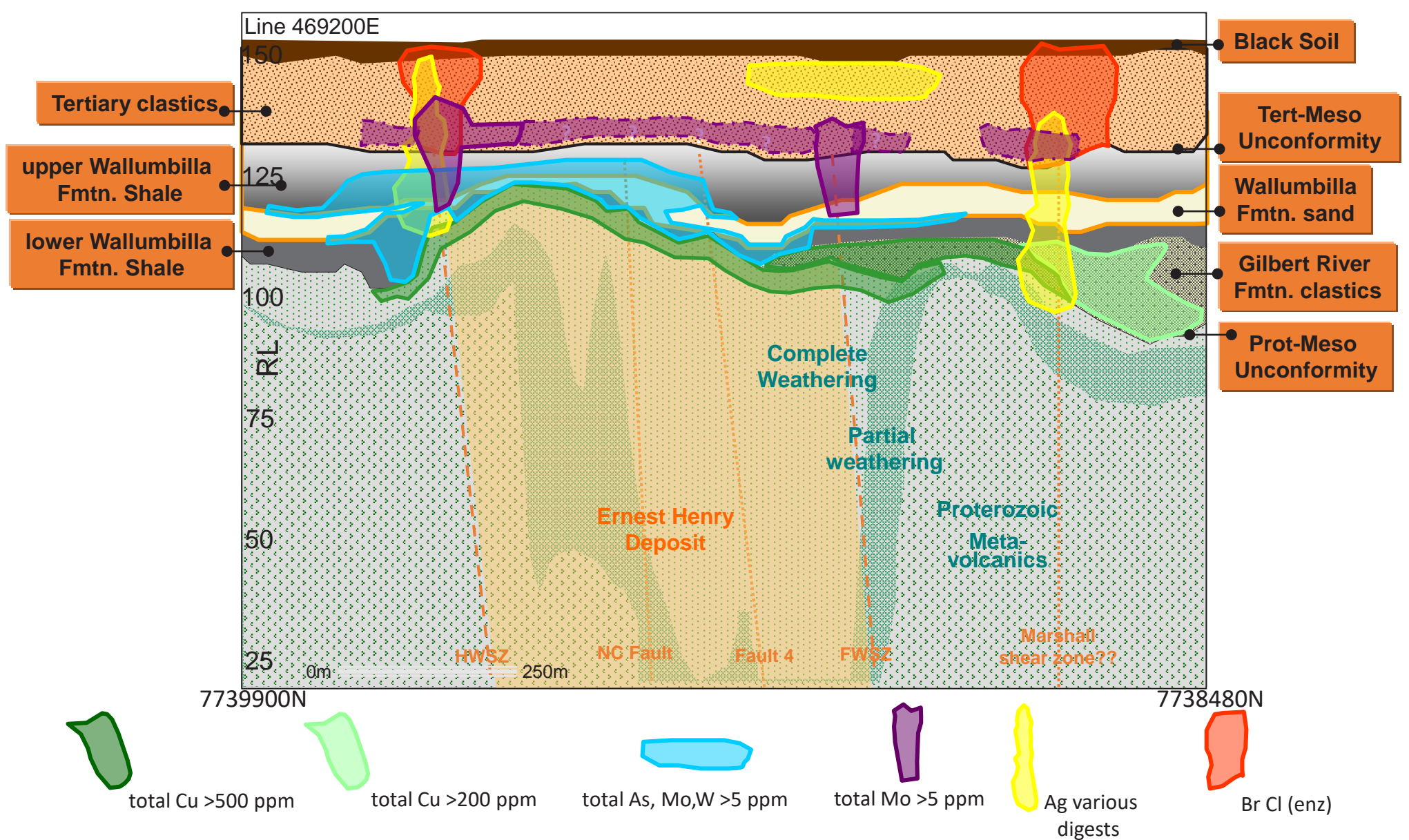
(see previous page for Figure 3.caption)



Figure 3.38. Photograph of the Ernest Henry pit looking to the south, showing the position of the Proterozoic unconformity.

Figure 3.39. Schematic diagram summarising the cover environment and geochemical dispersions associated with the Ernest Henry orebody (Lilly and Hannan, 2016).

### Schematic Diagram of Secondary Geochemical Dispersion



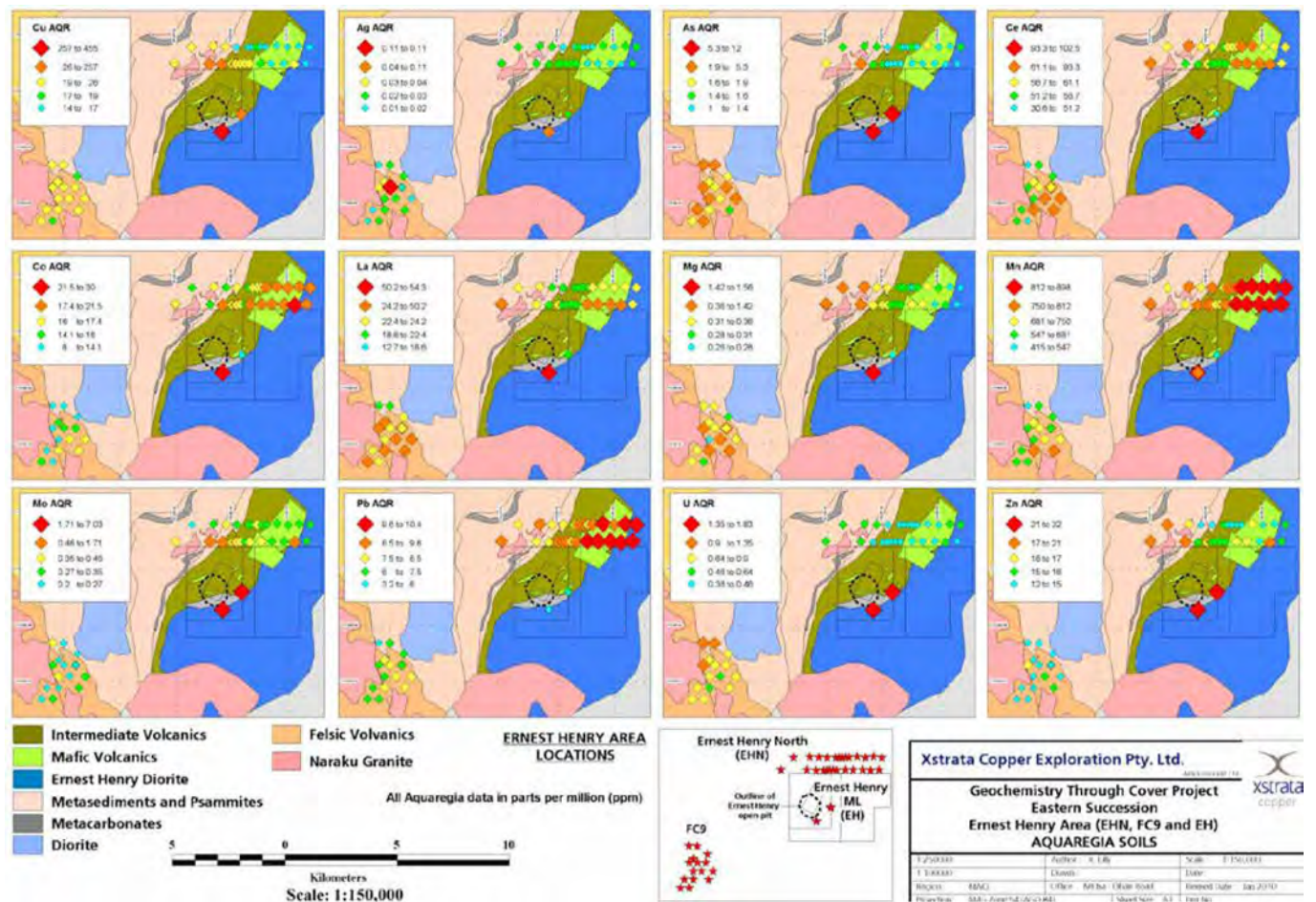


Figure 3.40. Diagram from Lilly et al (2014) showing aquaregia soil results for surveys in the Ernest Henry area.

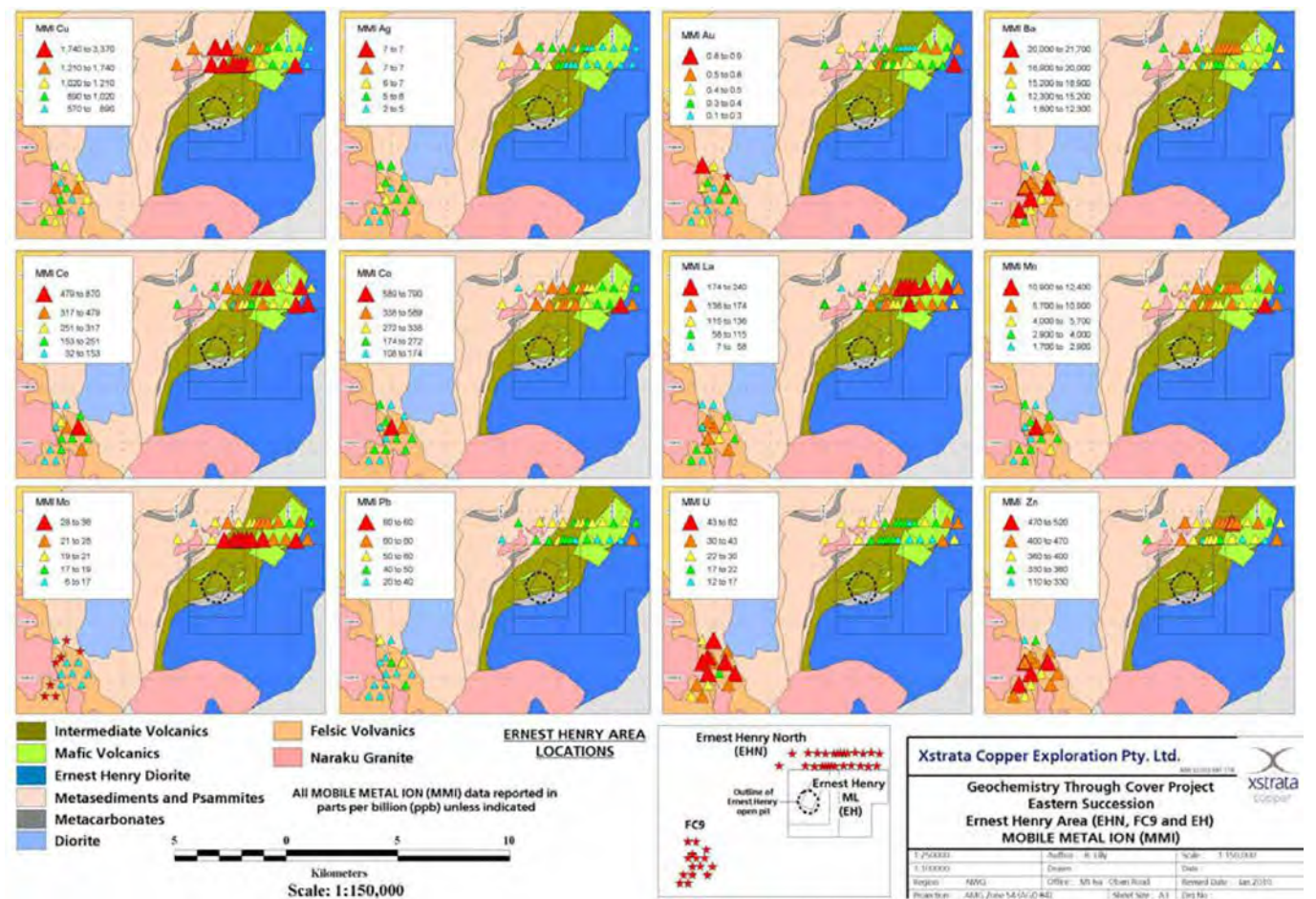


Figure 3.41. Diagram from Lilly et al (2014) showing Mobile Metal Ion (MMI) soil results for surveys in the Ernest Henry area.

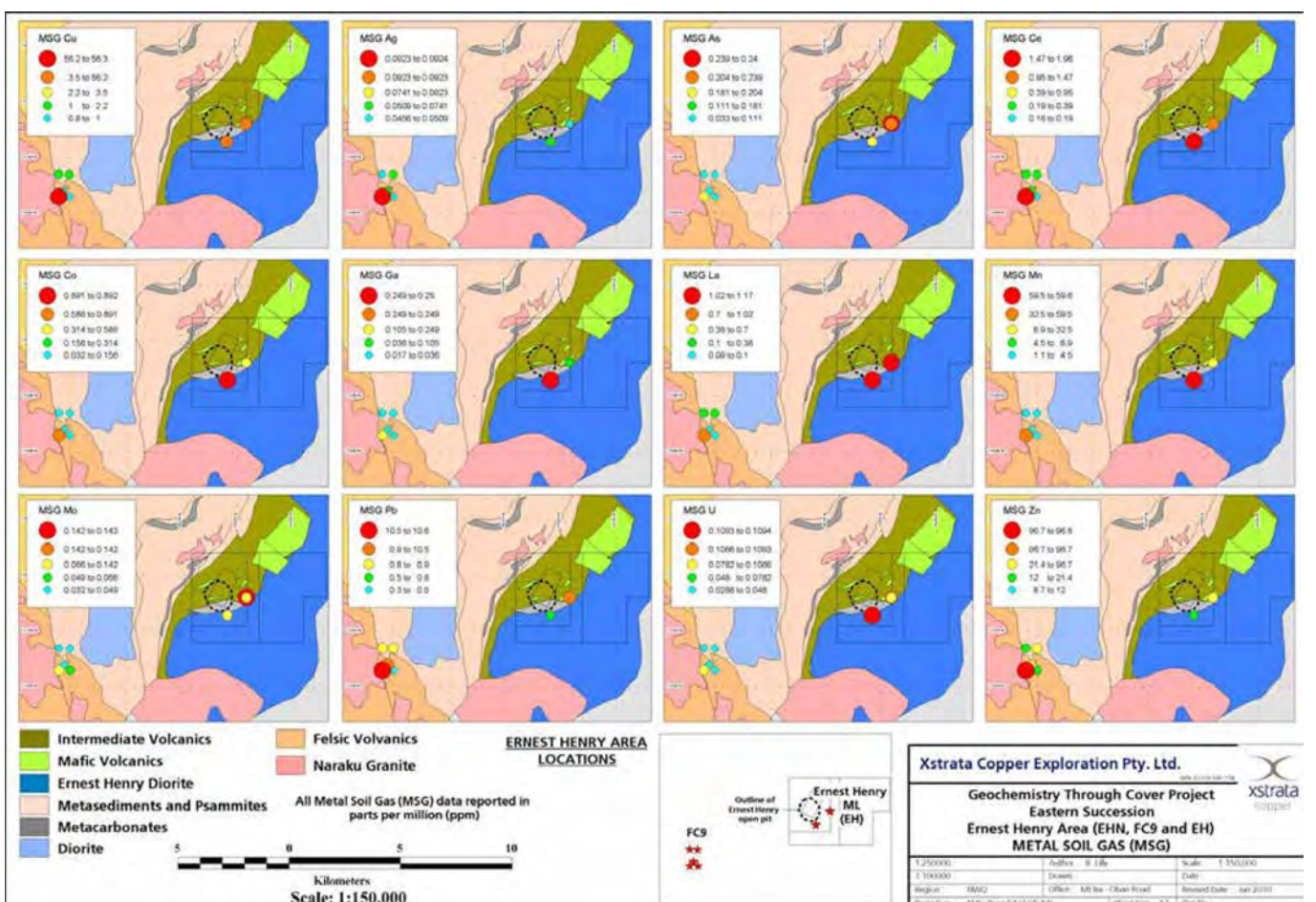
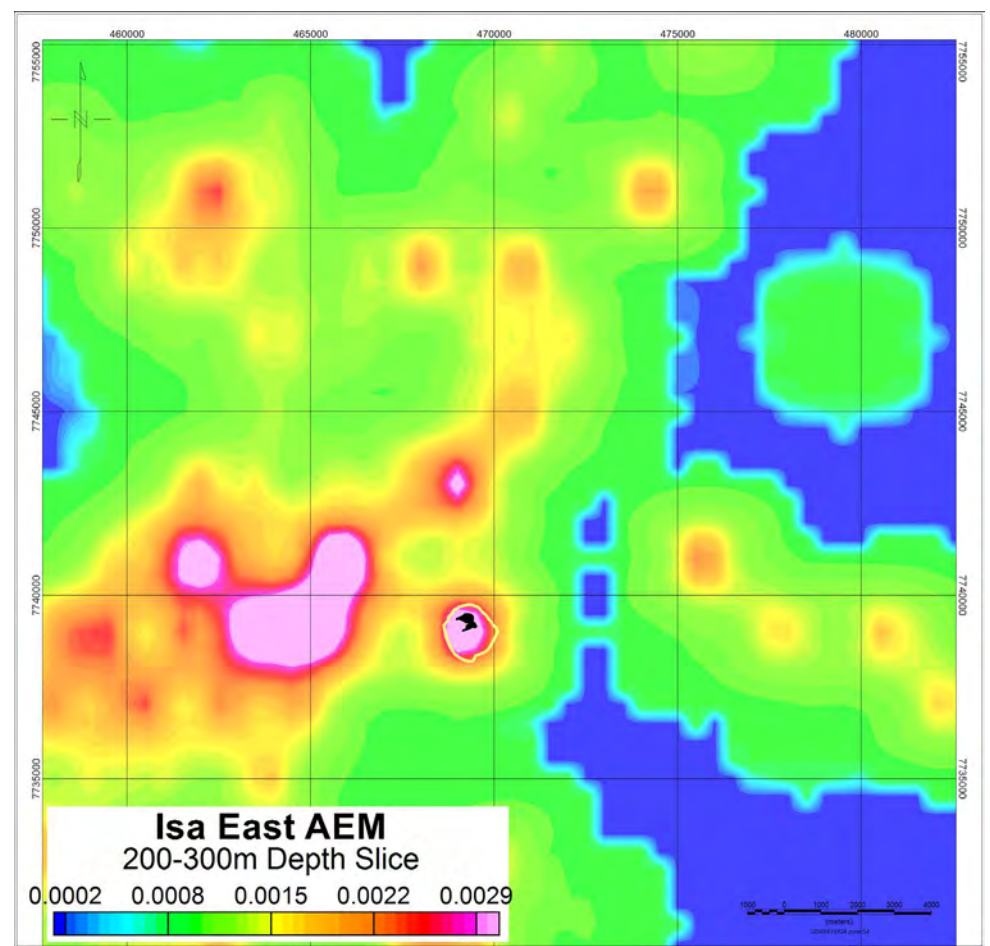
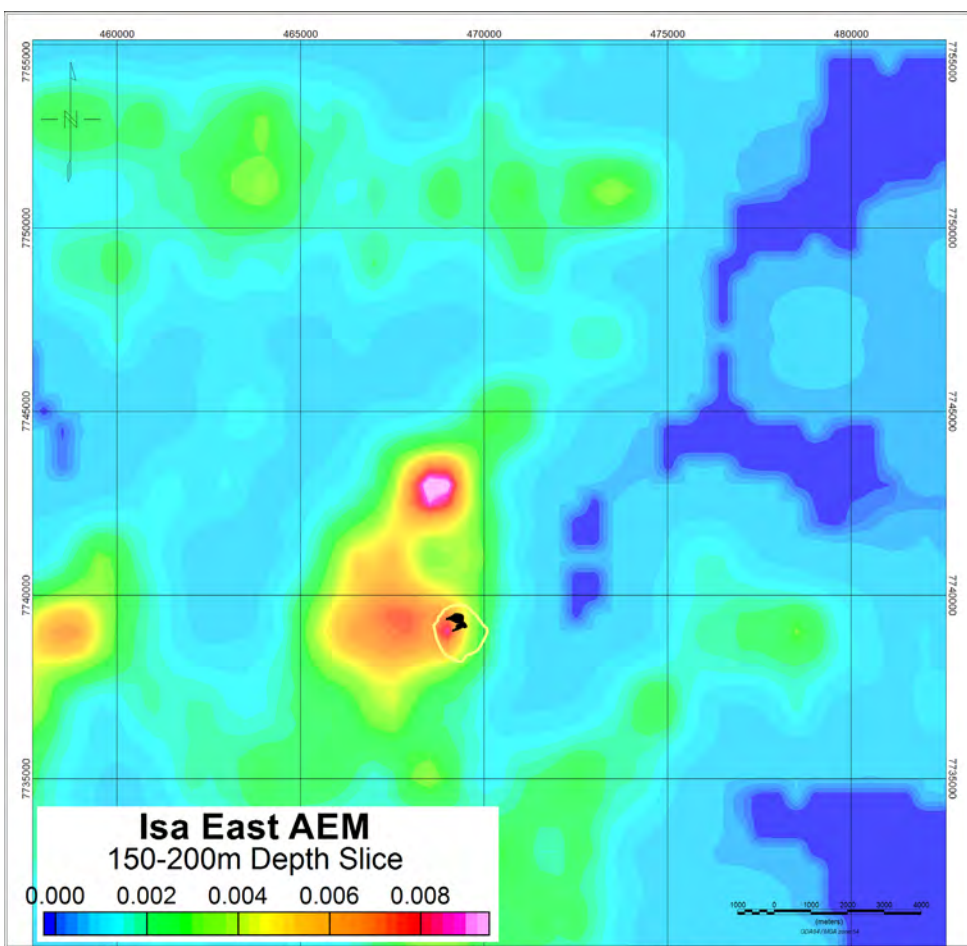
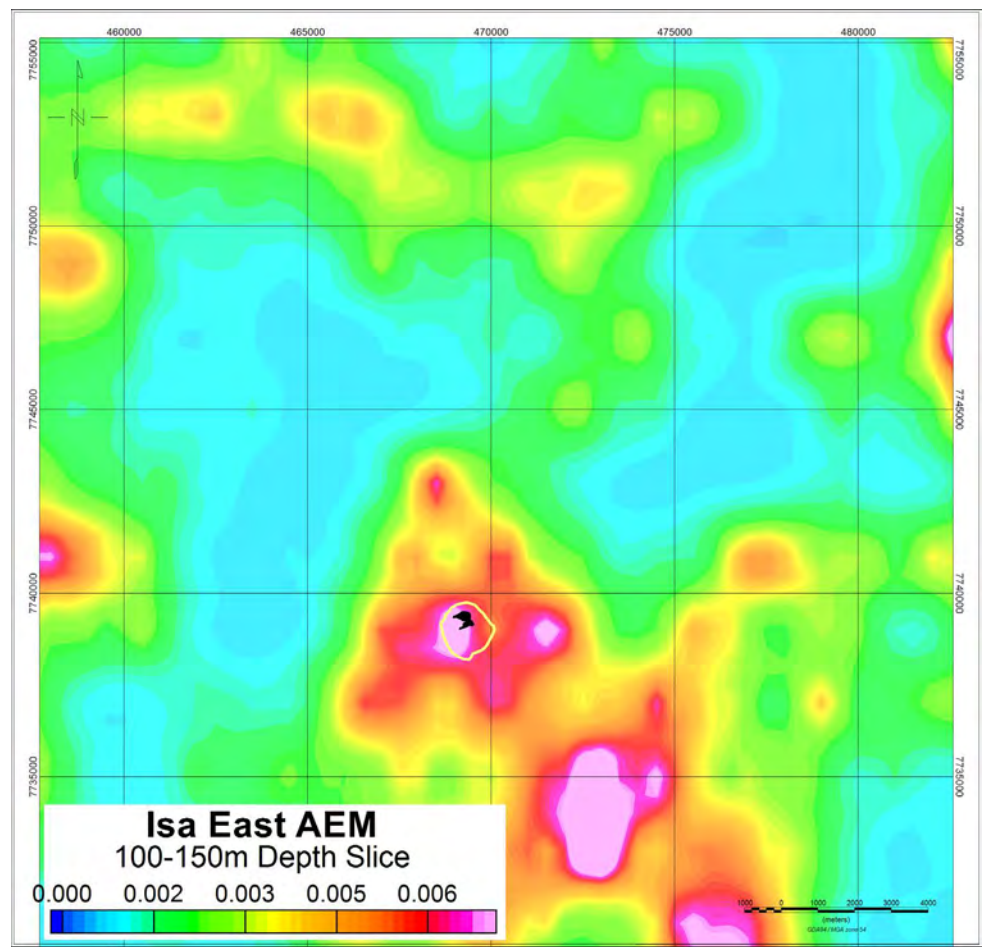
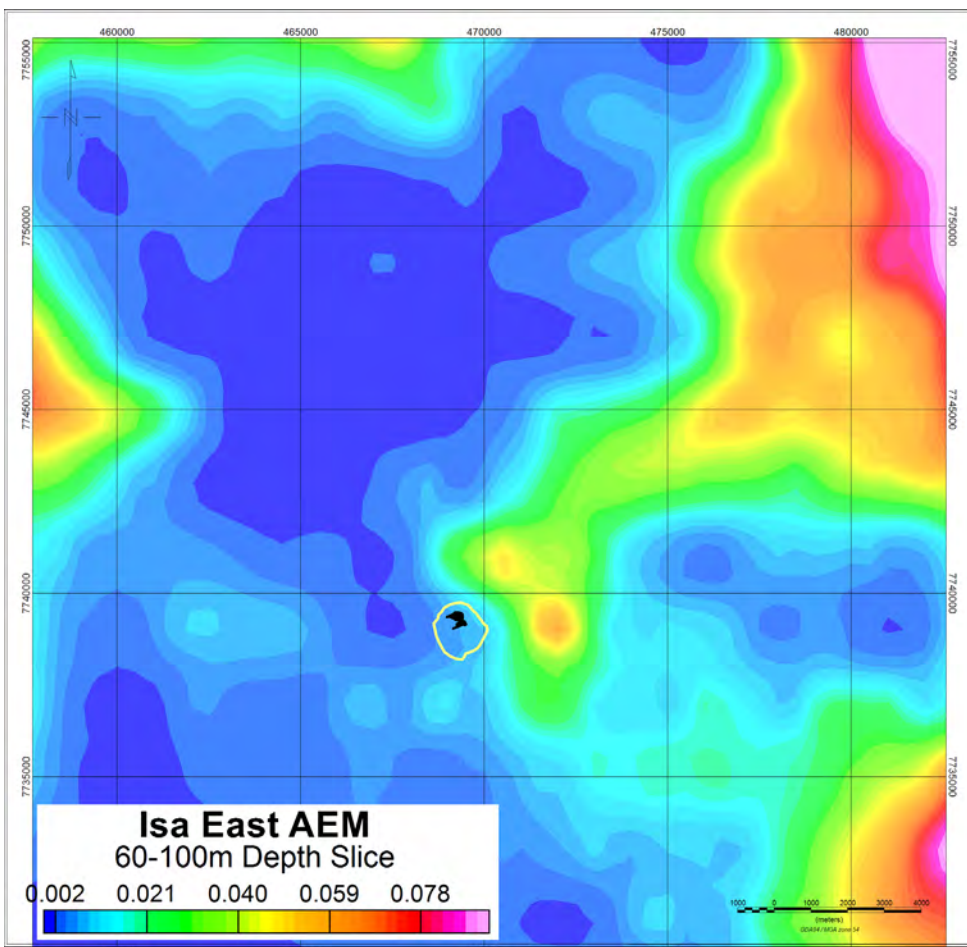
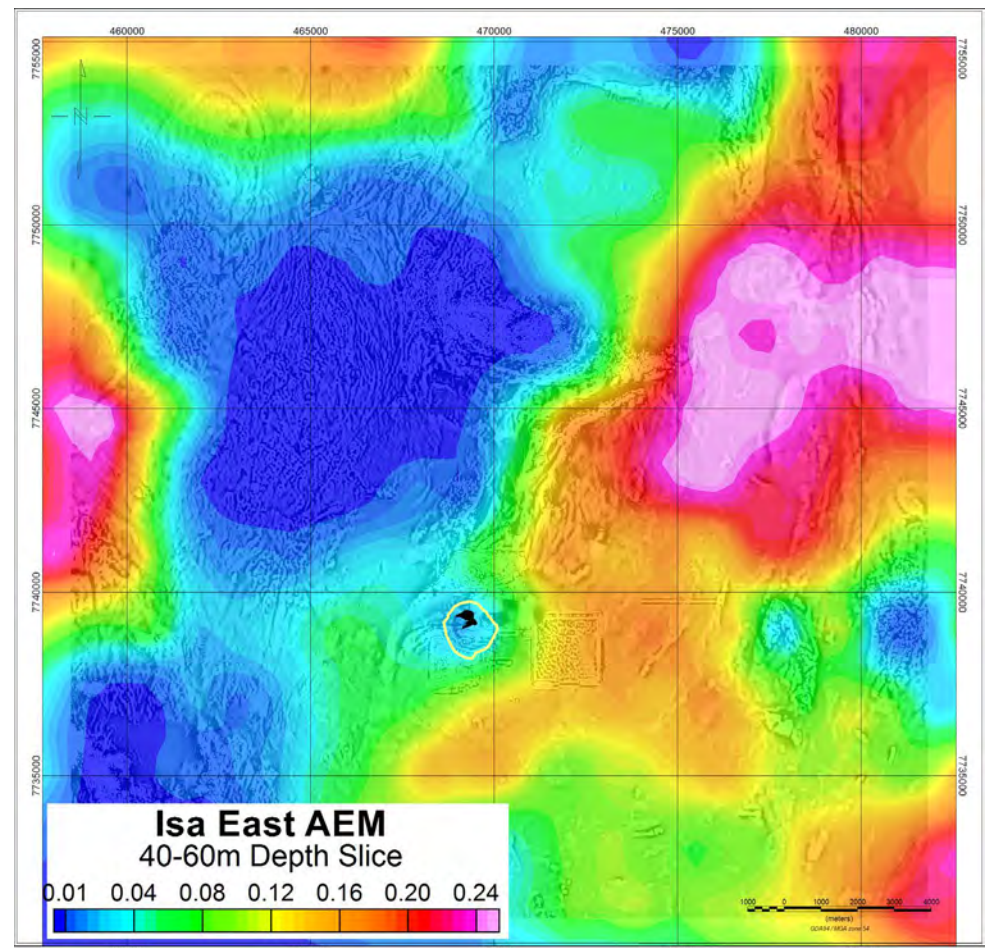
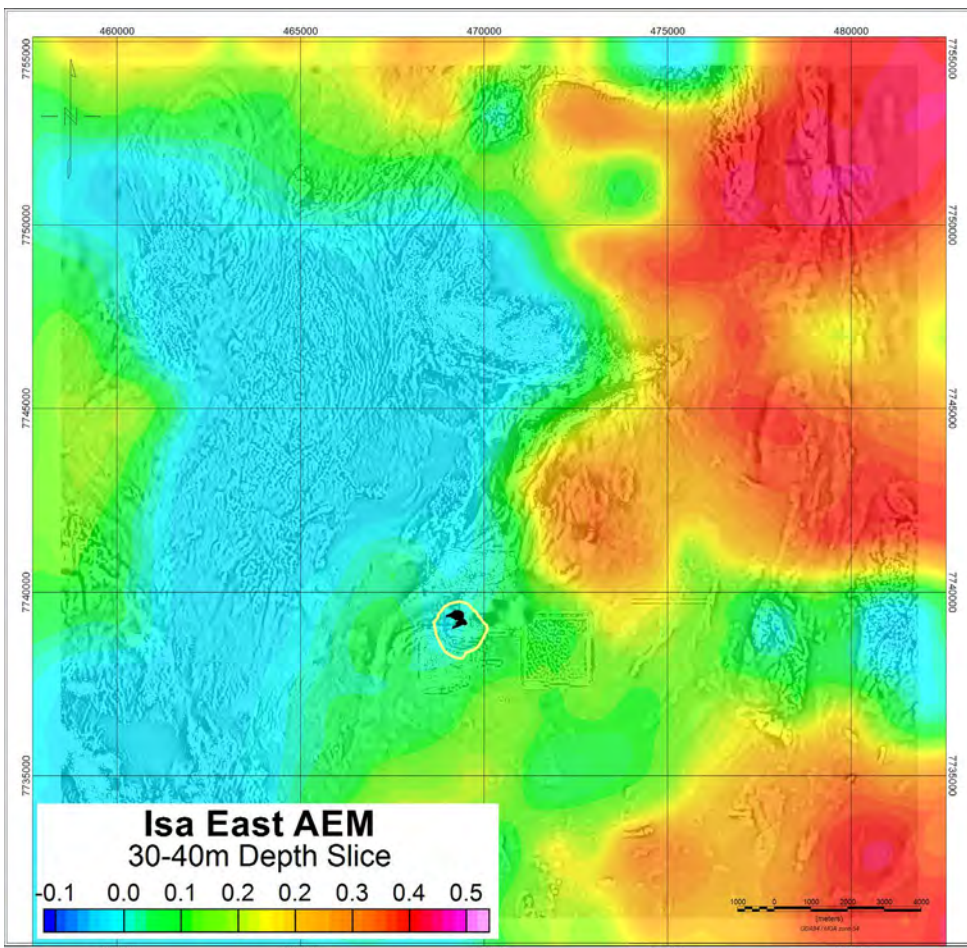


Figure 3.42. Diagram from Lilly et al (2014) showing Mobile Soil Gas (MSG) soil results for surveys in the Ernest Henry area.



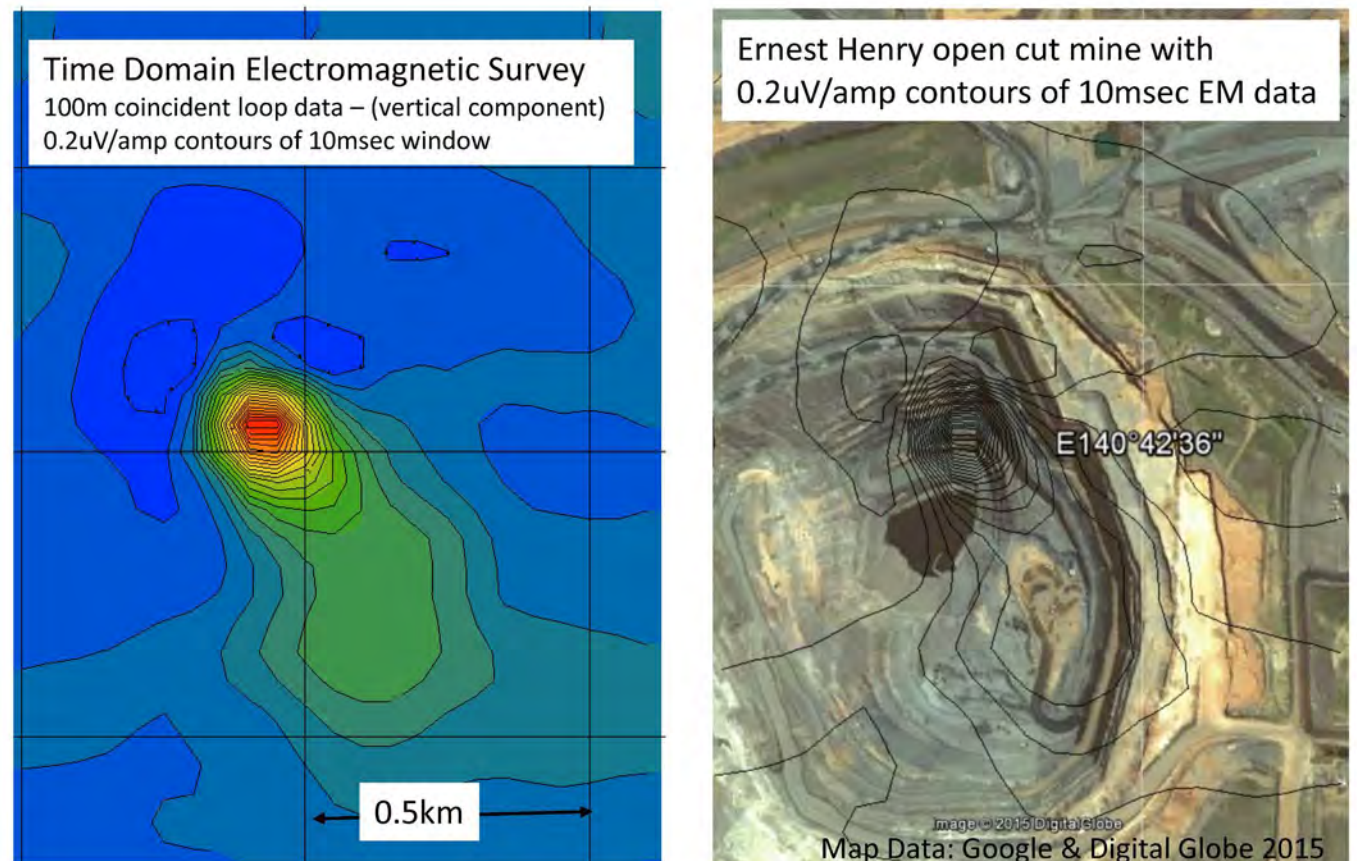


Figure 3.44. Diagram from Webb (2015) showing the ground time domain electromagnetic response attributed to supergene mineralisation (Webb and Rowston, 1995)

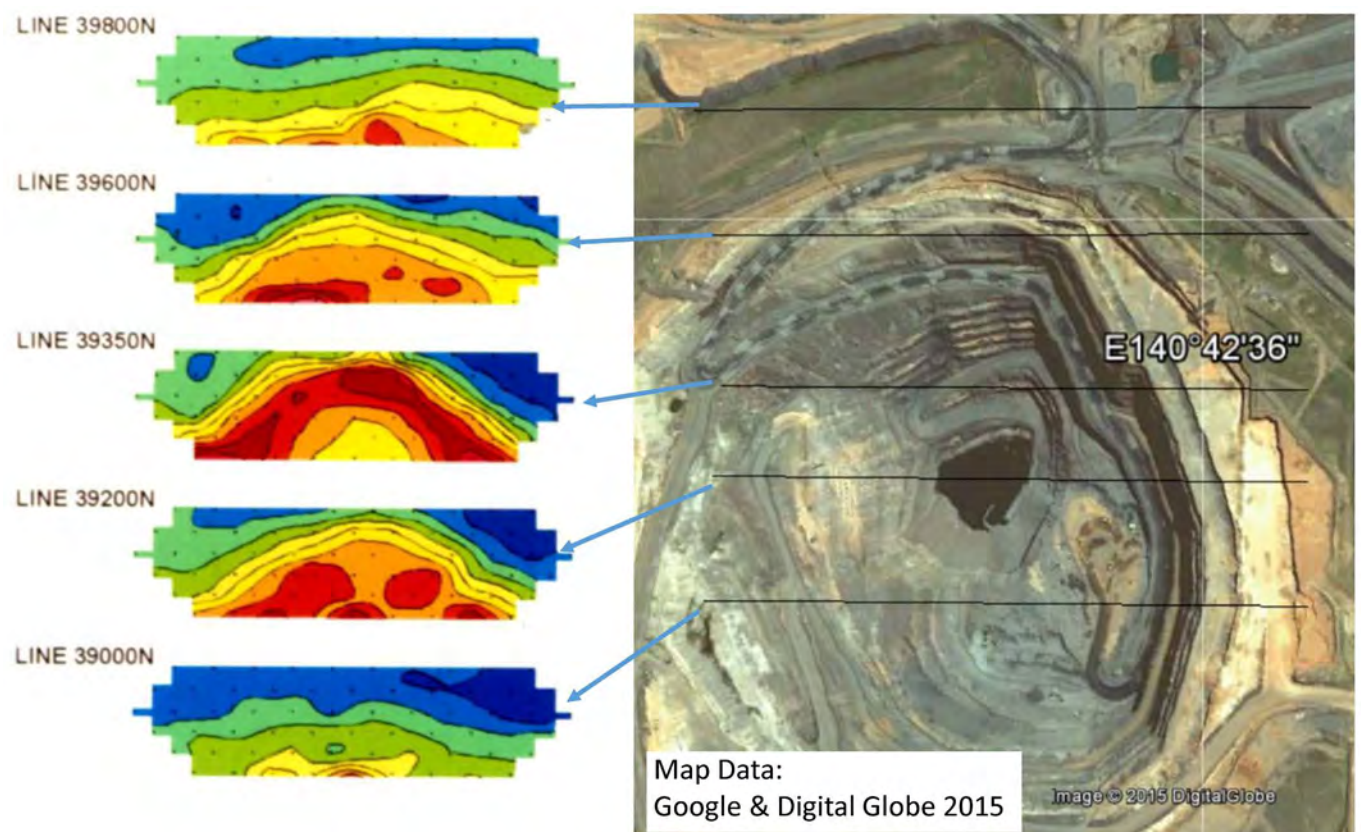


Figure 3.45. Diagram from Webb (2015) showing IP chargeability pseudosections over the Ernest Henry orebody.

Figure 3.43. (facing page) Depth slices from the Isa East Airborne EM survey (VTEM time domain EM flown at 2km line spacing). Depth slices based on EMflow models as supplied with the dataset. Yellow line shows outline of final pit and black solid represents the near-surface expression of the Ernest Henry orebody. Line 1701 of the survey passed directly over the orebody and pit at an altitude of up to 437 metres - about 400 metres more than the altitude recorded for the rest of the line. Map Projection GDA94, MGA54.

## REFERENCES

- Austin, JR, Walshe, JL, Gazley, MF, Ibrahimi T, Patterson, BO, leGras, M, 2016. The Ernest Henry Cu-Au deposit: Integrated Petrophysical and Geochemical analyses. CSIRO, Australia, pp. 56.
- Case, G., Blenkinsop, T., Chang, Z., Huizenga, J., Lilly, R., McLellan, J. 2017. Delineating the structural controls on the genesis of iron oxide-Cu-Au deposits through implicit modelling; a case study from the E1 Group, Cloncurry District, Australia. Special Publication - Geological Society of London, 453, Special Publication - Geological Society of London, Characterization of ore-forming systems from geological, geochemical and geophysical studies, 2017, Vol.453.
- Coward, M., 2001. Structural controls on ore formation and distribution at the Ernest Henry Cu-Au deposit, NW Queensland; BSc (Honours) Thesis, James Cook University, Townsville.
- Craske, T. 1995. Discovery of the Ernest Henry copper-gold deposit and E1 deposits, Cloncurry Qld - Geological aspects. AIG Seminar presentation.
- Lilly, R., & Hannan, K., 2016. Geochemistry Through Cover: Defining geochemical exploration parameters for the Cloncurry Mineral District, Queensland. Final report - Geochemistry through cover project (QDEX)
- Lilly, R., Case, G., & Miller, B. 2017. Ernest Henry iron oxide copper-gold deposit ,in Australian Ore Deposits (ed: G N Phillips), pp 501-506 (The Australasian Institute of Mining and Metallurgy: Melbourne).
- Lilly, R., Hannan, K., & Wang, M. 2014. Geochemical trials in weathered overburden: Defining exploration parameters for Mount Isa-style and IOCG mineralisation in NW Queensland, Australia. AusIMM Technical talk April 2014
- Mark, G., Oliver, N., & Williams, H. 2006. Mineralogical and chemical evolution of the Ernest Henry Fe oxide-Cu-Au ore system, Cloncurry district, northwest Queensland, Australia. Mineralium Deposita, 40(8), 769-801.
- Murphy, T., Hinman, M., Donohue, J., Pirlo, M., Valenta, R., Jones, M. & Pratt, A., 2017. Deep Mining Queensland: Prospectivity Analysis in the Southern Cloncurry Belt, Queensland, Australia. DNRM-GSQ Commissioned Industry Study.
- O'Brien, S. 2016. Structural and Mineralogical Controls on the Formation of the 'Inter-lens' at the Ernest Henry Deposit, Queensland. BSc honours thesis, Adelaide University
- Oliver, N.H.S., Butera, K.M., Rubenach, M.J., Marshall, L.J., Cleverley, J.S., Mark, G., Tulle-mans, F. and Esser, D., 2008. The protracted hydrothermal evolution of the Mount Isa Eastern Succession: A review and tectonic implications; Precambrian Research, v. 163, pp. 108-130.
- Page R.W., Sun S-S. 1998 Aspects of geochronology and crustal evolution in the Eastern Fold Belt, Mount Isa Inlier. Aust J Earth Sci 45:343-362
- Pollard PJ, McNaughton N 1997 U-Pb geochronology and Sm/Nd isotope characteristics of Proterozoic intrusive rocks in the Cloncurry district, Mount Isa Inlier, Australia. In: Pollard, PJ (compiler) AMIRA P438 Final Report: Cloncurry Base Metals and Gold Section 4, p 19
- Rusk, B.G., Oliver, N.H.S., Cleverley, J.S., Blenkinsop, T.G., Zhang, D., Williams, P.J. and Habermann, P., 2010 - Physical and Chemical Characteristics of the Ernest Henry Iron Oxide Copper Gold Deposit, Australia; Implications for IOCG Genesis; in Porter, T.M., (ed.), Hydrothermal Iron Oxide Copper-Gold and Related Deposits: A Global Perspective, v. 3 - Advances in the Understanding of IOCG Deposits; PGC Publishing, Adelaide, pp. 201-218.
- Sullivan, E. 2016. Geological Characteristics of the Ernie Junior Iron-Oxide-Copper-Gold Ore Body, Mt Isa Inlier, North West Queensland. BSc honours thesis, Adelaide University
- Twyerould, S.C., 1997. The geology and genesis of the Ernest Henry Fe-Cu-Au deposit, Northwest Queensland, Australia; Unpublished PhD thesis, University of Oregon, Eugene, 494p.
- Webb M., Rowston P. 1995 The geophysics of the Ernest Henry Cu-Au deposit (N.W.) Queensland. Expl Geophys 26:51-59
- Webb, M. 2015. Ernest Henry copper deposit - geophysics. Blue Sky Geoscience presentation.